

PARAMETERS AFFECTING PRODUCT
FORMATION IN THE GAMMA RADIOLYSIS OF
AQUEOUS BENZENE SOLUTIONS

By

LARRY LEE LAND

A DISSERTATION PRESENTED TO THE GRADUATE SCHOOL
OF THE UNIVERSITY OF FLORIDA IN PARTIAL FULFILLMENT
OF THE REQUIREMENTS FOR THE DEGREE OF
DOCTOR OF PHILOSOPHY

UNIVERSITY OF FLORIDA

2001

This dissertation is dedicated to my wife, Cynthia Isabel Mendoza Land. Without your unending love and continuous support, the completion of this work would not have been possible.

ACKNOWLEDGMENTS

The writer would like to express heartfelt gratitude without limit to Professor Robert J. Hanrahan for his untiring support and countless suggestions that immensely aided in making this project a success. The writer would also like to say thanks to Professor M. L. Muga for his quick wit and his introduction of the writer to the world of crossword puzzles. The writer would like to show appreciation to Dr. Kathryn R. Williams for her friendship down through the years and the use of her analytical instrumentation.

On a more personal note, the writer would like to offer thanks to several special people whose acquaintanceships made graduate school both enjoyable and memorable: Susan Rasmussen Pursley, Craig Hoag, David Miko, Lisa Spurlock and Mark Stoy. I feel that I am a better person for having known each of you.

TABLE OF CONTENTS

	<u>page</u>
ACKNOWLEDGMENTS	iii
LIST OF TABLES	vi
LIST OF FIGURES	viii
ABSTRACT	xiii
 CHAPTERS	
1 INTRODUCTION	1
Purpose of the Project	1
Scope of the Project	3
2 INTERACTION OF RADIATION WITH MATTER	4
Production and Decay of Cobalt-60	4
Photon and Particle Interactions with Matter	6
Gamma Radiolysis of Water	19
3 DOSIMETRY AND THE FRICKE DOSIMETER	30
General Background	30
Fricke Dosimetry	33
Application of Fricke Dosimetry	37
4 PRELIMINARY INVESTIGATIONS INTO THE AQUEOUS BENZENE SYSTEM	62
Test Tube Geometry, Geometry A	62
Screw-Top Vial Geometry, Geometry B	72
Open Tube Evaporation Study	74
5 ANALYTICAL METHODS FOR CO ₂ QUANTITATION	77
Trapping/Titration Experiment	77
Gas Chromatography Experiment	91

6	GAMMA IRRADIATION OF AQUEOUS BENZENE SOLUTIONS.....	104
	Low Dose Rate Experiments for Initial Product Determination.....	104
	High Dose Rate Experiments for CO ₂ Production.....	115
	GC-MS Experiments for Qualitative Determination of Trace Products.....	118
7	MECHANISM AND DISCUSSION.....	160
	Effect of Headspace Volume	160
	Effect of Headspace Gas.....	170
	Reactions of Benzene with Radical Transients.....	183
	Discussion of Reaction Mechanism.....	187
	Application of Mechanisms to Our Systems	198
8	CONCLUSION AND FUTURE WORK	217
	Summary of Results	217
	Implications for Detoxification Applicability.....	218
	Future Work	219
	LIST OF REFERENCES	220
	BIOGRAPHICAL SKETCH	230

LIST OF TABLES

<u>Table</u>	<u>Page</u>
1. Typical reactions involved in the Cobalt-60 gamma radiolysis of water.....	23
2. Main reactions in the Fricke dosimeter	34
3. Representative Fricke experimental data using each of the three sample geometries. The date on which each representative Fricke experiment was performed is listed along with the dose rate, DR, in various units	57
4. A portion of a decay correction table showing the additional time needed in the irradiator as the source decayed	61
5. Listing of concentrations of standard HCl, NaOH and Na ₂ CO ₃ solutions for titration experiments.....	81
6. Listing of volumes and concentrations of each solution used for the three pseudo-unknown titration experiments.....	82
7. Listing of the results from the three pseudo-unknown titration trapping experiments for determination of radiolytically produced CO ₂	91
8. Results from the three pseudo-unknown CO ₂ headspace experiments analyzed by gas chromatography	103
9. Listing of μ moles of compound in solution versus dose in Mrad for the short air system.....	114
10. Listing of μ moles of compound in solution versus dose in Mrad for the long oxygen system (LOD = Limit of Detection)	114
11. Listing of μ moles of compound in solution versus dose in Mrad for the long air system (LOD = Limit of Detection)	115
12. Listing of μ moles of compound in solution versus dose in Mrad for the long nitrogen system (LOD = Limit of Detection).....	115
13. Listing of μ moles of CO ₂ versus dose in Mrad for each of the four systems (LOD = Limit of Detection)	117

14. Experimental parameters for geometry B gas chromatography experiments GCMS1 – GCMS5	120
15. Experimental parameters for geometry C gas chromatography experiments GCMS6 – GCMS10	122
16. Mass spectral data for experiment GCMS1	129
17. Mass spectral data for experiment GCMS2	131
18. Mass spectral data for experiment GCMS3	134
19. Mass spectral data for experiment GCMS4	136
20. Mass spectral data for experiment GCMS5	138
21. Mass spectral data for experiment GCMS6	140
22. Mass spectral data for experiment GCMS7	142
23. Mass spectral data for experiment GCMS8	144
24. Mass spectral data for experiment GCMS9	146
25. Mass spectral data for experiment GCMS10	148
26. Mass spectral data for experiment GCMS11	150
27. Mass spectral data for experiment GCMS12	153
28. Mass spectral data for experiment GCMS13	157
29. Mass spectral data for experiment GCMS14	159
30. Listing of initial G-values for benzene and quantified radiolysis products for the short air and long air systems	170
31. Listing of initial G-values for benzene and quantified radiolysis products for the long oxygen, long air and long nitrogen systems (LOD = Limit of Detection).....	181
32. Rates of production, R, of radical and molecular products during the four experiments using geometry B	203
33. Airborne toxicity limits (TL) for benzene and identified products	212

LIST OF FIGURES

<u>Figure</u>	<u>Page</u>
1. Decay diagram of Cobalt-60 showing the two gamma photons of energies 1.17 MeV and 1.33 MeV produced in cascade	5
2. A diagram of the photoelectric effect showing the events that occur	10
3. A diagram of the Compton effect indicating the deflection angles of the scattered gamma photon, θ , and the ejected electron, ϕ , from the path of the incident gamma photon, γ	11
4. A diagram of pair production showing the production of an electron/positron pair and the resulting emission of annihilation radiation at an angle of 180° relative to each other	14
5. The radiation chemistry timescale showing the pertinent reactions that occur within each stage	20
6. Cross-section of the Cobalt-60 gamma irradiator	38
7. A side view of the wagon-wheel sample holder used in geometry A showing the spacing between plates	41
8. Top view of the wagon-wheel sample holder used in geometry A showing the relative distances from the source hole to the inner and outer sample holes	42
9. Top view of the solid aluminum sample holder resting on the solid aluminum plate. The holder is affixed using brackets. A handle is present on the bottom of the plate to aid in insertion and removal	44
10. Cutaway view of the solid-block aluminum sample holder showing the relative positions of the bottoms of the sample cells and the source rod	45
11. Top view of the solid-block aluminum sample holder used in geometry C showing the four sample positions and the source to sample distances used for total irradiator calibration	46
12. Fricke plot for the inner sample position using geometry A. This experiment was performed on 10/93 and resulted in a dose rate of 7023.2 rad/min	49

13.	Fricke plot for the inner and outer sample positions using geometry B. This experiment was performed on 4/94 and resulted in a dose rate of 5782.2 rad/min for the inner sample position, and 1421.1 rad/min for the outer sample position	50
14.	Fricke plot for sample position 1 using geometry C. This experiment was performed on 5/99 and resulted in a dose rate of 24591 rad/min.....	51
15.	Fricke plot for sample position 2 using geometry C. This experiment was performed on 5/99 and resulted in a dose rate of 5721.2 rad/min.....	52
16.	Fricke plot for sample position 3 using geometry C. This experiment was performed on 5/99 and resulted in a dose rate of 1660.0 rad/min.....	53
17.	Fricke plot for sample position 4 using geometry C. This experiment was performed on 5.99 and resulted in a dose rate of 245.48 rad/min.....	54
18.	Plot of dose rate versus source to sample distance for geometry C. This experiment resulted in total calibration of the irradiator.....	58
19.	Plot of dose rate versus the reciprocal of square distance for geometry C. This experiment resulted in total calibration of the irradiator.....	59
20.	Chemical structures of benzene, phenol, 2-phenylphenol and biphenyl	66
21.	Solution benzene concentration versus time of irradiation for geometry A for the first two hours of irradiation.....	67
22.	Phenol concentration versus time of irradiation for geometry A for the first two hours of irradiation	68
23.	2-Phenylphenol concentration versus time of irradiation for geometry A for the first two hours of irradiation	69
24.	Biphenyl concentration versus time of irradiation for geometry A for the first two hours of irradiation	70
25.	Apparent solution benzene concentration versus time of irradiation exhibiting improbable behavior.....	71
26.	Solution benzene concentration versus the length of time the vial had stood uncapped on the benchtop.....	76
27.	Pseudo-unknown titration experiment 1: pH plot for the titration of 5.000 mmoles CO_3^{2-} and 6.070 mmoles OH^- using 0.9127 M HCl as titrant	83
28.	Pseudo-unknown titration experiment 1: Second derivative plot for the titration of 5.000 mmoles CO_3^{2-} and 6.070 mmoles OH^- using 0.9127 M HCl as titrant	84

29.	Pseudo-unknown titration experiment 2: pH plot for the titration of 0.5000 mmoles CO_3^{2-} and 0.6070 mmoles OH^- using 0.04564 M HCl as titrant ...	85
30.	Pseudo-unknown titration experiment 2: Second derivative plot for the titration of 0.5000 mmoles CO_3^{2-} and 0.6070 mmoles OH^- using 0.04564 M HCl as titrant ...	86
31.	Pseudo-unknown titration experiment 3: pH plot for the titration of 5.000×10^{-2} mmoles CO_3^{2-} and 6.070×10^{-2} mmoles OH^- using 4.564×10^{-3} M HCl as titrant	87
32.	Pseudo-unknown titration experiment 3: Second derivative plot for the titration of 5.000×10^{-2} mmoles CO_3^{2-} and 6.070×10^{-2} mmoles OH^- using 4.564×10^{-3} M HCl as titrant	88
33.	Gas chromatography air calibration plot indicating the normalized peak area versus μmoles of injected air	96
34.	Gas chromatography CO_2 calibration plot indicating the normalized peak area versus μmoles of injected CO_2	97
35.	Diagram showing headspace gas transfer in progress. The large syringe contains acid solution that is added to the vial as the headspace is withdrawn into the smaller syringe	100
36.	A typical chromatogram of a sample containing air (N_2/O_2) and CO_2	102
37.	Cross section of the 500 mL roundbottom flask modified for use as an irradiation vessel	123
38.	GC-MS chromatogram for experiment GCMS1	128
39.	GC-MS chromatogram for experiment GCMS2	130
40.	GC-MS chromatogram for experiment GCMS3	133
41.	GC-MS chromatogram for experiment GCMS4	135
42.	GC-MS chromatogram for experiment GCMS5	137
43.	GC-MS chromatogram for experiment GCMS6	139
44.	GC-MS chromatogram for experiment GCMS7	141
45.	GC-MS chromatogram for experiment GCMS8	143
46.	GC-MS chromatogram for experiment GCMS9	145
47.	GC-MS chromatogram for experiment GCMS10	147

48.	GC-MS chromatogram for experiment GCMS11	149
49.	GC-MS chromatogram for experiment GCMS12	152
50.	GC-MS chromatogram for experiment GCMS13	156
51.	GC-MS chromatogram for experiment GCMS14	158
52.	Plot of μ moles of benzene in solution versus dose in Mrad for both the short air and long air systems	161
53.	Plot of the total number of μ moles of benzene contained in the radiolysis vessel versus dose in Mrad for both the short air and long air systems	162
54.	Plot of μ moles of phenol versus dose in Mrad for both the short air and long air systems	163
55.	Plot of μ moles of biphenyl versus dose in Mrad for both the short air and long air systems	164
56.	Plot of μ moles of 3-phenylphenol versus dose in Mrad for both the short air and long air systems	165
57.	Plot of μ moles of 4-phenylphenol versus dose in Mrad for both the short air and long air systems	166
58.	Plot of μ moles of CO_2 versus dose in Mrad for both the short air and long air systems	171
59.	Plot of μ moles of benzene in solution versus dose in Mrad for the long oxygen, long air and long nitrogen systems	172
60.	Plot of total number of μ moles of benzene versus dose in Mrad for the long oxygen, long air and long nitrogen systems	173
61.	Plot of μ moles of phenol versus dose in Mrad for the long oxygen, long air and long nitrogen systems	174
62.	Plot of μ moles of biphenyl versus dose in Mrad for the long oxygen and long air systems. Biphenyl was not observed in the long nitrogen system	175
63.	Plot of μ moles of 3-phenylphenol versus dose in Mrad for the long oxygen and long air systems. The compound 3-phenylphenol was not observed in the long nitrogen system	176
64.	Plot of μ moles of 4-phenylphenol versus dose in Mrad for the long oxygen and long air systems. The compound 4-phenylphenol was not observed in the long nitrogen system	177

65.	Plot of $\mu\text{moles of CO}_2$ versus dose in Mrad for the long oxygen, long air and long nitrogen systems	182
66.	Plot of Total Toxicity Units (TTU) versus dose in Mrad for the short air and long air systems	215
67.	Plot of Total Toxicity Units (TTU) versus dose in Mrad for the long oxygen, long air and long nitrogen systems.....	216

Abstract of Dissertation Presented to the Graduate School
of the University of Florida in Partial Fulfillment of the
Requirements for the Degree of Doctor of Philosophy

PARAMETERS AFFECTING PRODUCT
FORMATION IN THE GAMMA RADIOLYSIS OF
AQUEOUS BENZENE SOLUTIONS

By

Larry Lee Land

May, 2001

Chairman: Robert J. Hanrahan
Major Department: Chemistry

The gamma radiolysis of aqueous benzene solutions was studied under different conditions in order to ascertain the role that oxygen plays in the destruction of benzene to form carbon dioxide. Aqueous benzene solutions were studied using two different headspace volumes (small versus large) and three different headspace gases (oxygen, air and nitrogen). For three of the four headspace systems (small air, large oxygen and large air), phenol and biphenyl were determined to be the major quantified products. For the large nitrogen headspace system, phenol was the sole quantified product. Benzene was found to be consumed at nearly the same rate in each of the four systems; $G(-\text{benzene})$ was calculated to equal 4.2 to 4.7 molecules per 100 eV. Initial yields of phenol, $G(\text{phenol})$, were determined for each system and were found to equal 0.58, 1.2, 0.58 and 0.29 for the small air, large oxygen, large air and large nitrogen headspace systems, respectively. The yield of biphenyl, $G(\text{biphenyl})$, was also determined for each of the

three systems in which biphenyl was identified as a product. Values for $G(\text{biphenyl})$ of 0.12, 0.27 and 0.18 were calculated for the small air, large oxygen and large air systems, respectively. The percent conversion of benzene to CO_2 after an absorbed dose of 250 Mrad was determined for each of the four systems; conversion percents of 10.7%, 55.1%, 30.5% and 12.5% were found for the small air, large oxygen, large air and large nitrogen headspace systems, respectively. A proposed mechanism, dependent upon the presence or absence of oxygen, was presented for each system. Product yields were discussed in view of the proposed mechanism. Lastly, the total solution toxicity for each system was calculated by summing the individual toxicities of benzene and each identified product. For the small air, large oxygen and large air systems, the total solution toxicity was found to go through a maximum at a dose of 2.0 Mrad and then decrease to a value below that of the original solution. The total solution toxicity of the large nitrogen system was found to decrease from the onset of experimentation.

CHAPTER 1 INTRODUCTION

Aromatic hydrocarbons such as benzene are major constituents of groundwater contamination in many polluted water sites in the United States [1]. Many methods of pollutant removal (solution detoxification) are now being investigated such as aeration stripping, activated carbon adsorption, ozone oxidation, UV irradiation of titanium dioxide slurries, and the use of ionizing radiation such as accelerated electrons (linear accelerator beam) or Cobalt-60 gamma irradiation. Of these, the last three are particularly advantageous in that the organic contaminants are actually destroyed, not simply moved from one place to another. Gamma radiolysis of aqueous solutions is especially applicable because of the steady-state production of reactive radicals that occurs during irradiation not only of thin liquid layers but also of aqueous solutions as deep as a foot or more.

Purpose of the Project

The use of UV irradiation of titanium dioxide slurries as a method of water detoxification has received considerable attention during the last twenty years [2-10]. Aqueous slurries of TiO_2 are used for detoxification experiments due to the band gap structure of TiO_2 . When aqueous slurries of TiO_2 are irradiated with UV light, an electron is promoted from the valence band to the conduction band. This promotion leaves a positive hole, denoted as h^+ , in the TiO_2 structure.



The reaction of h^+ with water produces the hydroxyl radical, $\cdot OH$.



Reaction of $\cdot OH$ with the pollutant contained in the slurry leads to degradation of the contaminant. Total degradation of the pollutant leads to formation of carbon dioxide, CO_2 . In many cases, quantitative or near quantitative destruction is known to occur within moderate exposure times to UV light. This is in direct contrast to irradiation time or dose that is necessary for quantitative conversion to CO_2 when using Cobalt-60 gamma irradiation, as this work will demonstrate. It is believed that quantitative conversion to CO_2 is possible in TiO_2 slurries because the pollutant tends to adsorb on the surface of the titania. Upon irradiation with UV light, a much higher effective $\cdot OH$ concentration is possible in TiO_2 slurries than is possible in Cobalt-60 gamma radiolysis work.

In the early 1990's, however, Michael Nickelsen, William Cooper and associates reported the quantitative destruction of organic pollutants such as benzene, toluene and phenol when using a linear electron accelerator (LINAC) as a source of detoxifying radicals [11, 12]. During this time Cooper was director of the Electron Beam Research Facility (EBRF) located at the Miami-Dade Central District Wastewater Treatment Plant in Miami, Florida. At this facility, Cooper and associates studied the treatment of polluted waters with a 1.5 MeV electron beam. In their plant, polluted water was continually circulated from an 11,400 L holding tank, through a complex system of pipes, across a weir in front of the electron beam horn, and back to the holding tank. Samples of the water were taken at various points in the recirculating stream and analyzed for solute destruction.

Various aspects of Nickelsen's and Cooper's results raised questions in our research laboratory, for we felt that it was extremely unlikely that complete solute destruction to form CO_2 was possible as described in their work. Since electron beam irradiation and Cobalt-60 gamma irradiation are equivalent in terms of track effects, i.e., both methods lead to steady-state distributions of the same reactive radicals, we felt that an investigation of one of his systems was in order. We chose the aqueous benzene system, partly because Nickelsen and Cooper had studied the system, and partly because of the long history of research into the aqueous benzene system that had been performed in our laboratory and others.

Scope of the Project

We were interested in investigating the effects of oxygen and solute concentration on initial product formation, rate of degradation to CO_2 , and the mechanistic pathway that is followed during irradiation. Our laboratory had performed considerable work on the radiolysis of the tetraphenylborate system in connection with studies on the storage of nuclear waste [13, 14]. Our laboratory found that benzene was a product in the tetraphenylborate system. In addition, observed yields of benzene and other products were explainable in terms of $\cdot\text{OH}$ attack on the intermediate benzene. For this reason, we felt that further examination of the aqueous benzene system was in order.

CHAPTER 2 INTERACTION OF RADIATION WITH MATTER

Production and Decay of Cobalt-60

Production of Cobalt-60

The gamma ray emitters Cobalt-60 and Cesium-137 comprise the majority of radioactive sources in research gamma irradiators in use today. Cobalt-60 is prepared by irradiating slugs of Cobalt-59 in a nuclear reactor with thermal neutrons. In this flux, Cobalt-59 absorbs neutrons and converts into Cobalt-60 in an excited state. Cobalt-60 immediately relaxes to the ground state by the emission of a prompt gamma ray. This reaction scheme is commonly known as an n, γ reaction and may be written using standard nuclear reaction shorthand:



Cobalt-60 Decay Scheme

Cobalt-60, a radioactive nuclide with half-life of 5.27 years, decays by negative beta (negatron) decay to an excited nuclear level of Nickel-60, which decays to the ground state in two steps [15]. Gamma photons of energy 1.17 MeV and 1.33 MeV are produced in the decay, the scheme of which is shown in Figure 1 [15]. Since the two gamma photons are produced in cascade (as shown in Figure 1), equal numbers of photons of each energy are produced. Commonly, Cobalt-60 is described as emitting two gamma photons of energy 1.25 MeV, which is the average of 1.17 MeV and 1.33 MeV.

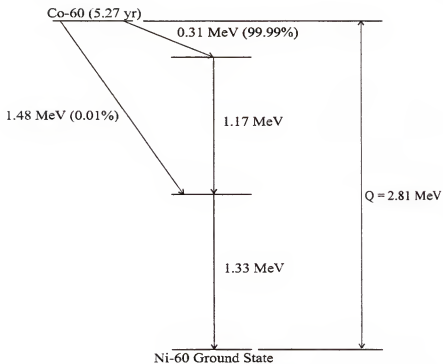


Figure 1: Decay diagram of Cobalt-60 showing the two gamma photons of energies 1.17 MeV and 1.33 MeV produced in cascade.

Photon and Particle Interactions with Matter

Description of Gamma Photons

Gamma rays versus X-rays

Gamma photons and X-rays are both electromagnetic radiation, EMR, of extremely short wavelength and are thus highly energetic and penetrating. However, one fundamental difference between gamma photons and X-rays lies in the origin of the radiation: gamma photons arise from transitions between energy levels in the atomic nucleus, whereas X-rays arise from transitions between electronic levels outside the nucleus and/or bremsstrahlung (braking radiation) as charged particles are stopped in matter.

The wavelength, λ , region of the electromagnetic spectrum in which gamma rays are found roughly exists from 3×10^{-11} m to 3×10^{-13} m. This wavelength range may be converted to an equivalent energy range:

$$E = h \frac{c}{\lambda} \quad (4)$$

In Equation (4), h is Planck's constant, 6.626×10^{-34} Js, and c is the speed of light, 2.998×10^8 m/s. Substituting wavelength extremes and the constants yields an energy range of 40 keV to 4 MeV for gamma photons.

Statistical nature of photon interactions

A gamma photon traveling through an absorber tends to lose most of its energy in one interaction, whereas a charged particle tends to lose its energy gradually, losing a small fraction with each interaction. When a gamma ray passes through a thin absorber, gamma photons may be transmitted with no change in energy or direction, or may be

removed from the ray in single events either through true absorption or through scattering, thus reducing the intensity of the beam exiting the absorber.

A gamma photon may travel a short or long distance before being absorbed. Therefore, gamma photons do not possess a definite range. As the distance traveled increases, the total probability of absorption increases but the probability of absorption per unit path length is essentially constant. For an initially monoenergetic population of photons, the statistical nature of the photon absorption process leads to an exponential relationship between the intensity of the beam versus the distance traveled through the absorber:

$$I = I_0 e^{(-\mu x)} \quad (5)$$

In Equation (5), I_0 is the initial intensity of the gamma ray beam, and I is the intensity of the beam after having traveled a distance x (in cm) through the absorber. The quantity μ is termed the linear absorption coefficient and has units of cm^{-1} . The magnitude of μ depends on both the energy of the gamma photon and the identity of the absorber.

From Equation (5), the half-thickness value for a given gamma photon and absorber can be calculated. Half-thickness, $x_{1/2}$, is defined as the thickness of absorber that reduces the intensity of the gamma ray beam to 50% of the initial value:

$$x_{1/2} = \frac{\ln(2)}{\mu} = \frac{0.693}{\mu} \quad (6)$$

Using the linear absorption coefficient for water, 0.064 cm^{-1} [16], the half-thickness for Cobalt-60 gamma photons in water is calculated to equal 10.8 cm.

Gamma Photon Interactions

Gamma photons interact with absorbers mainly by three mechanisms: photoelectric effect, Compton effect and pair production. In addition, two other minor

interaction mechanisms exist: coherent scattering and photonuclear reactions. The importance of each interaction mechanism depends on the energy of the gamma photon, E_γ , as well as the atomic number of the absorber, Z .

Photoelectric effect

In the photoelectric effect, a photon undergoes an inelastic collision with an orbital electron of an absorber molecule. The photon is completely absorbed and the orbital electron is ejected with kinetic energy, E_k , equal to the difference between the energy of the photon, E_γ , and the binding energy of the electron, E_b :

$$E_k = E_\gamma - E_b \quad (7)$$

Momentum is conserved by recoil of the remainder of the atom; for this reason, the photoelectric effect is not possible with free electrons.

If the energy of the photon is greater than the binding energy of a K-shell electron of an absorber atom, 80% of the ejected electrons come from the K-shell and 20% come from the L-shell. The photoelectron may then interact with other absorber atoms by charged particle mechanisms that are discussed later in this chapter.

The ejection of the photoelectron leaves a vacancy in an orbital of the absorber atom and an electron from an outer orbital level falls to fill this hole. This relaxation results in either the emission of an X-ray of energy equal to the energy difference between the two orbital levels (X-ray fluorescence), or the ejection of a second electron (Auger electron emission). Since X-ray fluorescence and Auger electron emission both leave an orbital vacancy in an orbital of higher principal quantum number, the relaxation process may be repeated several times, which results in the emission of several Auger

electrons or fluorescence X-rays for each initial photoelectron. The ejection of the photoelectron and subsequent relaxation mechanisms are shown in detail in Figure 2 [17].

The probability of the photoelectric interaction, $P_{\text{photoelectric}}$, is directly related to the atomic number of the absorber, Z , and indirectly related to the energy of the gamma photon, E_γ :

$$P_{\text{photoelectric}} \propto \frac{Z^5}{E_\gamma^{7/2}} \quad (8)$$

The photoelectric effect is thus favored for gamma photons of low energy passing through absorbers of high atomic number.

Compton effect

If the energy of the gamma photon is large in comparison to the binding energy of an orbital electron of an absorber atom, the photon may impart only a portion of its energy to the orbital electron. This interaction is known as the Compton effect, also known as incoherent scattering. The orbital electron is ejected and the photon emerges from the interaction scattered at a different angle with less energy. The kinetic energy of the ejected electron, E_k , is simply the difference in the energies of the incident and scattered photons, E_γ and E_γ' , respectively:

$$E_k = E_\gamma - E_\gamma' \quad (9)$$

Since the binding energy of the orbital electron is small in magnitude compared to the photon energy, the binding energy is usually not considered in Equation (9). The scattered photon may then participate in photoelectric interactions or further Compton interactions. The Compton interaction is shown schematically in Figure 3 [17].

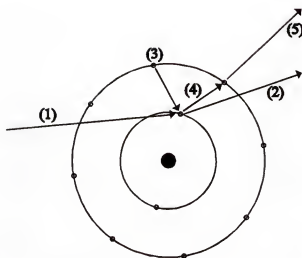


Figure 2: A diagram of the photoelectric effect showing the events that occur.

- (1) An incoming gamma photon kicks out an orbital electron.
- (2) The orbital electron is ejected from the absorber atom thus leaving an orbital vacancy.
- (3) An electron from a higher electron shell drops to fill the vacancy.
- (4) The relaxation process can emit a photon of energy equal to the difference in energy levels between the shells.
- (5) The relaxation process may result in the ejection of an Auger electron.

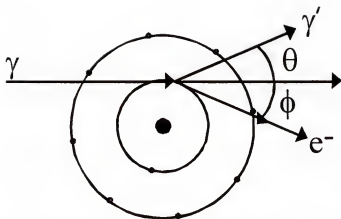


Figure 3: A diagram of the Compton effect indicating the deflection angles of the scattered gamma photon, θ , and the ejected electron, ϕ , from the path of the incident gamma photon, γ .

Using physical laws of conservation of energy and momentum, the equation that relates the energy of the scattered gamma photon, E_{γ}' , to the scattering angle, θ , may be derived:

$$\frac{1}{E_{\gamma}'} - \frac{1}{E_{\gamma}} = \frac{1 - \cos \theta}{E_0} \quad (10)$$

In Equation (10), E_{γ} is the energy of the incident gamma photon, and E_0 is the rest energy of the electron, 0.511 MeV. Equation (4) may then be employed to convert Equation (10) to its more usable form:

$$\lambda' - \lambda = \frac{h}{m_e c} (1 - \cos \theta) \quad (11)$$

The factor m_e is the rest mass of the electron, and c is the speed of light. The quantity $h/(m_e c)$ is termed the Compton wavelength of the electron and is equal to 2.426×10^{-10} cm. Equation (11) may be used to predict the scattering angle, θ , at which the energy of the scattered gamma photon is minimized, which implies that the kinetic energy of the Compton electron is maximized. Due to the variability of the cosine function versus scattering angle θ , this minimum occurs at a scattering angle of 180° . The energy of the scattered gamma photon at this angle can then be calculated:

$$E_{\gamma}'(\text{minimum}) = \frac{E_0}{2} \frac{1}{1 + \frac{E_0}{2E_{\gamma}}} \quad (12)$$

For energies above 0.5 MeV, the probability of the Compton interaction, p_{Compton} , is directly proportional to the atomic number of the absorber, Z , and indirectly proportional to the energy of the gamma photon, E_{γ} .

$$P_{\text{Compton}} \propto \frac{Z}{E_{\gamma}} \quad (13)$$

The Compton effect is the main mode of interaction for moderately energetic gammas with energies between 1 MeV and 5 MeV in absorbers of high atomic number, and over a much wider range in absorbers of low atomic number. In water, the Compton interaction is the principal mode of interaction with photons with energies 30 keV to 20 MeV, an energy range that covers the gamma photons resulting from the decay of Cobalt-60.

Pair production

In pair production, the incident gamma photon is completely absorbed in the vicinity of an atomic nucleus of an absorber atom, and an electron/positron pair is produced. The energy of the incident gamma photon minus twice the rest mass of an electron is shared equally between the electron and the positron.

$$E_{\gamma} = E_{\text{electron}} + E_{\text{positron}} + 2m_e c^2 \quad (14)$$

The quantity $2m_e c^2$ is the energy that must be consumed in the creation of the electron/positron pair. Momentum is conserved by the recoil of the nucleus. The electron and the positron interact with matter as charged particles. In an absorber with many electrons, the positron will travel a short distance and will combine with an electron to produce two gamma photons of energy 0.511 MeV that are emitted 180° relative to each other, which are termed annihilation radiation. The process of pair production is shown in Figure 4 [17].

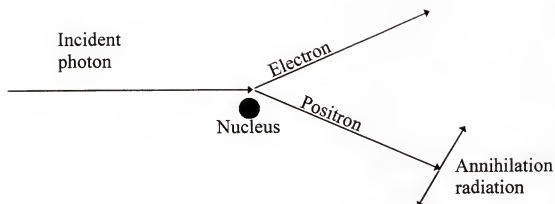


Figure 4: A diagram of pair production showing the production of an electron/positron pair and the resulting emission of annihilation radiation at an angle of 180° relative to each other.

Since 1.02 MeV of energy is needed for the creation of the electron/positron pair, the process of pair production is not possible at gamma photon energies below 1.02 MeV. In practice, pair production is favored only at much higher gamma photon energies. The probability of pair production, p_{pair} , varies directly with the square of the atomic number, Z .

$$p_{\text{pair}} \propto Z^2 \quad (15)$$

With absorbers of high atomic number, pair production is the main mode of interaction with high-energy gamma photons. In water, pair production only becomes important at gamma photon energies of 10 MeV or higher. Pair production is essentially negligible during the Cobalt-60 gamma radiolysis of water.

Coherent scattering

Unlike the three previously mentioned modes of interaction, coherent scattering does not result in degradation of the energy of the photon. Interactions with orbital electrons, termed Rayleigh scattering, are the most common type of coherent scattering. Photons with energies less than 0.1 MeV are scattered with little loss of energy, especially in absorbers of high atomic number, Z . The photon is usually not scattered by more than a few degrees and continues on a path very close to its original trajectory. Coherent scattering occurs in a gamma energy range in which the photoelectric probability is high.

Photonuclear reactions

In a photonuclear reaction, the absorption of a gamma photon may result in the ejection of a proton or a neutron from the nucleus of the absorber molecule. This interaction occurs with gammas with energies above 8 MeV for absorbers of high atomic

number, and in the region of 10 to 20 MeV for absorbers of low atomic number. In the energy range of interest in this work photonuclear reactions have cross-sections of essentially zero and may be ignored.

Charged Particle Interactions

Charged particles, such as electrons, traveling through absorbers undergo three types of interactions: elastic collisions, inelastic collisions and energy loss by bremsstrahlung. Of these three, elastic collisions are the only interactions that do not result in energy loss.

Elastic collisions

Elastic collisions occur when a charged particle is deflected by Coulombic (electrostatic) interactions with the electric field of the atomic nucleus of an absorber atom. The electron is deflected while the remainder of the atom remains almost stationary due to its much larger mass. Elastic collisions, also known as scattering, become more important as the absorber field increases (atomic number increases) or as the electron slows down. In this interaction, there is no change in the kinetic energy of the electron, but only a change in the direction of motion.

Inelastic collisions

Inelastic collisions result in degradation of the energy of the electron. The electric field of the charged particle, the electron, affects the electric field of an absorber atom as the electron approaches the atom. Some of the kinetic energy of the electron is transferred as internal energy to an electron of the absorber atom. This may result in excitation of an orbital electron of the absorber atom, or for greater energies, ionization in which the orbital electron leaves the absorber atom. The probability of energy transfer in this manner increases as the field of the charged particle increases (greater atomic

number) or as the speed of the particle decreases. This mode of interaction is also more probable for absorbers with greater electron densities. The equation relating the change in energy per unit length due to inelastic collisions was derived by Bethe and Ashkin [18]:

$$-\left(\frac{dE}{dl}\right)_{\text{col}} = \frac{2\pi N e^4 Z}{m_e v^2} \left[\ln \frac{m_e v^2 E}{2I^2(1-\beta^2)} - (2\sqrt{1-\beta^2} - 1 + \beta^2) \ln 2 + 1 - \beta^2 + \frac{1}{8}(1 - \sqrt{1-\beta^2})^2 \right] \quad (16)$$

In Equation (16), v is the velocity of the electron in m/s, β is the ratio v/c with c being the speed of light in m/s, I is the mean excitation potential for the absorber atoms in Joules, N is the number of atoms per liter, e is the charge on the electron in electrostatic units, m_e is the rest mass of the electron in kilograms and Z is the atomic number of the stopping material. The quantity dE/dl , which has units of J/m, is known as the specific energy loss or stopping power. As can be seen from Equation (16), dE/dl becomes larger as the electron loses velocity, which leads to greater excitation or ionization as the electron slows down.

Since both electrons involved in this interaction have the same mass, up to 1/2 of the energy of the impinging electron may be lost through one interaction, and large deflections in the angle of motion may result. Consequently, electrons show no fixed depth of penetration, but do show a maximum range that is much shorter than the true path length.

As the electron is slowed through numerous interactions, the intensity of ionization and excitation increases towards the end of the path length. At the end of the path, the ionization and excitation probability falls to zero because the electron does not possess sufficient energy to cause ionization or excitation. However, energy loss in the

low-energy region can occur due to the formation of transient negative ions [19]. A plot of the number of ion pairs formed versus the distance the particle has traveled is known as a Bragg plot.

Bremsstrahlung

When a high-speed charged particle, such as an electron, passes near an atomic nucleus, the particle is decelerated and the energy loss appears as a continuous X-ray spectrum known as bremsstrahlung (braking radiation). The energy range of bremsstrahlung extends from zero to the energy of the incident electron. The production of bremsstrahlung does not affect the absorber unless the absorber is susceptible to X-ray irradiation.

In the general case of electrons, bremsstrahlung is appreciable only at electron energies greater than 100 keV, and the percent of energy lost by an electron through bremsstrahlung increases as the energy of the electron increases. For 100 MeV electrons, approximately 50% of the energy is lost through bremsstrahlung. For electrons with energies greater than 150 MeV, most of the energy is lost by bremsstrahlung. Energy loss due to bremsstrahlung may be quantified:

$$-\left(\frac{dE}{dx}\right) = k \frac{z^2 Z^2}{m_e^2} \quad (17)$$

In Equation (17), z and m_e are the charge and mass of the electron, Z is the atomic number of the absorber nucleus, and k is a proportionality constant. Production of bremsstrahlung is the predominate interaction pathway for electrons with energies between 10 and 100 MeV [20].

For an electron with energy E in MeV, the ratio of energy loss by bremsstrahlung to energy loss by inelastic collision can be calculated [21].

$$\frac{(dE/dl)_{\text{brem}}}{(dE/dl)_{\text{coll}}} = \frac{EZ}{800} \quad (18)$$

In Equation (18), Z is the atomic charge of the absorber atom.

Gamma Radiolysis of Water

Radiation Chemistry Timescale

As previously stated, the main mode of interaction between gamma photons from Cobalt-60 and water is the Compton interaction, which results in the ejection of an orbital electron from a water molecule with average kinetic energy of 440 keV [22]. This fast electron ionizes and excites other absorber molecules before being degraded to thermal energy. The radiation chemistry timescale starts at the instant of bombardment of an absorber water molecule with a gamma photon, and ends with the re-establishment of chemical equilibrium in the solution. The overall timescale is divided into three stages, with different phenomena occurring within each stage. A complete overview of the three stages with pertinent reactions is shown in Figure 5 [23].

Physical stage

The physical stage of the radiation chemistry timescale occurs during the first 10^{-15} seconds or shorter. This stage is characterized by energy transfer to the medium through the Compton interaction, which results in the ejection of an orbital electron. This ejection may be represented by chemical reaction.



The ejected fast electron may travel a distance far enough to escape the Coulombic attraction of H_2O^+ and produce further ionization and excitation of water molecules. If the ejected electron does not escape the Coulombic attraction of H_2O^+ , the ejected electron and ionized water molecule recombine to produce an excited water molecule.

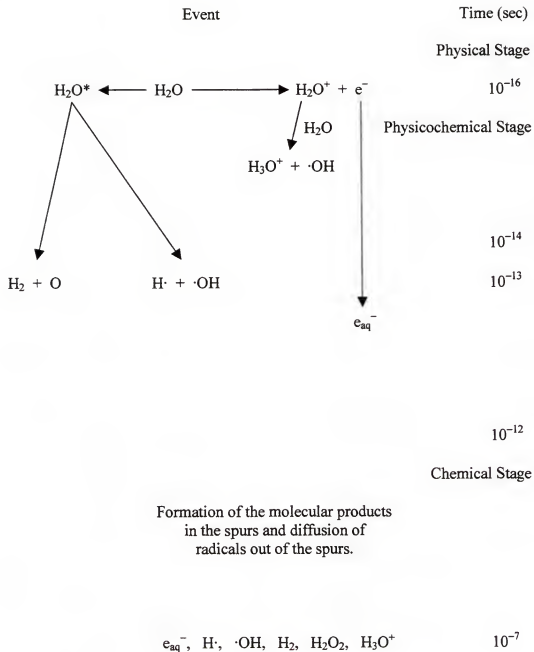


Figure 5: The radiation chemistry timescale showing the pertinent reactions that occur within each stage.



The excited water molecule would homolytically dissociate to produce two radicals.

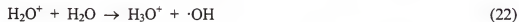


However, in a polar medium such as water, ejected electrons have a range of 5 nm [20], which is sufficient to escape the Coulombic attraction of H_2O^+ . Thus the contribution of the dissociation of H_2O^* to the production of radicals is negligible, although for nonpolar liquids the contribution of excited states to radical production must be considered.

Physicochemical stage

The physicochemical stage follows the physical stage and lasts approximately 10^{-11} seconds. Events that occur in this stage may be classified as processes that lead to the establishment of thermal equilibrium in the irradiated solution. The fast Compton electrons produce ionization and excitation in the absorbing medium. Since the average kinetic energy of a Compton electron is 440 keV [22], each Compton electron ionizes approximately 20,000 water molecules before being degraded to thermal energy and becoming hydrated to form e_{aq}^- , assuming that 25 eV are needed for each ionization.

In addition, H_2O^+ produced in Reaction (19) reacts with an unionized water molecule to produce hydronium ion, H_3O^+ , and hydroxyl radical, $\cdot\text{OH}$.



The species e_{aq}^- , $\cdot\text{OH}$ and H_3O^+ are produced in localized regions along the path of the incident gamma photon known as spurs. Regions in which spurs overlap are called blobs, and regions of high blob density are called tracks. The percentage of gamma photon energy deposited in spurs, blobs and tracks is dependent on the linear energy transfer, LET, of the radiation. The LET is a measure of the amount of energy

transferred to the medium per unit travel length of a particle. Fast electrons, such as Compton electrons, beta particles, X-rays and gamma photons are considered low LET species. High LET species include particles such as alpha particles, stripped nuclei and fission fragments. As the LET of the ionizing radiation increases, more energy is deposited in blobs and tracks, and less energy is deposited in spurs. In the case of Cobalt-60 gamma radiation in water, 64% of the energy is deposited in spurs, 11% in blobs and 25% is deposited in short tracks [24].

Chemical stage

The chemical stage begins after approximately 10^{-11} seconds in the spurs and 10^{-10} seconds in the bulk solution. This stage is characterized by radical-radical reactions inside the spurs and radical diffusion into the bulk solution, leading to the kinetic "steady-state" in *ca.* 10^{-7} seconds and ultimately to equilibrium. The species contained in the spur include the radical products e_{aq}^- , $\cdot OH$ and $H\cdot$, as well as H_3O^+ . These species may react with each other to produce the molecular products H_2 and H_2O_2 , or may diffuse into the bulk solution and react with solute. A complete description of the reactions that occur in the gamma radiolysis of water involves over forty reactions. Pertinent reactions and rate constants are listed in Table 1.

Radical Transients

G-values

After approximately 10^{-7} seconds from the time of the interaction with the ionizing species, the spur reactions are complete and the radical and molecular products have essentially diffused homogeneously throughout the solution. The primary yields of the highly-reactive radical transients e_{aq}^- , $H\cdot$ and $\cdot OH$, and the stable molecular products

Table 1: Typical reactions involved in the Cobalt-60 gamma radiolysis of water.

Reaction	k (M ⁻¹ s ⁻¹)	Reference	
$e_{aq}^- + e_{aq}^- \rightarrow H_2 + 2OH^-$	6.0×10^9	[25]	(23)
$e_{aq}^- + \cdot OH \rightarrow OH^-$	3.1×10^{10}	[26]	(24)
$e_{aq}^- + H^+ \rightarrow H\cdot$	2.4×10^{10}	[27]	(25)
$e_{aq}^- + HO_2^- \rightarrow \cdot OH + 2OH^-$	3.5×10^9	[28]	(26)
$e_{aq}^- + O^- \rightarrow 2OH^-$	2.2×10^{10}	[29]	(27)
$e_{aq}^- + H_2O_2 \rightarrow OH^- + \cdot OH$	1.2×10^{10}	[30]	(28)
$e_{aq}^- + O_2 \rightarrow O_2^{\cdot -}$	1.9×10^{10}	[31]	(29)
$e_{aq}^- + O_2^{\cdot -} \rightarrow O_2^{2-}$	1.3×10^{10}	[32]	(30)
$e_{aq}^- + H_2O \rightarrow H\cdot + OH^-$	1.9×10^1	[33]	(31)
$H\cdot + OH^- \rightarrow e_{aq}^-$	2.5×10^7	[34]	(32)
$H\cdot + H\cdot \rightarrow H_2$	5.0×10^9	[35]	(33)
$H\cdot + \cdot OH \rightarrow H_2O$	7.0×10^9	[36]	(34)
$H^+ + OH^- \rightarrow H_2O$	1.4×10^{11}	[37]	(35)
$H_2O \rightarrow H^+ + OH^-$	2.6×10^{-5}	[37]	(36)
$\cdot OH + H_2 \rightarrow H\cdot + H_2O$	3.4×10^7	[38]	(37)
$\cdot OH + H_2O_2 \rightarrow HO_2\cdot + H_2O$	2.7×10^7	[39]	(38)
$2HO_2\cdot \rightarrow H_2O_2 + O_2$	2.7×10^6	[33]	(39)
$O_2^{\cdot -} + HO_2\cdot \rightarrow HO_2^{\cdot -} + O_2$	4.4×10^7	[40]	(40)
$H\cdot + H_2O_2 \rightarrow \cdot OH + H_2O$	3.6×10^7	[41]	(41)
$HO_2\cdot + H\cdot \rightarrow H_2O_2$	2×10^{10}	[42]	(42)
$H\cdot + O_2 \rightarrow HO_2\cdot$	2.1×10^{10}	[33]	(43)

$O_2^- + H^+ \rightarrow HO_2\cdot$	5.0×10^{10}	[43]	(44)
$HO_2\cdot \rightarrow H^+ + O_2^-$	8×10^5	a	(45)
$H^+ + HO_2^- \rightarrow H_2O_2$	3×10^{10}	[44]	(46)
$H_2O_2 \rightarrow H^+ + HO_2^-$	3×10^{-2}	b	(47)
$H_2O_2 + OH^- \rightarrow HO_2^- + H_2O$	5.0×10^8	[26]	(48)
$HO_2^- + H_2O \rightarrow H_2O_2 + OH^-$	5.7×10^4	[26]	(49)
$\cdot OH + OH^- \rightarrow O^- + H_2O$	1.2×10^{10}	[45]	(50)
$O^- + H_2O \rightarrow \cdot OH + OH^-$	9.3×10^7	[40]	(51)
$\cdot OH + HO_2^- \rightarrow OH^- + HO_2\cdot$	6.8×10^9	[46]	(52)
$H\cdot + H_2O \rightarrow H_2 + \cdot OH$	1×10^1	[33]	(53)
$\cdot OH + O^- \rightarrow HO_2^-$	2×10^{10}	[47]	(54)
$\cdot OH + O_2^- \rightarrow OH^- + O_2$	1.0×10^{10}	[48]	(55)
$O^- + H_2 \rightarrow H\cdot + OH^-$	1.0×10^8	[49]	(56)
$O^- + H_2O_2 \rightarrow O_2^- + H_2O$	5×10^8	[33]	(57)
$O^- + HO_2^- \rightarrow O_2^- + OH^-$	4×10^8	[33]	(58)
$O^- + O_2 \rightarrow O_3^-$	3.5×10^9	[50]	(59)
$O^- + O_2^- + H_2O \rightarrow 2OH^- + O_2$	6.0×10^8	[51]	(60)

- a. Calculated to give $pK_a(HO_2\cdot) = 4.8$ with respect to Reaction (44).
b. Calculated to give $pK_a(H_2O_2) = 11.8$ with respect to Reaction (46).

H_2 , H_2O_2 and H_3O^+ are described using G-values. G-values are defined as the number of molecules either destroyed or produced per 100 eV of energy absorbed by the system and are written as $G(x)$ in which x is the species in question. The G-values for the gamma radiolysis of liquid water are constant over a wide range of conditions, including pH (between *ca.* 3 and 11) and temperature. The G-values, in units of molecules per 100 eV, as given by Draganic are as follows: e_{aq}^- , 2.63; $\cdot\text{OH}$, 2.72; $\text{H}\cdot$, 0.55; H_3O^+ , 2.63; H_2 , 0.45; H_2O_2 , 0.68; and $\text{HO}_2\cdot$, 0.026 [22].

Reducing agents (e_{aq}^- , $\text{H}\cdot$)

The hydrated electron is a powerful reducing agent with a reduction potential of 2.87 V [52] (for the reaction $e_{\text{aq}}^- + \text{H}^+ \rightarrow \frac{1}{2} \text{H}_2$) whereas the hydrogen atom is a moderate reducing agent with a reduction potential of 2.31 V [53]. The type of reaction that e_{aq}^- undergoes with organic molecules depends on the state of saturation of the molecule. Organic molecules with sites of unsaturation react quickly with e_{aq}^- , with e_{aq}^- adding to double or triple bonds. The reactivity of e_{aq}^- with the site of unsaturation is increased by the presence of electron withdrawing groups attached to the double or triple bond. With saturated organic molecules, e_{aq}^- reacts several orders of magnitude slower, unless the organic molecule has an electronegative group such as a halogen attached. In this case, e_{aq}^- reacts by an electron capture mechanism giving either non-dissociative or dissociative electron capture, forming RX^- or $\text{R}\cdot + \text{X}^-$, respectively.

The hydrogen atom reacts with saturated organic molecules by abstracting $\text{H}\cdot$ to produce H_2 , and with unsaturated organic molecules by adding to the site of unsaturation. In highly acidic solutions ($\text{pH} < 3$), e_{aq}^- reacts with H^+ to produce $\text{H}\cdot$.



Thus, in a highly acidic solution, each e_{aq}^- is converted into a H^\cdot , which is a slightly weaker reducing agent. This change in reducing agent may lead to alternative product formation.

The hydrated electron has a characteristic UV-VIS absorbance centered at 715 nm with a molar absorptivity coefficient of $18,000 \text{ M}^{-1}\text{cm}^{-1}$ [37]. This large coefficient dictates the experimental method that is usually employed to study the kinetics of electron reactions. In practice, it is convenient to follow spectrophotometrically the disappearance of e_{aq}^- in order to ascertain kinetic data. In contrast, H^\cdot exhibits negligible absorption in the UV-VIS spectrum, so the buildup of absorbance of product is usually monitored for kinetic experiments involving H^\cdot reactions.

Many reactions between e_{aq}^- and organic solutes have rate constants that are near the diffusion-controlled limit, whereas rate constants for reactions of H^\cdot are usually two or three orders of magnitude less. In slightly acidic ($\text{pH} > 3$), neutral or basic solutions, the G-value for formation of e_{aq}^- is four times as large as the G-value for formation of H^\cdot . Therefore, e_{aq}^- is considered to be the main reducing species in irradiated solution, and any contribution to the reducing character made by H^\cdot is relatively small and usually ignored.

Oxidizing agents ($\cdot\text{OH}$ and H_2O_2)

The hydroxyl radical is a powerful oxidizing agent with a reduction potential of 1.9 V in basic solution [54] (for the reaction $\cdot\text{OH} + e_{aq}^- \rightarrow \text{OH}^-$), and 2.7 V in acidic solution [55] (for the reaction $\cdot\text{OH} + \text{H}^+ + e_{aq}^- \rightarrow \text{H}_2\text{O}$). The hydroxyl radical reacts with saturated organic compounds by hydrogen atom abstraction and with unsaturated organic compounds by addition to the site of unsaturation.

The hydroxyl radical is unaffected by extremely acidic conditions. However, in extremely basic solutions ($\text{pH} > 11$), $\cdot\text{OH}$ may be deprotonated to form O^- , which tends to react with solutes in a different manner to lead to alternative products.



The hydroxyl radical has an absorption centered at 230 nm with a molar absorptivity coefficient of $530 \text{ M}^{-1}\text{cm}^{-1}$ [56]; however, in the higher UV or visible portion of the spectrum $\cdot\text{OH}$ absorbs negligibly. Therefore, it is not practical to follow spectrophotometrically the decay of $\cdot\text{OH}$ for kinetic studies unless a specially selected analytical light source with strong intensity in the lower UV region is available. In practice, it is common to follow the buildup absorbance of the $\cdot\text{OH}$ adduct for data analysis.

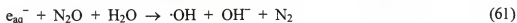
Rate constants of $\cdot\text{OH}$ with organic solutes are very large, with many approaching the diffusion-controlled limit. Since the other oxidizing species produced in the solution, H_2O_2 , is nearly chemically inert with most organics, $\cdot\text{OH}$ is considered to be the main oxidizer in deaerated aqueous solution.

System Modifications (Oxidizing Versus Reducing)

Due to the magnitudes of $G(e_{\text{aq}}^-)$ and $G(\cdot\text{OH})$, an irradiated aqueous solution has approximately equal amounts of reducing agent and oxidizing agent. However, at times it is necessary to study systems that are entirely oxidizing or entirely reducing in character. This goal can be accomplished by system modifications.

Entirely oxidizing solution

To convert a radiolytically treated solution into a solution of oxidizing-only character, the solution is saturated with nitrous oxide gas, N_2O . The hydrated electron reacts with N_2O with a rate constant of $9.1 \times 10^9 \text{ M}^{-1} \text{ s}^{-1}$ [57].



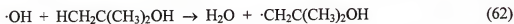
Since $G(e_{aq}^-)$ and $G(\cdot OH)$ are almost equal, the reaction of N_2O in saturated solution (ca. 0.024 M [20]) with e_{aq}^- nearly doubles the $\cdot OH$ concentration; however, there is a small correction due to interference in spur processes. As recommended by Buxton et al., when the product of the scavenger rate constant and concentration, $k[\text{scavenger}]$, is less than 10^7 s^{-1} , the primary yields are equal to those of pure water. When the product $k[\text{scavenger}]$ is greater than 10^7 s^{-1} , the primary yields can increase by 0.3 to 0.5 G-units for each 10-fold increase in the value of the product $k[\text{scavenger}]$ over 10^7 s^{-1} [33]. Accordingly, Schuler and coworkers give $G(\cdot OH)$ in N_2O -saturated solution as 6.0 molecules per 100 eV [58].

Reaction (61) eliminates the presence of e_{aq}^- , but does nothing to remove the other reducing species in solution, $H\cdot$. However, as mentioned previously, hydrogen atom rate constants are two or three orders of magnitude smaller than $\cdot OH$ or e_{aq}^- rate constants, and $G(H\cdot)$ is four times smaller than $G(\cdot OH)$ or $G(e_{aq}^-)$. For these reasons, any reducing contribution from $H\cdot$ is usually ignored and the N_2O -treated solution is considered entirely oxidizing in character.

Entirely reducing solution

The principle method utilized to eliminate the oxidizing capability of $\cdot OH$ is to convert $\cdot OH$, an extremely reactive oxidizing radical, into a much less reactive radical.

Aliphatic alcohols such as t-butanol are routinely used for this purpose. The $\cdot\text{OH}$ reacts with 0.1 M t-butanol completely, with a rate constant of $7.55 \times 10^8 \text{ M}^{-1}\text{s}^{-1}$ [59].



The product t-butoxy radical is unreactive in comparison to $\cdot\text{OH}$. As required, e_{aq}^- is unreactive with t-butanol. Therefore, the oxidizing capability of the solution has been greatly reduced and reactions of e_{aq}^- can be studied without interference from $\cdot\text{OH}$.

Indirect Effect

When a mixture of components is irradiated, each component absorbs radiation in proportion to its electron fraction in the mixture. If one component is minute in electron fraction in comparison to the others, as is the case in dilute aqueous solutions, then all radiation is absorbed through interactions with the solvent and none through interactions with the solute. As a rule, solutes in near-neutral pH solutions at concentrations of 0.1 M or less absorb negligible amounts of radiation [60]. Thus, in 10 mM aqueous solutions such as those studied in this work, all changes to the solute are brought about by reaction of the solute with the aforementioned radical transients produced from the solvent. Any direct action of the radiation on the solute may be ignored.

CHAPTER 3 DOSIMETRY AND THE FRICKE DOSIMETER

General Background

Definition and Common Units

Dose

The field of dosimetry is concerned with the determination of absorbed dose, which is defined as the amount of absorbed energy available to initiate chemical reactions and produce change in the substrate [17]. The SI unit of absorbed dose is the Gray, Gy, which is equal to the absorption of 1 Joule per kg of substrate. Older units, still in common use, include the rad and eV per g, or eV per mL if solution density is taken into account. These three dose units may be interconverted by noting that one rad is equal to 0.01 Gy or 6.241×10^{13} eV per g. Another radiation chemistry term that is commonly encountered is dose rate, DR. Dose rate is simply the absorbed dose, D, divided by the time, t, over which the dose is absorbed.

$$DR = \frac{D}{t} \quad (63)$$

In radiation chemistry, the term dose always refers to the absorbed dose and not dose rate.

Radiation exposure

Radiation exposure is based on the ionization of air [17]. Historically, this quantity was given in terms of the roentgen, R, which was defined as the amount of

radiation exposure that produced 2.58×10^{-4} Coulombs per kg or 1.62×10^{15} ion pairs per kg of dry air. By definition, exposure in roentgens can only be applied to photon radiation and not to charged particle radiation.

Equivalent dose

The equivalent dose, H, is the radiation unit used for biological monitoring [61]. This unit is calculated by multiplying the absorbed dose (in rads) by a quality factor, Q, that takes into account the relative damage produced by equivalent doses of different types of internal radiation. The common and SI units of equivalent dose are the roentgen equivalent mammal, rem, and the Sievert, Sv, respectively. Typical quality factors include 1 for gamma rays, 10 for fast neutrons, and 20 for alpha particles.

Primary Versus Secondary Dosimeters

Dosimeters, systems used to determine absorbed dose, may be classified as either primary or secondary [62]. Primary dosimeters provide a direct measure of the exposure or absorbed dose from physical measurements. Two common types of primary dosimeters include calorimetric dosimeters and gas ionization chambers. Secondary dosimeters, although much easier to use on a daily basis, must initially be calibrated using a primary dosimeter. The most common types of secondary dosimeters are chemical dosimeters though other types such as film dosimeters and thermoluminescent dosimeters do exist.

Primary dosimetry

In calorimetry, the temperature of an object that is placed in the radiation beam is monitored, and the increase in temperature yields the absorbed dose. In this method, it is essential that all absorbed radiation results in raising the temperature of the object, and not in initiating chemical reactions inside the object. In addition, good thermal

conductivity is necessary. For these reasons, blocks of graphite or metals are commonly used as calorimetry objects; however, the unit temperature change is very small for graphite or metal when using low-intensity radiation such as X-ray or gamma sources. For water, the change in temperature with absorbed dose is even smaller. Radak and Markovic report a change in water temperature of $2.39 \times 10^{-4} \text{ }^{\circ}\text{C}$ per Gy [63]. Due to this small temperature change, calorimetry is practical only for large doses.

Primary dosimeters of the ionization chamber type consist of a chamber that is filled with an ionizable gas. The chamber contains two electrodes across which a voltage is applied. When an ionizing photon or particle enters the chamber and ionizes the gas, all the ions produced by the radiation are collected at the electrodes. The collection of the ions directly yields exposure. It is then necessary to convert exposure to absorbed dose. Two types of ionization chambers that are commonly used include the Standard Free-Air chamber, and the Thimble Ionization chamber [20].

Secondary dosimetry

Secondary dosimeters are more suitable than primary dosimeters for routine measurements and are cheaper to maintain as well as simpler to operate. One central tenet of radiation dosimetry is that it is always desirable to use a dosimeter that mimics the system that is going to be irradiated; chemical dosimetry systems can easily be varied in order to model many different systems. In chemical dosimetry, the absorbed dose is calculated based on the chemical change that the radiation has produced in the substrate. This requires that the radiation change in the substrate be calibrated at some point using a primary dosimeter [62].

When choosing a chemical dosimeter, many qualifications are desirable for the ideal dosimeter to possess [16]:

1. The response of the dosimeter should be linear over a wide range of absorbed dose and be independent of the dose rate.
2. The response of the dosimeter should be independent of the linear energy transfer, LET, and energy of the radiation.
3. The response of the dosimeter should be independent of temperature fluctuations and be stable to normal lab conditions (light and air).
4. The response of the dosimeter should not vary with small changes in dosimeter composition.
5. The dosimeter should be easy to prepare from common laboratory reagents.

Fricke Dosimetry

Introduction

Although no single chemical dosimeter meets all of these criteria, one dosimeter that approaches ideality is the Fricke dosimeter, which was originally proposed by H. Fricke in 1927 as a dosimeter for aqueous X-ray systems [64]. In practice, however, the Fricke dosimeter is frequently used not only for aqueous solutions, but also for organic liquids, gases, or even solids, due to the convenience and reliability of the Fricke system. The standard Fricke dosimeter consists of 1 mM ferrous ion, Fe^{2+} , in an air-saturated, aqueous solution of 0.4 M H_2SO_4 . Fricke solutions are generally prepared both with and without 1 mM NaCl. The presence of NaCl serves as a diagnostic test for water impurities; in the presence of numerous impurities, different yields of Fe^{3+} are found in the presence and absence of NaCl. The central theme of Fricke dosimetry is the radiolytic conversion of ferrous ion, Fe^{2+} , to ferric ion, Fe^{3+} , the absorbance of which is measured via UV-VIS spectrophotometry. The dose rate, DR, is then determined through

suitable calculation. The procedure followed during a Fricke experiment and the calculations performed are thoroughly explained later in this chapter.

Fricke Chemical Reactions

The chemical reactions involved in the Fricke dosimeter are numerous, but the main reactions and rate constants are shown in Table 2.

Table 2: Main reactions in the Fricke dosimeter.

Reaction	k (M ⁻¹ s ⁻¹)	Reference	
$\text{Fe}^{2+} + \cdot\text{OH} \rightarrow \text{Fe}^{3+} + \text{OH}^-$	2.3×10^8	[65]	(64)
$e_{\text{aq}}^- + \text{H}^+ \rightarrow \text{H}\cdot$	2.3×10^{10}	[66]	(25)
$\text{H}\cdot + \text{O}_2 \rightarrow \text{HO}_2\cdot$	2.1×10^{10}	[67]	(43)
$\text{HO}_2\cdot + \text{Fe}^{2+} \rightarrow \text{Fe}^{3+} + \text{HO}_2^-$	2×10^6	[44]	(65)
$\text{HO}_2^- + \text{H}^+ \rightarrow \text{H}_2\text{O}_2$	3×10^{10}	[44]	(46)
$\text{H}_2\text{O}_2 + \text{Fe}^{2+} \rightarrow \text{Fe}^{3+} + \cdot\text{OH} + \text{OH}^-$	56	[44]	(66)

If these main reactions are multiplied by correct stoichiometric coefficients and summed with pertinent reactions arising from the radiolysis of water as listed in Table 1, the net chemical reaction that occurs in Fricke dosimetry can be determined [65]:



Several of the main reactions deserve note. Of these, Reaction (25) is of particular interest. Because the solution is 0.4 M in sulfuric acid, e_{aq}^- reacts with protons to produce $\text{H}\cdot$, which then react with oxygen to produce hydroperoxyl radicals, $\text{HO}_2\cdot$. Due to the scavenging of hydrated electrons by protons, the possibility of reduction of Fe^{3+} by e_{aq}^- to reform Fe^{2+} is eliminated. This is similar to the system modification described in Chapter 2, in which t-BuOH is used to convert a solution of equal oxidizing and reducing character into a solution of reducing-only character.

Reaction (66) is also of interest. As can be seen from the rate constants, most of the reactions are very fast, with several approaching the diffusion-controlled limit. However, Reaction (66) is not complete until several half-lives have passed (*ca.* 15 minutes). This slow reaction alters the experimental procedure that is followed when Fricke dosimetry is performed; the implications of this slow reaction are discussed later in this chapter.

Effects of Dissolved Substrates

Dissolved oxygen

Since these reactions consume oxygen as evidenced in the net reaction, the largest dose that can be measured accurately in an air-saturated solution (oxygen concentration *ca.* 0.025 M [14]) is approximately 500 Gy. In practice, samples are exposed for lengths of time such that the absorbed dose in air-saturated solutions is kept between 10 and 350 Gy. Moreover, when all oxygen is consumed, the value of $G(\text{Fe}^{3+})$ falls from 15.6 to approximately 8.2. The practical dose range can be extended by a factor of four or five to approximately 2000 Gy if the solution is saturated with oxygen (*ca.* 0.126 M [68]). If this extended dose range is desired, the standard solutions are prepared with Fe^{2+} concentrations between 20 and 50 mM instead of 1 mM Fe^{2+} [69].

Dissolved impurities

When an impurity such as an organic molecule is present, $\cdot\text{OH}$ will either add to the organic molecule, if it is unsaturated, or abstract a hydrogen atom from the molecule, if it is saturated, thus resulting in an organic radical [70]. Oxygen, if present, will then add to the organic radical to produce an organic peroxy radical. This peroxy radical can then undergo a chain reaction mechanism with Fe^{2+} to produce numerous Fe^{3+} ions. The

net result of the chain reaction is an overall increase in the G-value of Fe^{3+} . In contrast, if no oxygen is present, the organic impurity acts as an $\cdot\text{OH}$ scavenger thus lowering the value of $G(\text{Fe}^{3+})$. For these reasons, it is imperative that the presence of impurities be detectable.

The use of Fricke solutions prepared both with and without NaCl makes this detection possible. Chloride ion, Cl^- , masks the presence of impurities that can react with $\cdot\text{OH}$ by first reacting with $\cdot\text{OH}$ itself to produce the chlorine radical, $\text{Cl}\cdot$, with a rate constant of $4.3 \times 10^9 \text{ M}^{-1} \text{ s}^{-1}$ [71].



Due to the high concentration of Cl^- relative to the concentrations of impurities and the magnitude of the $\cdot\text{OH}/\text{Cl}^-$ rate constant, the reactivity of $\cdot\text{OH}$ with Cl^- is much greater than the reactivity of $\cdot\text{OH}$ with any impurities. Once formed, $\text{Cl}\cdot$ reacts with Fe^{2+} to produce Fe^{3+} with a rate constant of $1.3 \times 10^{10} \text{ M}^{-1} \text{ s}^{-1}$ [72].



The overall effect of the presence of Cl^- is the conversion of all $\cdot\text{OH}$ to $\text{Cl}\cdot$, which then reacts preferentially with Fe^{2+} instead of impurities due to greater reactivity. Thus the value of $G(\text{Fe}^{3+})$ is unchanged even though the water is contaminated with impurities.

Fricke Considerations

The lowest dose that can be measured using Fricke dosimetry is governed by the sensitivity of the analytical method used to quantify the concentration of ferric ion, Fe^{3+} . Since the absorbance of Fe^{3+} is usually measured spectrophotometrically, the lowest dose that leads to observable Fe^{3+} concentrations is approximately 3 to 5 Gy, assuming a

cuvette path length of 1 cm. A dose of this magnitude leads to an absorbance value on the order of 0.01, which can be determined within accuracy limits on modern spectrophotometers.

For low linear energy transfer, LET, radiation such as X-rays and gamma photons, $G(\text{Fe}^{3+})$ is independent of Fe^{2+} concentrations between 0.1 and 50 mM and independent of H_2SO_4 concentrations between 0.05 and 2.5 M. Temperature variations between 4 and 70°C also have no effect on $G(\text{Fe}^{3+})$. In addition, differing sample volumes from 2 to 470 mL have no effect on the observed dose rate. Lastly, $G(\text{Fe}^{3+})$ has no dependency on gamma energy for energies between 0.03 and 30 MeV [70]. The major disadvantage of the Fricke dosimeter is the rather narrow dose range that can be determined using the system. However, as can be seen from all the advantages listed above, it is no wonder that the Fricke dosimeter is the dosimeter of choice for aqueous systems.

Application of Fricke Dosimetry

In the course of this project, Fricke dosimetry was employed to determine the dose rate for three different fixed sample geometries. For each of the three geometries, equivalent Fricke solutions were prepared. Aliquots of these solutions were then placed into the Cobalt-60 gamma irradiator for specified times.

Description of the Cobalt-60 Gamma Irradiator

All Fricke irradiations were carried out at room temperature ($25 \pm 2^\circ\text{C}$) using a Wisconsin-type Cobalt-60 gamma irradiator that has been described in detail [73]. A cross-section of the irradiator with pertinent parts listed is shown in Figure 6. The

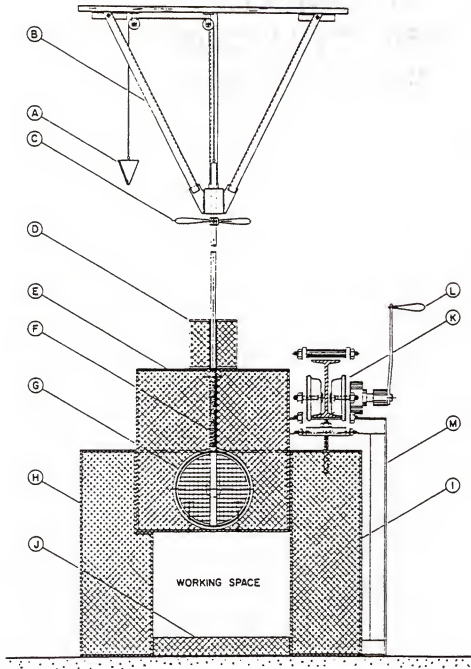


Figure 6: Cross-section of the Cobalt-60 gamma irradiator.

(A) counterweight, (B) upper support, (C) source rod handle, (D) extra top shielding, (E) storage turret, (F) 600 Curie Co-60 source, (G) shutter (shown open), (H) rear wall, (I) door, (J) downward shielding, (K) door carriage, (L) door crank and (M) door frame.

radioactive source consists of Cobalt-60 pellets that have been encapsulated in a cylinder made of type 316 stainless-steel. The dimensions of the cylinder are 1.40 inches (outer height) \times 0.445 inches (outer diameter). The wall thickness of the cylinder is 0.025 inches. The cylinder has been sealed into the end of a predrilled stainless-steel rod of dimensions 11 inches (length) \times 0.625 inches (diameter). Due to this design, the radioactive source is double-encapsulated for maximum safety. The double stainless-steel casing is also important because it effectively absorbs the beta radiation emitted during the decay of Cobalt-60. The stainless-steel rod/cylinder assembly is threaded onto the end of a vertical rod to form the control rod. The control rod is lowered to the sample position or raised to the storage position in order to begin or discontinue sample irradiations, respectively. When the source rod is in the storage (upper) position, the shutter mechanism (label G in Figure 6) is closed (rotated 90° from the orientation shown in Figure 6). Closing the shutter mechanism prevents the source rod from falling into the irradiation chamber and exposing the worker while the irradiator door is open. The irradiator is constructed such that the source rod must be in the storage (upper) position and the shutter must be closed before the irradiator door can be opened for sample insertion and removal.

The working volume of the irradiator measures 18 inches (depth) \times 16 inches (width) \times 15 inches (height), which provides ample room for large samples to be irradiated. In addition, the irradiator has inlet and outlet holes in the housing that allow for the connection of tubing for constant temperature experiments, although these were not used in this work. Each wall of the irradiator is constructed of steel plating welded together to form an empty cavity that is filled with lead. The lead acts as shielding to

protect the user from being exposed to a substantial dose during insertion and removal of samples. When a new source rod is installed (when the irradiator is recharged), the intensity of the source is equal to 600 Curies, which allows for large doses (on the radio-chemistry scale) to be administered in reasonable irradiation times.

Description of Different Sample Geometries

The phrase “sample geometry” is used to describe the choice and physical arrangement of sample cells, the sample cell holder, and the plate on which the sample holder rests inside the irradiator. Three different sample geometries (geometries A, B and C) were employed in the course of this work. The Cobalt-60 irradiator was recharged (a new source rod installed) in April, 1999. Geometries A and B were used with the old source (pre-April, 1999) for experiments to determine initial product identities and yields, and geometry C was used with the new source (post-April, 1999) to study the complete degradation of benzene, which results in the production of CO₂.

Sample geometry A

The first sample geometry for which Fricke dosimetry was employed consisted of a “wagon-wheel” type sample holder, which was affixed to a flat aluminum plate using duct tape. The flat aluminum plate was placed securely on a board that helped facilitate sliding the sample holder into and out of the irradiator. A side view of the sample holder is shown in Figure 7. The sample holder consists of three round, horizontal plates separated by vertical spacers (measurements given on Figure 7). The top two horizontal plates have matching holes drilled at a constant radial distance around the center source hole at three different radii: inner, middle, and outer source positions. The relative arrangement of source and sample holes is shown on Figure 8. This holder was milled specifically for use with 13 mm (outer diameter) × 100 mm (height) borosilicate test

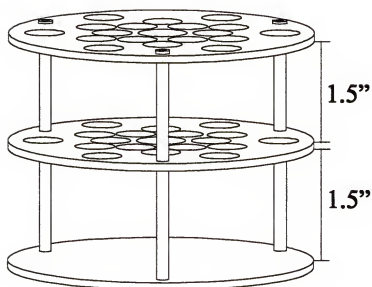


Figure 7: A side view of the wagon-wheel sample holder used in geometry A showing the spacing between plates.

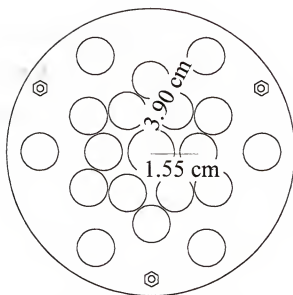


Figure 8: Top view of the wagon-wheel sample holder used in geometry A showing the relative distances from the source hole to the inner and outer sample holes.

tubes (Pyrex, model 9800) as sample cells. This sample geometry was used for preliminary experiments that were performed before the recharging of the irradiator (pre-April, 1999).

Sample geometry B

The second sample geometry, geometry B, consisted of a solid-block aluminum sample holder affixed to a solid aluminum plate using brackets. A top view of this geometry is shown in Figure 9. As with the wagon-wheel holder, the source rod slides into the center hole and two series of sample holes are drilled at equal radial increments around the source hole. In this sample holder, the source rod rests several millimeters below the bottoms of the sample cells during irradiation. The relationship between the bottoms of the sample cells and source rod is shown in Figure 10. This is in contrast to the wagon-wheel sample holder used for geometry A, in which the bottoms of the source rod and sample cells were at the same level during irradiation. This sample holder was milled specifically for use with screw top vials (National Scientific, model B7990-3) as sample cells instead of test tubes. This sample geometry was used with the old source (pre-April, 1999).

Sample geometry C

The third sample geometry used for Fricke dosimetry consisted of the same aluminum block sample holder with inner and outer positions and aluminum plate that were used in geometry B, and two other sample positions located inside the irradiator. Figure 11 illustrates these positions, four positions in total, as well as source to sample distances: 2.00 cm, 4.00 cm, 6.50 cm and 20.0 cm. This sample geometry was used after the irradiator was recharged with a new source (post-April, 1999).

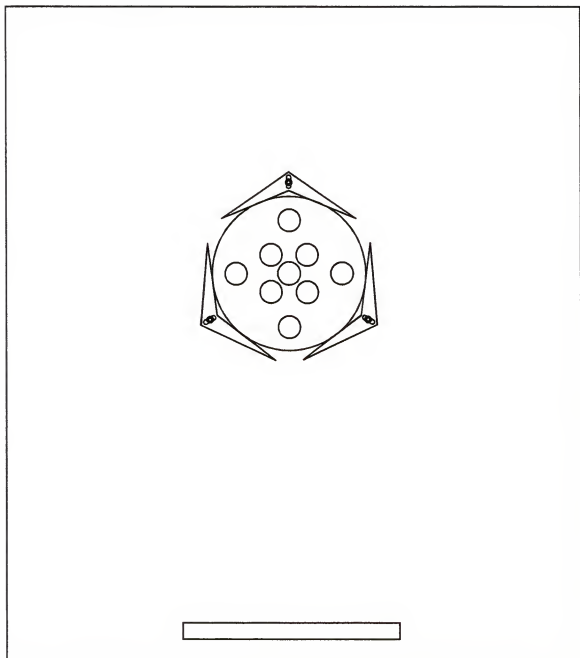


Figure 9: Top view of the solid aluminum sample holder resting on the solid aluminum plate. The holder is affixed using brackets. A handle is present on the bottom of the plate to aid in insertion and removal.

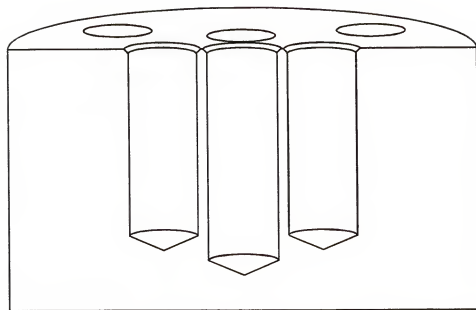


Figure 10: Cutaway view of the solid-block aluminum sample holder showing the relative positions of the bottoms of the sample cells and the source rod.

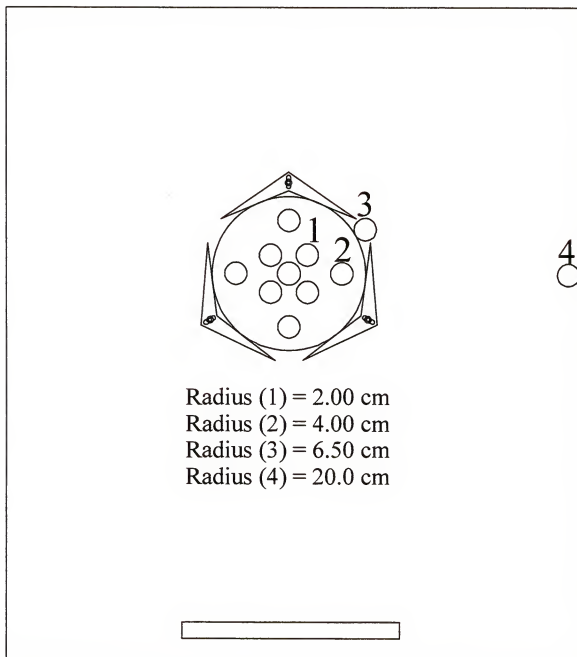


Figure 11: Top view of the solid-block aluminum sample holder used in geometry C showing the four sample positions and the source to sample distances used for total irradiator calibration.

Description of Experiment

Preparation of Fricke solutions

When using any chemical dosimeter it is imperative that the water be exhaustively purified. Commonly, laboratory deionized water is distilled from basic permanganate solution. This process yields so-called doubly-distilled water. Recently, however, filtration assemblies consisting of deionizing and carbon filtration beds, such as the MilliQue (MQ) system (MilliPore Systems, Bedford, Massachusetts), have been replacing distillation as the method of choice for water purification for radiation chemistry purposes. Precautions must also be taken to ensure that all glassware is similarly clean. One cleaning method that works well is the soaking of glassware in a solution of 50% concentrated nitric acid / 50% concentrated sulfuric acid for a minimum of 24 hours. The glassware is then rinsed well with doubly-distilled or MQ water.

Standard Fricke solutions of approximately 1 mM Fe^{2+} were prepared using $\text{FeSO}_4 \cdot 4\text{H}_2\text{O}$ (Fisher, ACS grade) in 0.4 M H_2SO_4 (Fisher, ACS grade) following the procedure of Weiss and Stein [74]. Solutions were prepared both with and without 1 mM NaCl (Mallinckrodt, analytical grade) and are called salted and saltless solutions, respectively. In practice, a large volume of the saltless solution (usually 1 L) was prepared. A mass of NaCl was added to a flask of smaller volume, and the saltless solution was used to prepare the salted solution by dissolving the pre-weighed solid (NaCl) to the final volume (usually 500 mL). This method ensured that the saltless and salted solutions were identical in all aspects save the presence of salt. All solutions were prepared using either doubly-distilled or MQ water and freshly cleaned, acid-soaked flasks. Once one of the three sample geometries (A, B or C) had been chosen for experimentation, 5.000 mL aliquots of Fricke solution were pipetted into acid-soaked

sample cells. Sample cells containing either salted or saltless Fricke solution were irradiated (one cell at a time) using the desired sample position within the irradiator.

Measurement of absorbances

After all cells had been irradiated, the absorbance of the solution in each cell was determined at 305 nm using a Beckman DU spectrophotometer equipped with Gilford electronics. This procedure (irradiating all tubes before measuring) was followed to allow the slow reaction between Fe^{2+} and H_2O_2 (Reaction (66)) to reach completion before measurement. All absorbance measurements were made using quartz cuvettes with pathlengths of 1 cm, with the respective unirradiated saltless or salted solution used as the blank.

Data workup

For each Fricke experiment, a plot of absorbance versus time of irradiation (in minutes) was prepared for each sample position for both the saltless and salted solutions. These plots are known as Fricke plots. A representative plot for geometry A is shown in Figure 12, and a representative plot for geometry B is shown in Figure 13. Lastly, representative plots using each sample position from geometry C are shown in Figure 14- Figure 17. The slope of each plot, m , a literature $G(\text{Fe}^{3+})$ of 15.6 [75], and a literature molar absorptivity, ϵ , of $2205 \text{ M}^{-1}\text{cm}^{-1}$ [75] were used to calculate the dose rate, DR, for each sample position for each solution.

The calculations used to determine the dose rate, DR, begin with Beer's Law:

$$A = \epsilon bc \quad (70)$$

In this equation, A is the blank corrected absorbance, ϵ is the molar absorptivity, b is the path length and c is the molar concentration. Each side of this equation is divided by

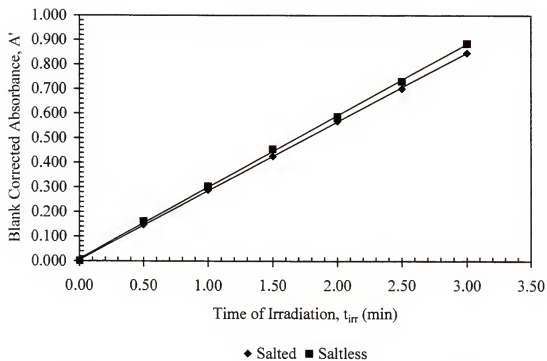
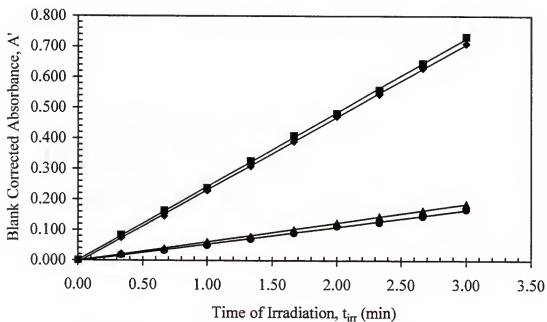


Figure 12: Fricke plot for the inner sample position using geometry A. This experiment was performed on 10/93 and resulted in a dose rate of 7023.2 rad/min.



◆ Inner Hole Salted ■ Inner Hole Saltless ● Outer Hole Salted ▲ Outer Hole Saltless

Figure 13: Fricke plot for the inner and outer sample positions using geometry B. This experiment was performed on 4/94 and resulted in a dose rate of 5782.2 rad/min for the inner sample position, and 1421.1 rad/min for the outer sample position.

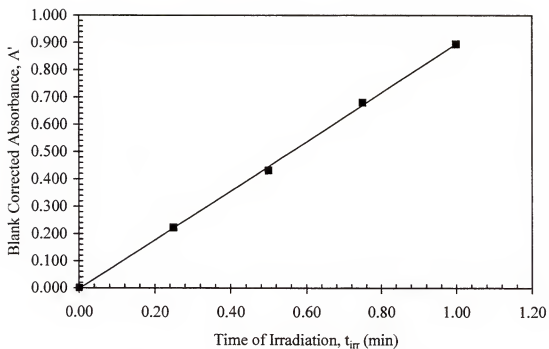


Figure 14: Fricke plot for sample position 1 using geometry C. This experiment was performed on 5/99 and resulted in a dose rate of 24591 rad/min.

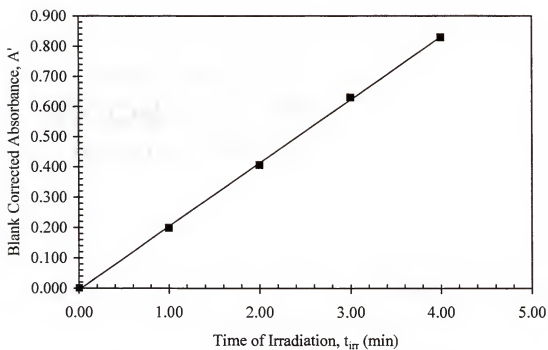


Figure 15: Fricke plot for sample position 2 using geometry C. This experiment was performed on 5/99 and resulted in a dose rate of 5721.2 rad/min.

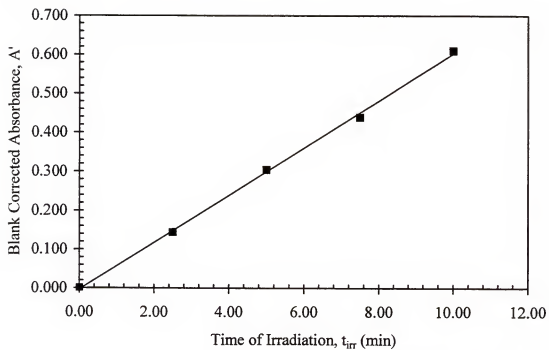


Figure 16: Fricke plot for sample position 3 using geometry C. This experiment was performed on 5/99 and resulted in a dose rate of 1660.0 rad/min.

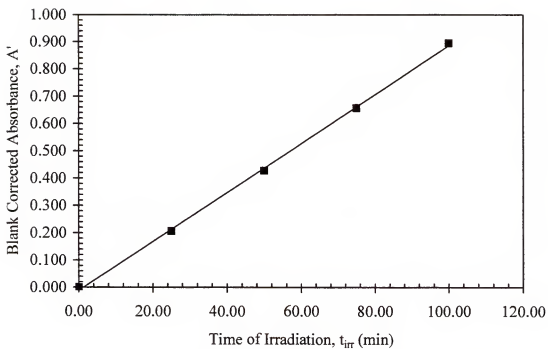


Figure 17: Fricke plot for sample position 4 using geometry C. This experiment was performed on 5.99 and resulted in a dose rate of 245.48 rad/min.

time, t , in minutes. The quantity A/t is equal to the slope of the plot of absorbance versus time of irradiation – the Fricke plot.

$$\frac{A}{t} = \epsilon b \frac{c}{t} = m \quad (71)$$

This equation was solved for the quantity c/t . The rationale for this manipulation is the isolation of c/t on one side of the equation. This rearrangement is desirable since c/t is the change in concentration of Fe^{3+} over time, which can be converted to the change in the number of molecules of Fe^{3+} over time by using Avogadro's number. Lastly, the value of $G(\text{Fe}^{3+})$ can be used to determine the dose rate, DR. This calculation can most easily be understood by examining the units of c/t , which are $\text{mol}/(\text{L} \cdot \text{min})$, and working towards the units of the desired dose rate, $\text{eV}/(\text{mL} \cdot \text{min})$:

$$\left(\frac{\text{mol}}{\text{L min}} \right) \left(\frac{1 \text{ L}}{1000 \text{ mL}} \right) \left(\frac{6.02 \times 10^{23} \text{ molecules}}{\text{mol}} \right) \left(\frac{100 \text{ eV}}{15.6 \text{ molecules}} \right) = \frac{\text{eV}}{\text{mL min}} \quad (72)$$

Substitution of symbols for each unit conversion factor leads to the following equation for dose rate:

$$\text{DR} = \frac{m N_A}{156 \epsilon b} \quad (73)$$

In this equation, m is the slope of the Fricke plot in units of min^{-1} , N_A is Avogadro's number, ϵ is the molar absorptivity coefficient in $\text{L}/(\text{mol} \cdot \text{cm})$, and b is the path length in cm. The quantity 156 arises from the 1000, 100, and 15.6 factors in Equation (72). Equation (73) yields the dose rate in units of $\text{eV}/(\text{mL} \cdot \text{min})$. The dose rate may be converted to rads per minute or Gray's per minute through the use of the appropriate factors:

$$\left(\frac{\text{eV}}{\text{mL min}} \right) \left(\frac{1 \text{ rad}}{6.241 \times 10^{13} \frac{\text{eV}}{\text{g}}} \right) \left(\frac{1 \text{ mL}}{1.024 \text{ g}} \right) = \frac{\text{rad}}{\text{min}} \quad (74)$$

$$\left(\frac{\text{rad}}{\text{min}} \right) \left(\frac{1 \text{ Gy}}{100 \text{ rad}} \right) = \frac{\text{Gy}}{\text{min}} \quad (75)$$

In Equation (74), use is made of the density of 0.4 M H₂SO₄ solution, 1.024 g/mL.

This calculation was repeated for each sample position for each solution (salted and saltless). Lastly, the percent difference between the two dose rates (salted and saltless solutions) for each sample position was examined. In a given sample position, percent differences in dose rates for the saltless versus salted solution of less than two percent were taken as an indicator that the water used for solution preparation was adequately pure.

Results

Data analysis

Table 3 lists the average dose rate (average of salted and saltless solutions) for each sample position using sample geometries A, B and C. In this table, dose rates are listed in eV/(mL*min), rad/min and Gy/min. The date on which each representative Fricke experiment was performed is also listed. When using geometry B, the outer dose rate was equal to one-fourth of the respective inner dose rate. This result is confirmation of the relationship between source intensity and distance, $I \propto \frac{1}{d^2}$, which is characteristic of gamma radiation emitting from a point source, given the distance from the source to inner sample position of 2.00 cm, and the distance from the source to outer sample position of 4.00 cm.

Table 3: Representative Fricke experimental data using each of the three sample geometries. The date on which each representative Fricke experiment was performed is listed along with the dose rate, DR, in various units.

Date (month/year)	Geometry	Position	Average Dose Rate		
			(eV/(mL*min))	(rad/min)	(Gy/min)
10/93	A	Inner	4.4884×10^{17}	7023.2	70.232
4/94	B	Inner	3.6953×10^{17}	5782.2	57.822
	B	Outer	9.0820×10^{17}	1421.1	14.211
5/99	C	1	1.5716×10^{18}	24591	245.91
	C	2	3.6563×10^{17}	5721.2	57.212
	C	3	1.0608×10^{17}	1660.0	16.600
	C	4	1.5688×10^{16}	245.48	2.4548

A more exhaustive data treatment was performed on the dose rates obtained using geometry C. First, the curve of the dose rate, DR, in rad/min versus source to sample distance, r , in cm was fitted using a power function.

$$DR \left(\frac{\text{rad}}{\text{min}} \right) = 89992 r^{-2.0081} \left(\frac{\text{rad}}{\text{min}} \text{cm}^2 \right) = \frac{89992}{r^{2.0081}} \left(\frac{\text{rad}}{\text{min}} \text{cm}^2 \right) \quad (76)$$

The correlation coefficient for this power-function fit was found to equal 0.99326. The experimental dose rate versus distance curve is shown in Figure 18. Since source intensity decreases with the square of the distance, a value of 2 for the exponent of distance in this formula was expected and the experimentally determined exponent, 2.0081, was indeed close.

In addition, a plot was made of the dose rate, DR, in rad/min versus reciprocal of distance squared, $1/r^2$, in cm^{-2} . This plot was fitted using a second order equation:

$$DR = -3.4502 \times 10^{-11} \left(\frac{1}{r^2} \right)^2 + 1.0923 \times 10^{-5} \left(\frac{1}{r^2} \right) + 2.2109 \times 10^{-3} \quad (77)$$

The correlation coefficient for this fit was equal to 0.99952. The plot of dose rate versus reciprocal of distance squared is shown in Figure 19. By using either of these two fitting

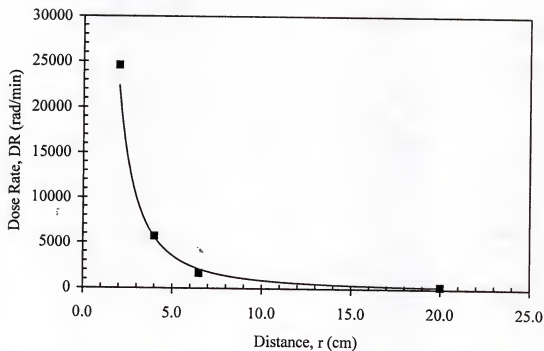


Figure 18: Plot of dose rate versus source to sample distance for geometry C. This experiment resulted in total calibration of the irradiator.

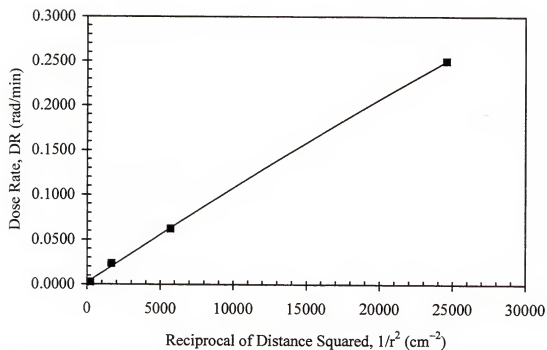


Figure 19: Plot of dose rate versus the reciprocal of square distance for geometry C. This experiment resulted in total calibration of the irradiator.

functions, the source to sample distance for a desired dose rate can be calculated as can the dose rate for a given source to sample distance, thus leading to total dose rate calibration of the Cobalt-60 irradiator.

Decay corrections

As described in Chapter 2, the activity of the source is constantly decreasing due to decay of the Cobalt-60 source, which implies that the dose rates obtained over time are similarly decreasing. The dose rates listed in Table 3 were valid only near the time of measurement listed in the table. To correct for the decay of the source in later experiments, a chart of t_{corr} per hour versus months after the date of the Fricke experiment was prepared. A portion of this table is presented in Table 4. For example, if near the date of the Fricke experiment for geometry A, 10/93, a sample was irradiated for three hours, a dose of 1.26 Mrad was absorbed by the sample. If at a latter time, say 6 months later, it was desired that a sample receive the same dose using geometry A, extra time in the irradiator was allotted so that the same dose was delivered. Table 4 lists a value of 3.8 minutes per hour for t_{corr} at 6 months. This is the additional time (in minutes per hour of irradiation) that must be added for equivalent dose. Since t_{corr} at 6 months is equal to 3.8 minutes per hour, this sample must spend 3 hours, 11.4 minutes in the irradiator for equivalent dose.

It is also of interest to note that the dose rate decreases by approximately 1% per month. This decrease is an artifact of the Cobalt-60 half-life being equal to 5.27 years, or 63.24 months. The decay constant λ , another nuclear quantity, is the amount the source decays per unit time. This quantity may be calculated by using the relationship between the half-life and the decay constant:

$$\lambda = \frac{\ln(2)}{t_{1/2}} = \frac{0.693}{63.24 \text{ month}} = 0.0110 \text{ month}^{-1} = 1.10\% \text{ month}^{-1} \quad (78)$$

This equation rationalizes the ~1% per month decrease in dose rate as well as provides a quick and easy method to estimate the dose rate at any future date.

Table 4: A portion of a decay correction table showing the additional time needed in the irradiator as the source decayed.

t_{elapsed} (months)	Dose Rate (eV/(mL*min))	(rad/min)	(Gy/min)	%decay	t_{corr} (min/hour)
0	4.4884×10^{17}	7023.2	70.232	0.00	0.0
1	4.4431×10^{17}	6952.4	69.524	1.10	0.6
2	4.3983×10^{17}	6882.3	68.823	2.20	1.2
3	4.3540×10^{17}	6812.9	68.129	3.30	1.9
4	4.3101×10^{17}	6744.2	67.442	4.40	2.5
5	4.2666×10^{17}	6676.2	66.762	5.50	3.1
6	4.2236×10^{17}	6608.9	66.089	6.60	3.8

Fricke dosimetry was repeated numerous times for each sample geometry throughout the course of this project. On average, a new Fricke experiment was conducted two or three times per year for each sample geometry. Experiments were replicated mainly for two reasons: repeat experiments provided verification of the decay predicted dose rate (1.10% per month), and more importantly, repeat experiments provided confirmation that the water source (doubly-distilled or MQ) had not become impure and could thus be trusted for preparation of aqueous benzene samples for irradiation.

CHAPTER 4 PRELIMINARY INVESTIGATIONS INTO THE AQUEOUS BENZENE SYSTEM

Test Tube Geometry, Geometry A

The earliest radiolysis experiments performed in this project utilized the test tube based geometry with the wagon-wheel sample cell holder, which was described in detail in Chapter 3 as geometry A. Fricke dosimetry was performed and the dose rate using an inner hole of the wagon-wheel sample holder was calculated. Aqueous benzene samples were prepared using two different preparation techniques. After irradiation, each sample was subjected to HPLC chromatography for product determination using two different developmental procedures. The applicability of each sample preparation and developmental method was determined.

Description of HPLC Instrumental Setup

The HPLC instrumental setup that was used during this phase of the project consisted of an ISCO high-pressure HPLC pump (model 2300), which was set to a flow rate of one mL per minute. The pump was fitted with a VALCO injector (model C6W) with an ISCO 10 μ L injection loop. The detector in the system was an ISCO variable wavelength UV-VIS detector (model V⁴) that was set to a wavelength of 255 nm, which was obtained using the deuterium lamp setting of the detector. The analytical column used for separations was an ISCO C-18 reverse phase column of dimensions 25 cm \times 5 mm filled with 5 μ m diameter packing (model 68-2207-013). A mobile phase

of 25/75 V/V (volume to volume) doubly distilled water/acetonitrile (Fisher, HPLC grade) was used for elutions. Chromatograms were obtained via a Linear chart recorder (model 500), which was set to a chart speed of 1 cm per minute and a full scale voltage of 10 mV for all experimental runs.

Sample Preparation Techniques

Preparation method SA, stock solution

The first method of aqueous benzene sample preparation that was tested consisted of preparing a 2 L stock solution of benzene in water. The stock solution was prepared by pipetting a 2.000 mL aliquot of benzene (Fisher, ACS grade, thiophene free) into a 2.000 L volumetric flask and then diluting to the mark with doubly distilled water. This resulted in a benzene concentration of 11.08 mM. The stock 2.000 L solution was kept refrigerated between uses in order to minimize evaporation of the benzene. To prepare samples for irradiation, the stock solution was removed from the refrigerator and allowed to warm to room temperature. Aliquots of 5.000 mL were pipetted into acid-soaked test tubes (Pyrex, model 9800) of dimensions 13×100 mm. Each test tube was stoppered with a pre-rinsed aluminum foil covered cork and shaken for two minutes. After sample preparation was complete, the 2.000 L stock solution was immediately returned to the refrigerator.

Preparation method SB, individually prepared tubes

The second method of sample preparation consisted of preparing sample tubes individually instead of using a 2 L stock solution. Sample preparation was accomplished by pipetting a 5.000 mL aliquot of doubly distilled water into a 13×100 mm acid-soaked test tube. Next, a 5.0 μ L aliquot of benzene (Fisher, ACS grade, thiophene free) was added to the tube using a pre-calibrated 20 μ L gas-chromatography syringe. Each tube

was immediately capped with a pre-rinsed aluminum foil covered cork and shaken for two minutes.

Irradiation and HPLC Development Techniques

While using geometry A, two different HPLC developmental procedures were employed and tested. The two procedures differed with respect to the amount of time that elapsed from removal from the irradiator to sample development via HPLC.

Development method DD, delayed development

In this method, all six inner sample holes of the wagon-wheel wheel sample holder were filled with tubes prepared using sample preparation method SA or SB. All six sample tubes were irradiated simultaneously, with one tube being removed at the end of each desired irradiation time interval. After all six tubes had been irradiated, each irradiated sample as well as a non-irradiated blank were developed using the HPLC setup previously described.

Development method PD, prompt development

In this method, sample tubes were prepared using one of the aforementioned sample preparation techniques SA or SB, and then irradiations were carried out. An HPLC analysis of the irradiated sample was performed immediately upon removal of the tube from the irradiator. Irradiations were planned such that each tube was chromatographed immediately upon removal. In addition, a non-irradiated blank was developed on each day when irradiations and elutions were performed.

Analysis of Experimental Methods

Failure of sample preparation method SA

After only a few experiments, chromatograms of non-irradiated blank samples indicated that the use of a 2 L stock solution of benzene was unacceptable. Even though

the 2 L solution was stored in a refrigerator at 3°C, and only allowed to warm to room temperature for sample tube preparation, the concentration of benzene in the stock solution was continually decreasing due to evaporation. For this reason, the 2 L stock benzene solution preparation technique, technique SA, was abandoned and the practice of individually preparing sample tubes, technique SB, was adopted for subsequent work. With practice, it became possible to prepare individual sample tubes using technique SB with solution benzene concentrations varying 5% or less as determined by HPLC analysis.

Failure of HPLC developmental method DD

Using the individual preparation technique solely (technique SB), several series of tubes were irradiated so that the applicability of the delayed versus prompt development HPLC technique could be determined. The observation was made that when using the delayed development technique, product concentrations varied according to the length of time between sample removal from the irradiator and sample development via HPLC. These changes were attributed to post-irradiation reactions. This observation is especially significant for radiochemistry laboratories in which the analytical services division is unable to process irradiated samples promptly. Any time lag between sample removal and sample development leads to a so-called "Civil Service Effect", a change in concentrations due to analytical time lag. Accordingly, irradiated samples were developed via HPLC promptly upon removal from the irradiator in all subsequent work.

Results and Discussion

Determination of products

Using individual sample preparation method SB and prompt development technique PD, sample tubes were individually irradiated using sample geometry A for

times of 0.5 to 2 hours. Products were identified based on retention times; the compounds 2-phenylphenol, phenol and biphenyl were observed. The structures of these compounds as well as the reactant benzene are shown in Figure 20. Quantitation of radiolysis products was made possible by injecting standard solutions and calculating peak areas. All standard solutions were made using ACS grade reagents with mobile phase as dilutant. Care was taken so that concentrations of standard solutions reasonably approximated concentrations of radiolysis products.

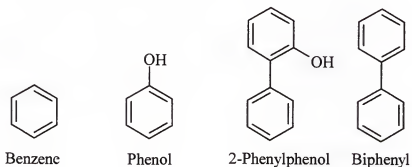


Figure 20: Chemical structures of benzene, phenol, 2-phenylphenol and biphenyl.

Discussion

Over the irradiation time span of 0 to 2 hours, reactant and all product concentrations are consistent with an $A \rightarrow B + C + D$ kinetic scheme. Concentration versus time of irradiation data are shown for benzene and the three products in Figure 21- Figure 24. However, upon further irradiation (2-10 hours), the plot of benzene concentration versus time of irradiation did not exhibit the simple shape expected. Instead of decreasing throughout the irradiation timescale, the area of the peak attributed to benzene decreased from 0 to 3 hours, increased from 3 to 5 hours, and then decreased again from 6 to 10 hours and presumably beyond. This anomalous concentration versus time of irradiation behavior is shown in Figure 25.

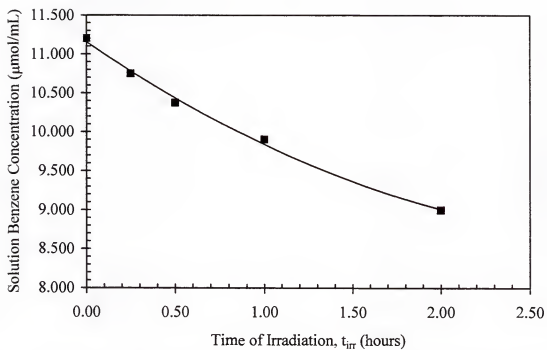


Figure 21: Solution benzene concentration versus time of irradiation for geometry A for the first two hours of irradiation.

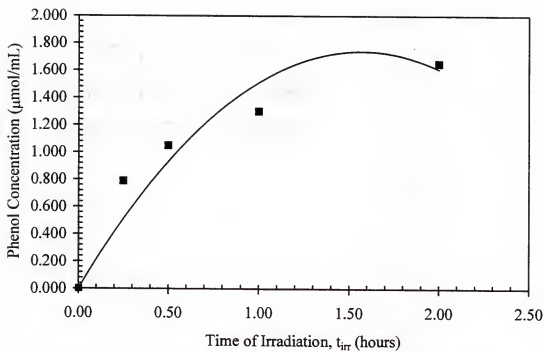


Figure 22: Phenol concentration versus time of irradiation for geometry A for the first two hours of irradiation.

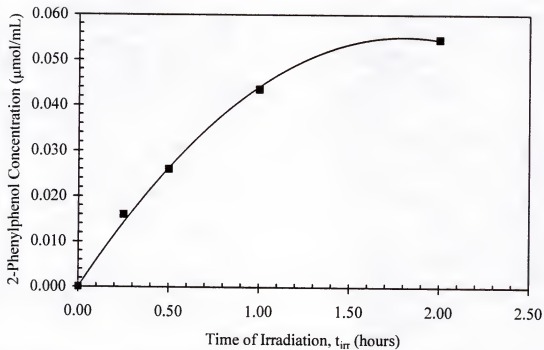


Figure 23: 2-Phenylphenol concentration versus time of irradiation for geometry A for the first two hours of irradiation.

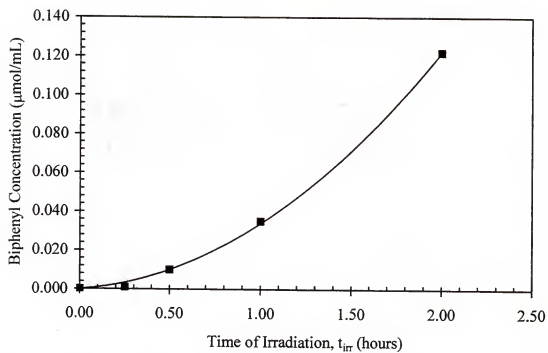


Figure 24: Biphenyl concentration versus time of irradiation for geometry A for the first two hours of irradiation.

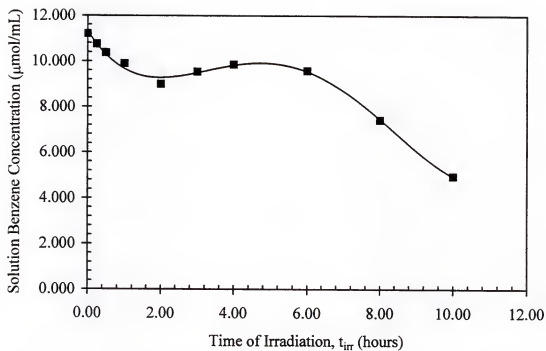


Figure 25: Apparent solution benzene concentration versus time of irradiation exhibiting improbable behavior.

Since the apparent concentration behavior was improbable, experiments were undertaken in order to rationalize the observed plot of benzene concentration versus time of irradiation. It was postulated that the ISCO reverse phase column that was in use was not adequately separating radiolysis product(s) from reactant benzene. It was suggested that the peak on the chromatogram that was assigned to benzene was actually a composite peak that was composed of benzene and other radiolysis product(s). Efforts were made at varying the mobile phase composition from 25/75 water/acetonitrile in order to improve separations, but ultimately a decision was made to purchase a new C-18 HPLC column.

It was also decided at this juncture that the foil-covered cork closure of the radiolysis tubes was inadequate. A new cell design was selected consisting of screw-top vials sealed with caps, each of which accommodated a septum port. This change in sample cell design was made in hopes of eventually performing gas headspace analyses on the irradiated samples. A search was made in vain for 13×100 mm test tubes with screw tops, so a new sample geometry consisting of screw-top chromatography vials instead of test tubes was selected.

Screw-Top Vial Geometry, Geometry B

Modification of Experimental Procedure

Change in sample cell

Chromatography vials of dimensions 16×62 mm and volume 8.0 mL (National Scientific, model B-7990-3) were chosen as sample cells because of the open screw-top enclosures that allowed for syringe penetration through the septum in the open cap. Since the diameter of these vials was different from the diameter of the previously used test tubes (16 mm versus 13 mm), a new sample holder was constructed using a solid

cylindrical block of aluminum. This sample geometry, geometry B, was described in detail in Chapter 3.

Change in analytical column

The ISCO C-18 reverse phase analytical column was replaced with a Whatman PAH C-18 reverse phase analytical column of dimensions 25 cm \times 4.6 mm (model 4691-2721) with 5 μ m packing. The PAH designation of this column indicates that the column has been optimized for separation of polyaromatic hydrocarbons. This column proved superior for separations in comparison to the previously used ISCO column.

Change in mobile phase composition

For these chromatographic runs utilizing geometry B and the new Whatman column, multiple mobile phases consisting of doubly distilled water/methanol (Fisher, HPLC grade) were used for elutions instead of the previously used 25/75 water/acetonitrile mobile phase. The different mobile phases that were used were 25/75, 33/66, 40/60, 50/50, 60/40, 66/33 and 75/25 water/methanol (V/V). These multiple mobile phases served as a "manual" approximation of gradient elution, since the ISCO model 2300 HPLC pump is an isocratic-only pump, incapable of gradient elution.

Preparation method SC, daily stock solution

At this time, a third sample preparation technique was also tested for efficiency. In this technique, a fresh, stock aqueous solution of benzene was prepared at the beginning of each working day. For this preparation, a 50.00 mL volumetric flask was filled to the mark with doubly distilled or MQ water. A 50.0 μ L aliquot of benzene (Fisher, ACS grade, thiophene free) was added to the flask using a precalibrated 50 μ L GC syringe. The flask was capped with a ground glass stopper, shaken for 2 minutes, and then allowed to sit for 15 minutes in order to establish equilibrium between the liquid

and vapor phases. Aliquots of 5.000 mL were pipetted into the National Scientific chromatography vials, which were then capped with pre-rinsed aluminum foils and open screw-top caps containing Teflon-backed silicone septa. Each cap was screwed as tightly as possible to minimize evaporation of the benzene from the vial. This technique of preparing a daily stock solution proved superior to the technique of preparing individual sample tubes. Thus, the daily stock benzene solution preparation technique SC was used for all subsequent work. Note at this point that the headspace consisted of laboratory air. Use of other filling gasses including oxygen and nitrogen is discussed in Chapter 6.

Use of Phenol as a Daily "Internal" Standard

As a precaution to guard against detector instability and drift, a practice was adopted in which a standard solution of phenol was injected into the HPLC several times during each day of HPLC use. The use of the phenol standard was to serve as a pseudo "internal" standard. A phenol solution of concentration ~ 8 mM was prepared by placing a mass of phenol (Fisher, ACS grade) into a 100 mL volumetric flask and dissolving and diluting to the mark with doubly distilled or MQ water. Usually, injections of the phenol standard were made before and after the development of each irradiated sample as well as each unirradiated blank. Since aqueous phenol solutions decompose slowly over time, fresh standard phenol solutions were prepared biweekly. The utility of the pseudo "internal" standard solution method to correct for detector drift is described in detail in Chapter 6.

Open Tube Evaporation Study

Description of the Experiment

As stated previously, benzene was seen to evaporate readily from solution in a 2 L volumetric flask stoppered with a ground glass stopper. In order to quantify the effect of

air-stripping on an aqueous solution of benzene in an open sample vial, an experiment was performed in which a 50.00 mL stock aqueous benzene solution was prepared according to preparation method SC. Aliquots of 5.000 mL were pipetted into National Scientific chromatography vials, but the vials were left uncapped and undisturbed on the benchtop. After a specified time interval, one injection was made from each vial into the HPLC instrumental setup previously described. The benzene solution concentration at each time-period was determined through suitable calculation.

Results and Discussion

A plot was prepared of solution benzene concentration versus the amount of time the uncapped sample vial had sat on the benchtop undisturbed. This plot is shown in Figure 26. As can be seen from the plot, a significant amount of the benzene, 50%, had evaporated from solution in just four hours. This plot serves to reinforce the necessity of proper closures, such as screw-top caps with septa, for aqueous samples of highly volatile compounds such as benzene.

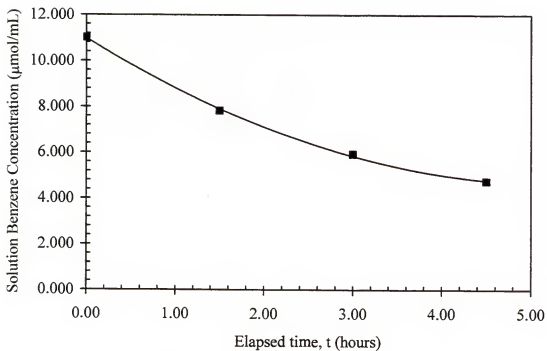


Figure 26: Solution benzene concentration versus the length of time the vial had stood uncapped on the benchtop.

CHAPTER 5

ANALYTICAL METHODS FOR CO₂ QUANTITATION

In this project an analytical method was needed for the determination of radiolytically produced CO₂ in sealed radiolysis vessels. For this purpose, two different analytical methods were chosen and tested: a procedure in which gaseous CO₂ was trapped in basic solution by conversion to CO₃²⁻, with the amount of trapped CO₂ being determined by subsequent titration with acid; and a procedure in which the amount of gaseous CO₂ was determined through the use of gas chromatography.

Trapping/Titration Experiment

Method development for the titration analysis of radiolytically produced CO₂ consisted of two prongs: (1) the study of titration behaviors of OH⁻/CO₃²⁻ mixed standards and pseudo-unknowns; and (2) the determination of headspace purging parameters for radiolysis samples. The aim of this method was to determine the amount of radiolytically produced CO₂ in a sealed radiolysis sample cell by sweeping the headspace of the sample cell through an aqueous solution of NaOH, thus trapping gaseous CO₂ by conversion to aqueous CO₃²⁻. The amount of trapped CO₂ would then be determined by subsequent acid titration of the reacted trapping solution. Analysis of endpoint volumes for the reacted trapping solution would be used to quantify the amount of CO₃²⁻ produced and to calculate the amount of CO₂ trapped. Accordingly, standard NaOH solutions, standard Na₂CO₃ solutions and standard mixed OH⁻/CO₃²⁻ solutions were prepared, and their titration behaviors when titrated against HCl were investigated.

Experimental Background

In order to understand the basis for this choice of quantitation methods, the behavior of gaseous CO_2 in both pure water and basic aqueous solution will be presented.

CO_2 in pure water

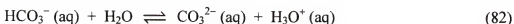
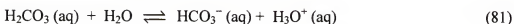
When CO_2 (g) is passed through pure water, it dissolves in the water to produce CO_2 (aq) with an equilibrium constant of 0.0344 [76].



Due to the magnitude of the equilibrium constant, it is evident that only a small percentage (~3%) of CO_2 (g) dissolves in water. The small percentage that does dissolve reacts with water to form aqueous carbonic acid, H_2CO_3 , with an equilibrium constant of 1.3×10^{-3} [76].



The kinetics of this dissolution process have been measured [77]. The reaction times are typically in the millisecond time range. Carbonic acid undergoes two acid dissociation steps to produce hydronium ion.



The equilibrium constant for reaction (81) is 4.30×10^{-7} [78], and for reaction (82) is 5.61×10^{-11} [78]. The magnitudes of these constants lead to slight acidification of the saturated solution: an aqueous, saturated solution in contact with gaseous CO_2 at pressure of 1 atm has a pH of 6.35.

CO₂ in basic solution

The fate of CO₂ (g) bubbled through a basic solution is quite different. As in the case with pure water, CO₂ (g) dissolves to produce CO₂ (aq) as shown in Reaction (79); CO₂ (aq) reacts with water to produce carbonic acid as shown in Reaction (80). Carbonic acid, H₂CO₃, dissociates as in Reactions (81) and (82), but the ionization equilibria are shifted entirely to product, CO₃²⁻, by reaction of hydroxide with hydronium ions produced in Reactions (81) and (82).



Therefore, the net effect of the presence of OH⁻ in the trapping solution is the conversion of gaseous CO₂ to aqueous CO₃²⁻.

Experimental Methods and Materials

Description of titration instrumentation

All titrations were performed using an Orion Research digital ionanalyzer (model 801A) that was set to pH mode. The titration unit was equipped with a Cole Parmer glass pH electrode (model 05991-80). When not in use, the electrode was stored in Fisher brand electrolyte solution (4 M KCl saturated with AgCl). At the beginning of each titration experiment, the instrument was calibrated using pH 2, 7 and 10 buffers (Fisher Scientific). All titrant was delivered using a Kimax 50 mL buret that was graduated in 0.1 mL increments. During each titration, the solution was stirred using a Cole Parmer stirrer/hotplate (model 4658) and a Teflon coated stir bar. The heating capability of the stirrer/hotplate was not used, as each titration was carried out at room temperature, 25 ± 2°C.

Description of solution preparation

A stock solution of approximately 1 M NaOH, a stock solution of approximately 1 M HCl, and a stock solution of approximately 1 M Na_2CO_3 were prepared using ACS grade reagents (Fisher Scientific). Solutions were prepared using MilliQue (MQ) or doubly distilled water. Several dilutions were made from each stock solution to produce diluted solutions with concentrations that spanned the range 1 M to 0.005 M. As before, MQ or doubly distilled water was used for all dilutions. Solutions were stored in 500 mL Nalgene bottles (Fisher Scientific) with screw-top lids.

List of Experiments

Standardization of NaOH

The ~1 M NaOH solution was standardized by reaction with the primary standard potassium hydrogen phthalate, KHP. Potassium hydrogen phthalate (Fisher, ACS grade) was dried in a drying oven at 110°C until a constant mass was obtained. Samples of approximately 5 g dried KHP were dissolved in 100 mL MQ water and titrated using the ~1 M NaOH solution as titrant. Using the mass and molecular weight of KHP and the volume of NaOH titrant, the molarity of the ~1 M NaOH solution was calculated. This process was repeated until a %RSD (random standard deviation) of less than 2% was obtained. (%RSD is defined as the quotient of the standard deviation and mean converted to percent.) The concentrations of the diluted NaOH solutions were calculated by applying the dilution formula. The concentrations of the stock and diluted NaOH solutions are listed in Table 5.

Standardization of HCl

The concentration of the ~1 M HCl solution was determined by titrating aliquots of the solution against the standardized 1.214 M NaOH solution. Titrations were

repeated until a %RSD of less than 2% was obtained for the concentration of the ~1 M HCl solution. The concentration of each diluted HCl solution was calculated by applying the dilution formula. The concentrations of the stock and diluted HCl solutions are also listed in Table 5.

Standardization of Na_2CO_3 solutions

The concentration of the stock ~1 M Na_2CO_3 solution was determined by using the molecular weight of Na_2CO_3 and the solution volume. This calculation resulted in a stock Na_2CO_3 solution concentration of 1.001 M. The concentration of each diluted Na_2CO_3 solution was determined by applying the dilution formula to the concentration of the stock 1.001 M Na_2CO_3 solution. The concentrations of the stock and diluted Na_2CO_3 solutions are also listed in Table 5.

Table 5: Listing of concentrations of standard HCl, NaOH and Na_2CO_3 solutions for titration experiments.

HCl (M)	NaOH (M)	Na_2CO_3 (M)
0.9127	1.214	1.001
0.04564	0.1214	0.1001
0.004564	0.01214	0.01001

Mixed solution (NaOH and Na_2CO_3) titrations

As stated previously, a basic solution used to trap CO_2 (g) contains CO_3^{2-} and excess OH^- after the trapping reaction is complete. In order to study the titration behavior of used trapping solutions, several pseudo-unknown solutions were prepared. Each pseudo-unknown was prepared by pipetting known aliquots of one of the NaOH solutions and one of the Na_2CO_3 solutions into the titration vessel. Each pseudo-unknown solution was titrated using one of the previously prepared HCl solutions as titrant. Each particular HCl solution was chosen as to obtain the most appropriate

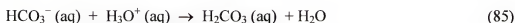
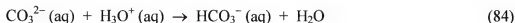
titrant volume. After each titration, the resulting titration curve was used to back-calculate the number of mmoles of CO_3^{2-} present in each pseudo-unknown. The calculated number of mmoles of CO_3^{2-} was compared to the number of mmoles pipetted into the titration beaker in order to determine the feasibility of this analytical method. Table 6 lists the concentrations and volumes of the NaOH, Na_2CO_3 , and HCl solutions used in each pseudo-unknown titration experiment. Each experiment was performed in triplicate at a minimum.

Table 6: Listing of volumes and concentrations of each solution used for the three pseudo-unknown titration experiments.

Experiment Number	C_{NaOH} (M)	V_{NaOH} (mL)	$C_{\text{Na}_2\text{CO}_3}$ (M)	$V_{\text{Na}_2\text{CO}_3}$ (mL)	C_{HCl} (M)
1	1.214	5.000	1.001	5.000	0.9127
2	0.1214	5.000	0.1001	5.000	0.04564
3	0.01214	5.000	0.01001	5.000	0.004564

Results and Discussion

A titration plot consisting of pH versus volume of titrant (in mL) and a plot consisting of the second derivative versus average volume of titrant (in mL) were prepared: a representative plot for each experiment is shown in Figure 27-Figure 32. In theory, each titration plot should exhibit three endpoints corresponding to the following reactions in order of volume of titrant.



In order to determine the number of mmoles of CO_3^{2-} present in each pseudo-unknown solution, the data from each titration experiment were interpreted in a strict

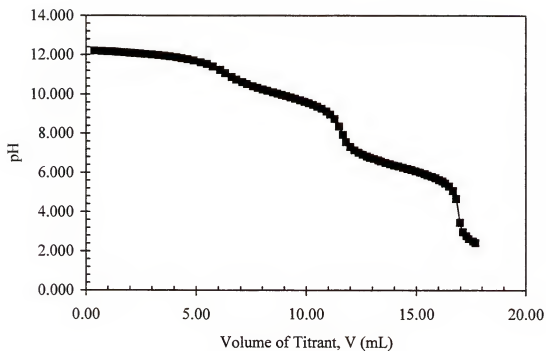


Figure 27: Pseudo-unknown titration experiment 1: pH plot for the titration of 5.000 mmol CO_3^{2-} and 6.070 mmol OH^- using 0.9127 M HCl as titrant.

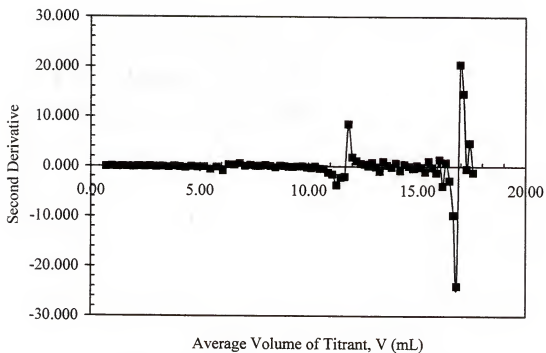


Figure 28: Pseudo-unknown titration experiment 1: Second derivative plot for the titration of 5.000 mmol CO_3^{2-} and 6.070 mmol OH^- using 0.9127 M HCl as titrant.

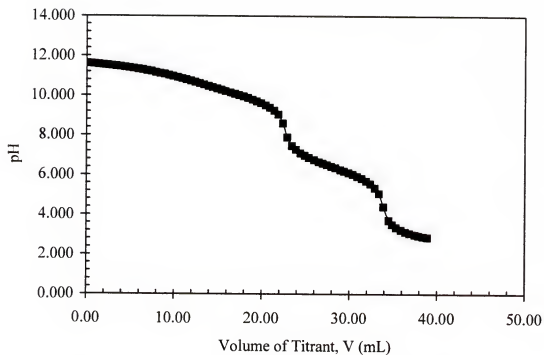


Figure 29: Pseudo-unknown titration experiment 2: pH plot for the titration of 0.5000 mmol CO_3^{2-} and 0.6070 mmol OH^- using 0.04564 M HCl as titrant.

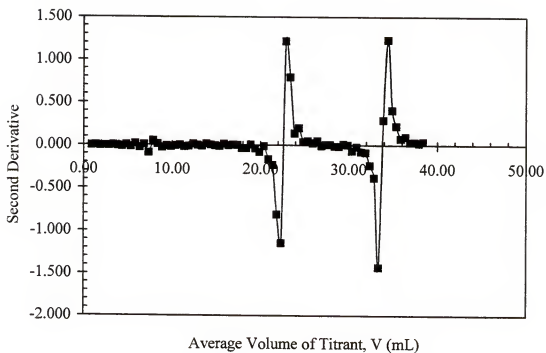


Figure 30: Pseudo-unknown titration experiment 2: Second derivative plot for the titration of 0.5000 mmoles CO_3^{2-} and 0.6070 mmoles OH^- using 0.04564 M HCl as titrant.

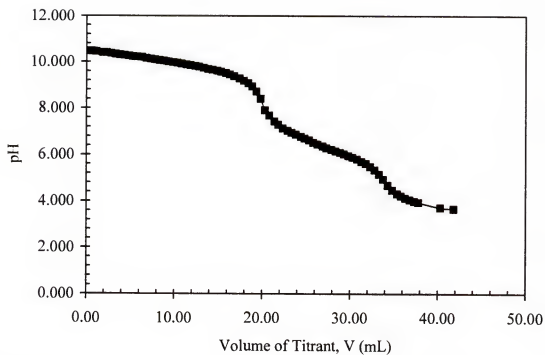


Figure 31: Pseudo-unknown titration experiment 3: pH plot for the titration of 5.000×10^{-2} mmoles CO_3^{2-} and 6.070×10^{-2} mmoles OH^- using 4.564×10^{-3} M HCl as titrant.

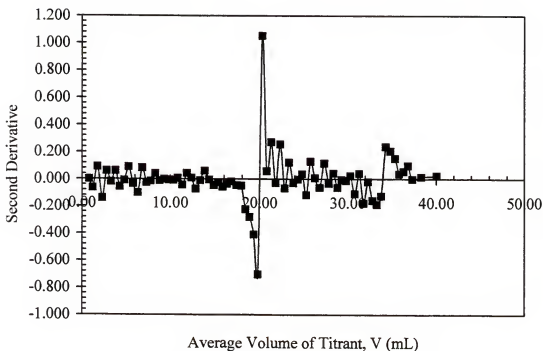


Figure 32: Pseudo-unknown titration experiment 3: Second derivative plot for the titration of 5.000×10^{-2} mmoles CO_3^{2-} and 6.070×10^{-2} mmoles OH^- using 4.564×10^{-3} M HCl as titrant.

manner. The total volume of titrant necessary to reach endpoint two (corresponding to Reaction (84) – conversion of CO_3^{2-} to HCO_3^-) was subtracted from the total volume of titrant necessary to reach endpoint three (corresponding to Reaction (85) – conversion of HCO_3^- to H_2CO_3). This volume difference (the difference in endpoint volumes for endpoints two and three) was then multiplied by the concentration of the HCl titrant to yield the mmoles of CO_3^{2-} present in the titration vessel.

In the first experiment listed in Table 6, a solution containing 5.005 mmoles CO_3^{2-} and 6.070 mmoles OH^- was titrated against 0.9127 M HCl. The plot of pH versus volume of titrant is shown in Figure 27, and the plot of the second derivative versus average volume of titrant is shown in Figure 28. Each of the plots exhibits three endpoints, although the first endpoint, which corresponds to Reaction (83), is barely visible. The two remaining endpoints are quite sharp. Based on the data analysis method previously described, the amount of CO_3^{2-} present was calculated to equal 4.755 mmoles. This result was 5.00% lower than the true value of 5.005 mmoles.

In the second experiment listed in Table 6, a solution containing 0.5005 mmoles CO_3^{2-} and 0.6070 mmoles OH^- was titrated against 0.04564 M HCl. The plot of pH versus volume of titrant is shown in Figure 29, and the plot of the second derivative versus average volume of titrant is shown in Figure 30. In comparison to titration experiment 1, the pH plot and the second derivative plot indicate two endpoints with both endpoints having approximately the same degree of sharpness. Although the first endpoint, which corresponds to Reaction (83), is visible on the second derivative plot, it is absent on the pH plot. This absence illustrates the utility of the second derivative plot in determining endpoints that are not visible when using the standard pH

plot. Using the same data analysis technique, the amount of CO_3^{2-} present was calculated to equal 0.5102 mmoles CO_3^{2-} . This result was 1.94% higher than the true value of 0.5005 mmoles.

In the third experiment listed in Table 6, a solution containing 0.05005 mmoles CO_3^{2-} and 0.06070 mmoles OH^- was titrated against 0.004564 M HCl. The plot of pH versus volume of titrant is shown in Figure 31, and the plot of the second derivative versus average volume of titrant is shown in Figure 32. As in experiment 2, the pH plot and the second derivative plots possess two endpoints corresponding to Reactions (84) and (85). In this experiment, the first endpoint, which corresponds to Reaction (83), is absent from both plots. In addition, the second derivative plot exhibits fluctuations that make accurate endpoint detection difficult. Based upon the same data analysis, the amount of CO_3^{2-} present was calculated to equal 0.06470 mmoles CO_3^{2-} . This result was 29.27% higher than the true value of 0.05005 mmoles CO_3^{2-} .

Evaluation of Method

Table 7 lists the experimentally determined number of mmoles of CO_3^{2-} found in each representative experiment and the true value for each solution. The percent error in each experiment is also listed. These results indicate that the amount of CO_3^{2-} in basic solution can be accurately determined in the more concentrated solutions. Numerous replications of experiments 1 and 2 yielded percent errors in CO_3^{2-} amounts within $\pm 5\%$. However, the experimentally determined concentration of CO_3^{2-} in titration experiment 3 never agreed with the true value, no matter how many times the experiment was repeated. Percent errors of +25% to +35% were common. The positive systematic error was attributed to atmospheric CO_2 dissolving into the titration solution during the experiment,

thus skewing the results in a positive direction. Since the concentrations of OH^- , CO_3^{2-} and HCl in experiment 3 were concentrations chosen to approximate those necessary for actual trapping experiments of irradiated samples, this analytical method for CO_2 determination was discarded and another quantitation method was tested. Moreover, the second prong of the two-fold method development plan, purging parameters, was never investigated, and no irradiated aqueous benzene samples were analyzed via this titration method.

Table 7: Listing of the results from the three pseudo-unknown titration trapping experiments for determination of radiolytically produced CO_2 .

Experiment Number	$n_{\text{CO}_2^-} \text{, calc}$ (mmoles)	$n_{\text{CO}_2^-} \text{, true}$ (mmoles)	%error
1	4.755	5.005	-5.00
2	0.5102	0.5005	+1.94
3	0.06470	0.05005	+29.27

Gas Chromatography Experiment

In this experimental method, the amount of CO_2 (g) contained in a sealed radiolysis vessel was determined using gas chromatography, GC. First, the response of the gas chromatography instrumental system was calibrated by preparing calibration plots of peak area versus injected μmoles of gas for both air and CO_2 . Then, a procedure was developed for transferring the headspace gas from a sealed radiolysis vessel into a syringe for injection. Lastly, the amount of CO_2 (g) in several pseudo-unknowns was determined through use of the calibration plots and suitable calculation.

Experimental Methods and Materials

Description of gas chromatography instrumentation

The gas chromatography instrumental setup consisted of a Tracor model 550 gas chromatograph fitted with a $\frac{1}{4}$ inch x 6 foot stainless-steel analytical column packed with

silica gel. This column was found in the laboratory pre-packed with no labeling information given, so the source and mesh particle size of the silica gel are unknown. The GC unit is equipped with a linear temperature programming control unit that allows for temperature ramping at a rate from 0.5°C per minute to 25°C per minute. Helium (BOC Group, UHP grade) was used as carrier gas for all elutions and was used as received. The detector on this unit is a thermal conductivity detector, TCD, (GOW-MAC, model 13-002), which is a four-filament detector of the quad (pretzel) design with elements made of rhenium tungsten. The current source used to power the TCD is a control unit/power supply (GOW-MAC, model 40-001), which was set to a current setting of 150 mA. All chromatograms were obtained via a Linear chart recorder (model 500) that was set to a chartspeed of 1 cm per minute and full-scale voltage setting of 1 mV. The flow rate through the analytical column was determined by using a soap bubble meter connected to the exit port of the detector and was set to a value of 25 mL per minute for all elutions. The composite N₂/O₂ peak and the CO₂ peak were well separated using the column and chromatographic conditions employed.

Source of calibration gases

Carbon dioxide (BOC Group, Industrial grade) was used for all calibration work including temperature program determination and calibration plot development. The gas was used as received. A 25 mL glass bulb fitted with a rubber septum was used as a reservoir so that accurate volumes of CO₂ at atmospheric pressure could be obtained for injection. Chromatographic analysis revealed no observable impurities.

The atmosphere of the laboratory was used for calibrations requiring air.

Calibration of System

Air calibration plot

Volumes of air at room temperature, $26 \pm 1^\circ\text{C}$, and room pressure, 760 ± 5 mm Hg, were injected into the GC and eluted isothermally at 70°C . Using this column temperature and a flow rate of 25 mL per minute, the air injections eluted at retention times from 3.5 to 4.5 minutes. Air volumes of 0.25 mL to 5 mL were injected into the GC for preparation of the calibration plot. Injections were made using either a 5 mL plastic syringe (Beckton Dickinson) or a 1 mL plastic syringe (Beckton Dickinson) fitted with a 2" 24 gauge leur-lock needle.

To prepare the calibration plot, a derivation to calculate the number of μmoles of gas in each injection was needed. This derivation was developed by first writing the ideal gas law twice: once for lab conditions, L, and once for standard temperature and pressure conditions, STP.

$$P_L V_L = n_L R T_L \quad (86)$$

$$P_{\text{STP}} V_{\text{STP}} = n_{\text{STP}} R T_{\text{STP}} \quad (87)$$

Each of these equations was solved for R, and the two were set equal to each other.

$$\frac{P_L V_L}{n_L T_L} = \frac{P_{\text{STP}} V_{\text{STP}}}{n_{\text{STP}} T_{\text{STP}}} \quad (88)$$

This equation was rearranged to solve for the quotient n_L/V_L , the molar gas volume at lab conditions.

$$\frac{n_L}{V_L} = \left(\frac{n_{\text{STP}}}{V_{\text{STP}}} \right) \left(\frac{P_L}{P_{\text{STP}}} \right) \left(\frac{T_{\text{STP}}}{T_L} \right) \quad (89)$$

Substituting the values for the molar gas volume, the pressure, and the temperature at STP (22.4 L per mole, 760 mm Hg, and 273 K, respectively) along with the laboratory

temperature and pressure on the day of the calibration plot experiment (298 K and 759 mm Hg) allowed for the calculation of the molar gas volume at lab conditions on the day of calibration.

$$\frac{n_L}{V_L} = \left(\frac{1 \text{ mole}}{22.4 \text{ L}} \right) \left(\frac{759 \text{ mm Hg}}{760 \text{ mm Hg}} \right) \left(\frac{273 \text{ K}}{298 \text{ K}} \right) = 4.084 \times 10^{-2} \frac{\text{moles}}{\text{L}} \quad (90)$$

This quantity was then converted to μmoles per mL.

$$\frac{n_L}{V_L} = \left(4.084 \times 10^{-2} \frac{\text{moles}}{\text{L}} \right) \left(\frac{1 \text{ L}}{10^3 \text{ mL}} \right) \left(\frac{10^6 \mu\text{moles}}{\text{mole}} \right) = 40.84 \frac{\mu\text{moles}}{\text{mL}} \quad (91)$$

For a 2 mL injection, the number of μmoles of gas was calculated as shown.

$$n_{2 \text{ mL}} = \left(40.84 \frac{\mu\text{moles}}{\text{mL}} \right) (2 \text{ mL}) = 81.68 \mu\text{moles} \quad (92)$$

This calculation was repeated in order to determine the number of μmoles of air in each injection.

The normalized peak area, A' , was calculated by multiplying each peak area, A , by the detector attenuation setting that was used for elution of the peak. For example, a peak area of 1000 units measured at an attenuation setting of 8 was normalized as follows:

$$A' = A \times s = 1000 \times 8 = 8000 \quad (93)$$

Normalizing peak areas yielded areas that would have been obtained had all elutions been achieved using a detector attenuation setting of 1, which is the most sensitive setting available on the GOW-MAC current source.

A plot was made of normalized peak area, A' , versus number of injected μmoles of air, n_{air} . The air calibration plot is shown in Figure 33. A linear fit of the data was made in Excel that yielded the equation of the air calibration line.

$$A'_{\text{air}} = (458.1 \mu\text{mol}^{-1})(n_{\text{air}}) - 24.18 \quad (94)$$

CO₂ calibration plot

On the same day during which the air calibration plot injections were made, injections of CO₂ (g) at lab temperature and pressure were also made into the GC. A temperature program consisting of 5 minutes at 70°C, then 5°C per minute temperature ramp was used for all CO₂ elutions. Using a flow rate of 25 mL per minute and this temperature program, CO₂ eluted at retention times of 20 to 22 minutes. Volumes of 0.25 mL to 5 mL CO₂ were removed from the 25 mL glass bulb and injected into the Tracor unit. Injections were made using the same syringes as were used for the air injections.

Using the same ideal gas law derivation, the number of μmoles of CO₂ (g) in each injection was calculated. Peak areas of CO₂ were normalized as before. A calibration plot consisting of the normalized peak area versus the number of injected μmoles of CO₂ was prepared. This plot is shown in Figure 34. The equation of the CO₂ calibration plot line was determined using Excel.

$$A'_{\text{CO}_2} = (521.2 \mu\text{mol}^{-1})(n_{\text{CO}_2}) - 24.83 \quad (95)$$

In this equation A'_{CO_2} is the normalized peak area for CO₂ and n_{CO_2} is the number of μmoles of CO₂ injected into the GC.

Once both calibration plot equations had been determined, the slopes of the air calibration line and CO₂ calibration line were used to calculate the slope ratio, m_{rat} .

$$m_{\text{rat}} = \frac{m_{\text{CO}_2}}{m_{\text{air}}} = \frac{521.2 \mu\text{mol}^{-1}}{458.1 \mu\text{mol}^{-1}} = 1.138 \quad (96)$$

The utility of the slope ratio will be explained shortly.

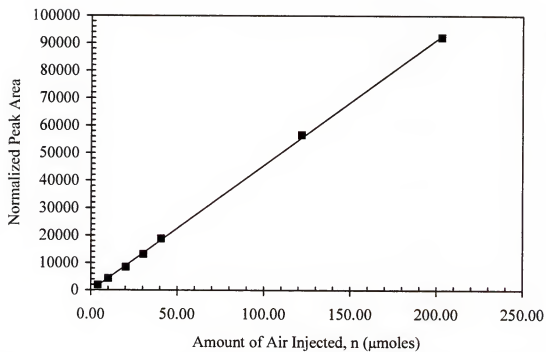


Figure 33: Gas chromatography air calibration plot indicating the normalized peak area versus μmoles of injected air.

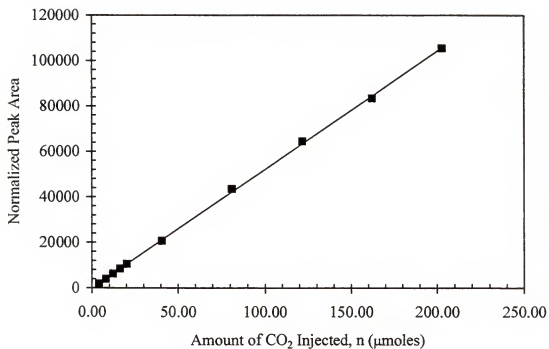


Figure 34: Gas chromatography CO₂ calibration plot indicating the normalized peak area versus μmoles of injected CO₂.

Description of Experimental Method

On each day of an experimental CO₂ determination run, a very specific procedure was followed. This procedure included preparing a daily air calibration plot, transferring the headspace that contained CO₂ from the irradiated sample tube to a syringe, injecting the syringe contents, and performing proper data workup.

Daily air calibration plot

Shortly after beginning to use the Tracor GC unit, the observation was made that the detector response was rather constant throughout the day, but varied by $\pm 10\%$ from day to day. Therefore, a method was needed to eliminate the shift in detector response from day to day. For this reason, a practice was begun of preparing a "daily air calibration plot" by making triplicate injections of 1 mL, 3 mL and 5 mL of air at room temperature and room pressure at the beginning of each working day. The use of this daily air calibration plot is explained shortly.

Technique for removal and injection of tube headspace gas

A technique was developed for the removal of headspace gas in an irradiated chromatography vial that was sealed with a open screw-top cap containing a rubber septum as described in Chapter 4 (National Scientific, model B-7990-3). Immediately upon removal from the irradiator, the vial was inverted. A 10 mL plastic syringe (Becton Dickinson) was fitted with a push-button gas valve (SGE, model 031915). Onto this syringe, a 5" leur-lock 26 gauge needle was attached and the needle was inserted through the septum all the way to the top of the inverted vial. Next, a 25 mL glass syringe (SGE, model 009462) was filled with 1 M H₂SO₄, which was prepared using concentrated Fisher ACS grade H₂SO₄ (a highly non-volatile acid) with MQ water as dilutant. A 2" 26 gauge leur-lock needle was fitted onto the 25 mL acid-containing glass syringe, and

the needle was inserted through the septum into the inverted sample vial. The acid solution was added to the vial as the headspace gas was removed. A transfer in progress is shown in Figure 35. The choice to use acid as a displacement solution instead of using water was made in order to force the various forms of carbonic acid mentioned earlier in this chapter to revert to CO_2 (g), which could be collected. After all the headspace volume had been transferred into the 10 mL syringe, the push-button valve was closed, and the 10 mL syringe was withdrawn from the inverted vial. The 5" long needle was removed and a 1.5" 23 gauge leur-lock needle was fitted onto the syringe.

The gas contents of the syringe (the headspace containing CO_2) were injected into the GC. All headspace samples were eluted using the same temperature ramping program as was used to prepare the CO_2 calibration plot: 5 minutes at 70°C , then 5°C per minute to 250°C . The column was held at 250°C for a minimum of 30 minutes after each headspace run in order to remove any tightly held components.

Data analysis technique

Once the chromatogram of the headspace sample was obtained, the areas of the triplicate injections of 1 mL, 3 mL, 5 mL of air (the daily air calibration plot injections), and CO_2 peak were measured. The normalized peak areas from the air injections were used to prepare a "daily air calibration plot", and the slope of this plot, $m_{\text{daily air}}$, was determined using Excel. Before the μmoles of CO_2 could be calculated, the fluctuating day-to-day response of the detector had to be determined and corrected. This was accomplished by using the slope of the daily air calibration plot and the slope ratio that had been determined on the day during which the air and CO_2 calibration plots were obtained, m_{rat} , which is equal to $m_{\text{CO}_2} / m_{\text{air}}$. In this procedure, the slope ratio that was

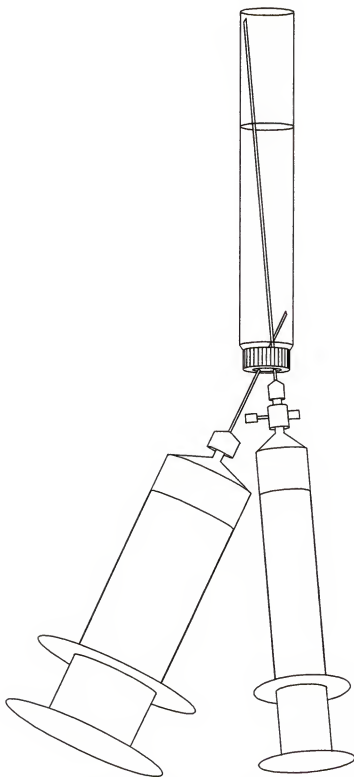


Figure 35: Diagram showing headspace gas transfer in progress. The large syringe contains acid solution that is added to the vial as the headspace is withdrawn into the smaller syringe.

obtained from the air and CO₂ calibration plots on the day of calibration was multiplied by the daily air slope to yield the slope of the CO₂ calibration line, had it been determined using that day's detector sensitivity.

$$m_{\text{CO}_2} = m_{\text{rat}} m_{\text{daily air}} = \frac{m_{\text{CO}_2}}{m_{\text{air}}} m_{\text{daily air}} = m_{\text{CO}_2, \text{ today}} \quad (97)$$

Next, the normalized peak area of the CO₂ peak was divided by "today's" CO₂ slope to yield the injected μmoles of CO₂ (g).

$$n_{\text{CO}_2} (\mu\text{moles}) = \frac{A'_{\text{CO}_2}}{m_{\text{CO}_2, \text{ today}}} \quad (98)$$

This data analysis technique was followed for all CO₂ (g) headspace injections.

Results and Discussion

A typical chromatogram obtained from the elution of a headspace gas sample is shown in Figure 36. The chromatogram consists of two peaks, air and CO₂, which are well separated. When using a silica gel column, air is not separated into its constituent gases and therefore appears as one peak.

Pseudo-unknown injections

Several mock irradiated samples were prepared in order to test the efficiency of this method for CO₂ analysis. Samples were prepared by injecting volumes of CO₂ (g) (at room temperature and room pressure) from 0.5 mL to 4 mL into inverted sample vials containing 5.000 mL MQ water (the same liquid volume used for sample irradiations) that were closed with open-top caps containing septa. The vials were shaken well and allowed to sit for 3 to 5 minutes. The aforementioned headspace extraction technique was applied to these vials. Each headspace sample was injected into the GC using the temperature program that was used for actual irradiated samples.

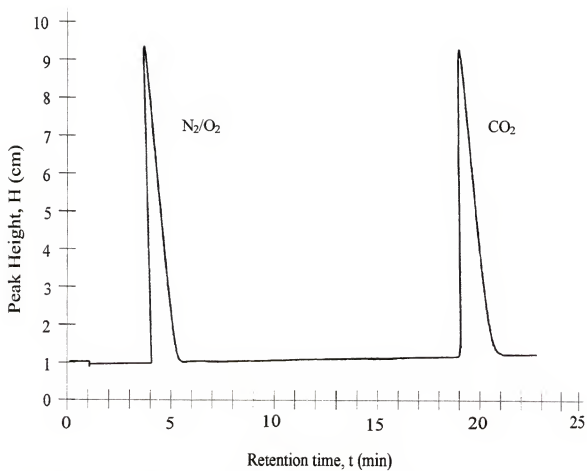


Figure 36: A typical chromatogram of a sample containing air (N_2/O_2) and CO_2 .

The results for the pseudo-unknown headspace injection experiments were quite encouraging. Table 8 lists the results from the pseudo-unknown experiments. As can be seen from Table 8, the calculated number of μmoles of CO_2 , $n_{\text{CO}_2, \text{calc}}$, agreed with the injected number of μmoles , $n_{\text{CO}_2, \text{inj}}$, for all experiments to within 6.78%.

Table 8: Results from the three pseudo-unknown CO_2 headspace experiments analyzed by gas chromatography.

Pseudo-unknown experiment	$V_{\text{CO}_2, \text{inj}}$ (mL)	$n_{\text{CO}_2, \text{inj}}$ (μmoles)	$n_{\text{CO}_2, \text{calc}}$ (μmoles)	% difference
1	0.5	20.42	19.07	-6.61
2	2.5	102.1	95.18	-6.78
3	4.0	163.4	154.4	-5.51

Evaluation of Method

Armed with the results of the pseudo-unknown experiments, the decision was made to use this method of CO_2 quantitation for all future aqueous benzene sample irradiation experiments in which CO_2 production information was desired. The only caveat to this method is that the irradiated solution must be made sufficiently acidic so that equilibria of carbonic acid, Reactions (81) and (82), are shifted toward reactants, therefore ensuring that the amount of CO_2 (g) in the headspace is maximized. Since the headspace is displaced with 1 M H_2SO_4 , this caveat is not a concern. A final solution pH of ~ 0.5 is far too acidic for any CO_2 to exist in the form of HCO_3^- or CO_3^{2-} , thereby assuring that the maximum amount of CO_2 is collected for injection.

CHAPTER 6

GAMMA IRRADIATION OF AQUEOUS BENZENE SOLUTIONS

Aqueous benzene solutions were irradiated under static conditions in order to ascertain parameters affecting both initial product yields and conversion percents of benzene to CO_2 . Samples were prepared using two different headspace volumes and three different headspace gases, and were irradiated using two different sample geometries. Lastly, the product mixtures from several experiments were analyzed via GC-MS in hopes of determining qualitative identities of trace products. This chapter focuses on experimental descriptions and result listings. Reaction mechanisms and product rationalization are discussed in Chapter 7.

Low Dose Rate Experiments for Initial Product Determination

Low dose rate irradiations of aqueous benzene solutions were performed using air-saturated samples prepared on the benchtop with both small and large headspaces. In addition, large headspace samples were prepared in a glovebox so that the solution would be saturated with, and the headspace would contain, either O_2 or N_2 .

Sample Preparation Techniques

Benchtop air-saturated samples

Air-saturated aqueous benzene solutions were prepared following the procedure listed at the end of Chapter 4. In this procedure, a 50.00 mL stock solution was prepared at the beginning of each working day, and this daily stock solution was used to prepare the samples for the day's irradiations as well as non-irradiated blank samples. To prepare

the daily stock solution, a 50.00 mL volumetric flask was filled to the mark with MilliQue (MQ) water (Millipore Systems, Bedford, Massachusetts), and a 50.0 μ L aliquot of benzene (Fisher, ACS grade, thiophene free) was added to the flask through the use of a precalibrated GC syringe. The flask was stoppered with a ground glass stopper, shaken for two minutes, and then allowed to stand undisturbed for 15 minutes in order to establish equilibrium between the liquid and vapor phases. Aliquots of 5.000 mL were pipetted using a class A volumetric pipet into sample vials (National Scientific, model B-7990-3). Each vial was immediately closed with a pre-washed layer of aluminum foil, a rubber septum and an open screw-top cap (National Scientific, model B7807-15). The cap was closed as tightly as possible in order to minimize evaporation of the benzene. Blank samples prepared in this manner exhibited minimal benzene loss for up to 24 hours. The screw-top caps that were used for sample vials were of the open-top variety, which allowed for the penetration of a syringe needle through the septum. This cap design was crucial for later headspace analyses.

In these experiments as well as in subsequent experiments, two different types of sample vials were used. For the air-saturated samples with small headspace volumes, referred to as “short” tubes, chromatography vials (National Scientific, model B-7990-3) were used as radiolysis vessels. These vials measure 60 mm tall and have outer diameters of 16 mm. The volume of each tube is a nominal 8.0 mL. Therefore, when a sample vial is prepared by pipetting 5.000 mL of aqueous benzene solution, a headspace volume of 3.0 mL remains. These vials were described in detail at the end of Chapter 4. Air-saturated aqueous benzene solutions prepared on the benchtop using these “short” sample vials are referred to as “short air tubes” throughout the remainder of this work.

For samples with large headspaces, new sample cells were constructed by joining two of the “short” National Scientific vials. This work was done by the departmental glassblower, Karl Wahler. For this joining, the bottom of one tube and the top of another tube were removed, the two remaining pieces were fused together and the resulting “long” tube was annealed in an oven. For sample preparation using these “long” tubes, 5.000 mL aliquots of the stock, air-saturated 50.00 mL aqueous benzene solution were pipetted into the “long” tubes using a class A volumetric pipet. Each tube was then sealed with aluminum foil, a septum, and an open, screw-top cap. Due to the lengthening of the tube, each “long” sample consisted of 5.000 mL solution and 11.0 mL headspace volume. Air-saturated samples prepared in these “long” sample tubes on the benchtop are referred to as “long air tubes” in the remainder of this work.

Glovebox O₂- or N₂-saturated samples

A laboratory glovebox (Lab Con Corporation) was used to prepare aqueous benzene sample tubes in which the solution was saturated with, and the headspace contained, either O₂ or N₂. The glovebox consists of a large inner chamber that measures approximately 3 feet (width) × 3 feet (height) × 2 feet (depth) and a side airlock box that measures approximately 1.5 feet (width) × 1 foot (height) × 1 foot (depth). The glovebox is fitted with two large neoprene gloves that allow the user to work inside the box. The glovebox is also plumbed with several gas valves that allow for purging. Initially, the glovebox was purged with two cylinders of either O₂ (BOC Group, Industrial grade) or N₂ (BOC Group, Industrial grade), and then the glovebox was kept under positive pressure for continuous purge as evidenced by the gloves of the glovebox being extended at all times. By proper adjustment of the purge gas cylinder regulator, it was found that

one cylinder of purge gas was sufficient to keep the glovebox in a state of constant purge for four or five days.

The procedure used to prepare the glovebox samples was followed exactly each day of sample preparation. While sitting on the benchtop, the 50.00 mL volumetric flask was filled to the mark with MQ water. A number of “long” tubes sufficient for the day’s irradiations and blanks were rinsed well with MQ water, and an equal number of aluminum foils, septa and open-top caps were prepared. The volumetric flask, foils, septa, caps and tubes were introduced into the side airlock box of the glovebox, which was then purged with industrial O₂ or N₂ for 45 minutes. Next, the flask, foils, septa, caps and tubes were introduced into the inner chamber of the glovebox. The volumetric flask was sparged with O₂ (BOC Group, grade 4.7) or N₂ (BOC Group, grade 4.8) for one hour. After sparging, a 50.0 µL aliquot of benzene (Fisher, ACS grade, thiophene free) was added to the volumetric flask inside the glovebox. A small volume of benzene (50 mL) and a precalibrated GC syringe were stored inside the glovebox for this purpose. The flask was shaken for two minutes and allowed to stand undisturbed for 15 minutes in the glovebox. Samples were immediately prepared by pipetting 5.000 mL aliquots from the 50.00 mL volumetric flask into “long” sample tubes using a class A volumetric pipet. Each tube was closed with a foil, a septum, and a cap. As before, each cap was closed as tightly as possible in order to minimize evaporation of the benzene. Care was taken so that the pressure of the gas in the headspace was as close to atmospheric as possible. Lastly, the 50.00 mL volumetric flask and prepared samples were removed from the glovebox, which was then returned to a state of constant purge. Samples prepared in the glovebox in which the aqueous layer was saturated with either O₂ or N₂, and the

headspace was filled with the respective gas, are referred to as "long oxygen tubes" and "long nitrogen tubes" throughout the remainder of this work. As was the case with long air tubes, these "long" glovebox samples consisted of 5.000 mL of solution and 11.0 mL of headspace volume.

Experimental Techniques

Sample irradiation procedure

After the dose rate had been determined using sample geometry B, as described in Chapter 3, aqueous benzene samples were irradiated using an inner sample position of the solid-block aluminum sample holder. Short air tubes were irradiated for up to 10 hours, which corresponded to a total dose of 4.2 Mrad. Long tubes (air, O₂ and N₂) were irradiated for up to 48 hours, which corresponded to a total dose of 18.1 Mrad. Decay corrections were taken into account so that each sample tube received the desired dose. The inclusion of decay corrections for equivalent doses to be absorbed necessitated the exposure of sample tubes for longer and longer times as the source decayed. The practical application of decay corrections was described in Chapter 3.

Sample development procedure

Samples were analyzed via HPLC immediately upon removal from the irradiator. This development procedure was described in Chapter 4 as the "prompt development" technique. The HPLC instrumental setup used for the entirety of this portion of the project consisted of an ISCO HPLC pump (model 2300) equipped with an ISCO UV-VIS detector (model V⁴), which was set to a wavelength of 255 nm for all elutions. This wavelength of light was selected using the deuterium setting on the detector. The pump was equipped with a VALCO injector (model C6W) fitted with an ISCO 10 µL injection loop, which was filled using a 50 µL HPLC syringe. All chromatograms were obtained

via a Linear chart recorder (model 500), which was set to a full-scale voltage setting of 10 mV and a chart speed of 1 cm per minute for all runs.

Separation of reactant benzene and radiolysis products was made using a Whatman PAH HPLC column (model 4691-2721), a reverse phase column packed with 5 μ m particles of C-18. The dimensions of the column are 25 cm \times 5 mm. The designation PAH signifies that the column has been optimized for the separation of polyaromatic hydrocarbons.

Because the instrument was an isocratic HPLC system, seven mobile phases of MQ water and Methanol (Fisher, HPLC grade) were used for elutions: 25/75, 33/66, 40/60, 50/50, 60/40, 66/33 and 75/25 (V/V percent water to percent methanol). A freshly irradiated sample was used for each mobile phase for each dose (time of irradiation). For example, determination of products for the "short air" system at one hour of irradiation required 7 irradiated tubes (one for each mobile phase); a freshly irradiated sample was used for each elution. The HPLC column was flushed with 100% methanol after each run in order to remove tightly held components. As a rule, experiments were repeated in at least triplicate to minimize the possibility of spurious results.

In order to eliminate detector drift, an aqueous solution of *ca.* 8.5 mM phenol was injected into the HPLC system before and after each run (both blank and irradiated samples). The purpose of the phenol standard was to serve as a pseudo-internal standard. In this manner, any long-term drift of the detector could be observed and all resulting peak areas could be drift corrected. Fresh aqueous phenol solutions were prepared biweekly because aqueous phenol solutions decompose slowly over time. Care was taken so that the concentration of each phenol standard solution reasonably approximated

the concentration of phenol in irradiated samples, at least within a factor of 10 to 20 times. Phenol was chosen to serve as an internal standard for two reasons: phenol was a product in the radiolysis system and would have to be quantified in any event, and phenol was found to elute within a reasonable elution time using any of the 7 mobile phase compositions. Using the Whatman column, phenol was found to elute within 5 minutes while using the fastest mobile phase, 25/75, and within 16 minutes while using the slowest mobile phase, 75/25. Thus, the phenol standard solution could be injected into the HPLC and eluted within a reasonable elution time irrespective of the mobile phase composition.

Sample quantitation procedure

Reactant benzene and radiolysis products were identified based on retention times in a minimum of two different mobile phase compositions. By using two or more mobile phases, the probability of product misidentification was minimized. Quantitation was made possible by preparing and injecting standard solutions of each identified compound. Analytical grade reagents were used in the preparation of standard solutions. The mobile phase composition that resulted in maximum resolution was used to prepare each standard solution. The standard solutions were injected into the HPLC using the same mobile phase for elution as was used for standard solution preparation.

The response of the detector to standard phenol solutions was used to eliminate detector drift in the following manner. On any particular day of experimentation, an approximately 8.5 mM solution of phenol was injected into the HPLC before and after each sample injection. The purpose of injecting the standard phenol solution before and after each sample injection was to "bracket" the response of the detector. If the detector response, as noted by peak area of the standard phenol solution, was the same before and

after the elution of the sample, then the probability of significant detector drift during the elution of the sample was minimal. Continual use of the ISCO V⁴ detector revealed that the response was reasonably constant throughout the day to within $\pm 3\%$, but did vary by $\pm 10\%$ from day to day.

Standard solutions of phenol, radiolysis products and reactant benzene were injected into the HPLC in order to calculate a response factor, relative to phenol, for each compound. The response factor for a generic compound X, relative to phenol, was determined by injecting a standard solution of compound X and a standard solution of phenol on the same day. The response factor, f_x , for the compound relative to phenol was then calculated. For the phenol standard, the peak area, A_p , detector attenuation setting, s_p , and concentration, C_p , were determined. In addition, the peak area, A_x , detector attenuation setting, s_x , and concentration of the standard, C_x , were calculated for the generic compound X. For each compound, the peak area was multiplied by the ratio of the detector attenuation setting used for the peak to the detector's maximum attenuation setting, 0.002. This conversion resulted in the determination of the normalized peak area, A' , which would equal the peak area had all compounds been eluted using the detector's maximum attenuation setting of 0.002. Using phenol as an example,

$$A'_p = A_p \frac{s_p}{0.002} \quad (99)$$

The response factor for phenol, f_p , was then calculated by dividing the normalized peak area, A'_p , by the concentration of the phenol solution, C_p .

$$f_p = \frac{A'_p}{C_p} \quad (100)$$

This calculation was repeated for all other radiolysis products as well as for reactant benzene.

A response factor ratio, F , relative to phenol was determined for each compound. Using the generic compound X , the response factor ratio was calculated by dividing the response factor of the compound, f_X , by the response factor of phenol, f_p .

$$F_X = \frac{f_X}{f_p} = \frac{A'_X C_p}{A'_p C_X} \quad (101)$$

Once the response factor ratio had been determined for each compound relative to phenol, the chromatographic data from each experimental run were used to determine the concentration of each radiolysis product. The data from the phenol standard used to bracket the detector response for the particular run and the data from the radiolysis product were analyzed. For the phenol standard, the peak area, A_p , detector attenuation setting, s_p , and concentration, C_p , were noted. Equivalent quantities were noted for the compound of interest. Using benzene as an example, the peak area, A_B , detector attenuation setting, s_B , and response factor ratio, F_B , were used to calculate the concentration of benzene in the solution. After the normalized peak area of each compound was determined as previously shown, the concentration of benzene was calculated:

$$C_B = \frac{A'_B C_p}{A'_p F_B} \quad (102)$$

This procedure was used to calculate the concentrations of all identified compounds in each irradiated solution. Lastly, the number of μ moles of each component in solution, n_X , was calculated by multiplying the concentration in μ moles per mL, C_X , by the sample volume, V_S .

$$n_x = C_x * V_s \quad (103)$$

Results

For each system, the concentrations of "typical" first generation radiolysis products as well as reactant benzene were determined in hopes of observing a shift in mechanistic pathway as a function of headspace volume and gas. Results for the four systems are listed in the following section. All discussion and rationalization are presented in Chapter 7.

Short air system

For the short air system, the amount of benzene in solution was measured as a function of absorbed dose. Phenol was found to be the major identified product. Biphenyl was also found among the radiolysis mixture. Lastly, 3-phenylphenol and 4-phenylphenol were quantified at each dose. Table 9 contains the amounts of products found in solution (in μmoles) at each dose (in Mrad) for the short air system.

Long oxygen system

For the long oxygen system, reactant benzene and the same radiolysis products were quantified at each absorbed dose: phenol, biphenyl, 3-phenylphenol and 4-phenylphenol. The amounts of each compound present in solution (in μmoles) versus dose (in Mrad) for the long oxygen system are listed in Table 10.

Long air system

For the long air system, the amount of benzene in solution was calculated at each absorbed dose. As in the short air system, phenol was found to be the major identified product. Biphenyl, 3-phenylphenol and 4-phenylphenol were found among the radiolysis mixture. Table 11 contains the amounts of these compounds (in μmoles) versus dose (in Mrad) for the long air system.

Long nitrogen system

For the long nitrogen system, the amounts of benzene and phenol in solution were determined for each absorbed dose. The amounts of benzene and phenol in solution (in μmoles) versus dose (in Mrad) for the long nitrogen system are listed in Table 12.

Strikingly, Biphenyl and the two aforementioned phenylphenols were not observed in this system.

Table 9: Listing of μmoles of compound in solution versus dose in Mrad for the short air system.

Dose (Mrad)	Benzene (μmoles)	Phenol (μmoles)	Biphenyl (μmoles)	3-Phenylphenol (μmoles)	4-Phenylphenol (μmoles)
0	55.2	0	0	0	0
0.408	46.3	1.437	0.2888	0.007361	0.02759
0.817	39.8	2.423	0.7263	0.02875	0.06743
1.22	29.8	2.757	0.7842	0.04399	0.09112
1.63	21.2	2.935	1.107	0.06521	0.1274
2.04	18.1	3.402	1.239	0.08742	0.1576
2.45	13.3	3.035	1.403	0.09936	0.1882
3.27	5.66	2.063	1.264	0.09959	0.1837
4.08	0.813	0.6262	1.192	0.05233	0.1256

Table 10: Listing of μmoles of compound in solution versus dose in Mrad for the long oxygen system (LOD = Limit of Detection).

Dose (Mrad)	Benzene (μmoles)	Phenol (μmoles)	Biphenyl (μmoles)	3-Phenylphenol (μmoles)	4-Phenylphenol (μmoles)
0	37.8	0	0	0	0
0.376	20.1	2.46	0.415	0.0181	0.0347
0.751	23.8	3.33	1.08	0.0572	0.101
1.13	19.0	3.81	1.37	0.0861	0.148
1.50	17.7	4.40	1.62	0.115	0.195
1.88	15.8	4.20	1.64	0.123	0.216
2.25	12.5	3.70	1.70	0.126	0.216
3.00	7.85	3.17	1.78	0.124	0.237
3.76	3.96	1.73	1.57	0.0719	0.220
5.63	1.98	0.792	0.851	0.0550	0.176
9.01	< LOD	< LOD	0.500	0.0271	0.102
13.5	< LOD	< LOD	0.364	0.0169	0.0802
18.0	< LOD	< LOD	0.201	0.0127	0.0582

Table 11: Listing of μmoles of compound in solution versus dose in Mrad for the long air system (LOD = Limit of Detection).

Dose (Mrad)	Benzene (μmoles)	Phenol (μmoles)	Biphenyl (μmoles)	3-Phenylphenol (μmoles)	4-Phenylphenol (μmoles)
0	38.6	0	0	0	0
0.376	32.2	1.11	0.364	0.0127	0.0265
0.751	27.7	1.82	0.712	0.0312	0.0572
1.13	20.8	2.06	0.993	0.0480	0.0791
1.50	15.9	2.21	1.26	0.0603	0.0973
1.88	11.2	1.61	1.34	0.0754	0.120
2.25	8.17	1.19	1.37	0.0787	0.132
3.00	5.84	0.972	1.23	0.0712	0.138
3.76	3.54	0.570	0.588	0.0344	0.0769
5.63	1.04	0.281	0.363	0.0159	0.0381
9.01	< LOD	< LOD	0.221	0.00829	0.0258
13.5	< LOD	< LOD	0.109	0.00441	0.0187
18.0	< LOD	< LOD	0.0481	0.00151	0.00999

Table 12: Listing of μmoles of compound in solution versus dose in Mrad for the long nitrogen system (LOD = Limit of Detection).

Dose (Mrad)	Benzene (μmoles)	Phenol (μmoles)	Biphenyl (μmoles)	3-Phenylphenol (μmoles)	4-Phenylphenol (μmoles)
0	37.6	0	0	0	0
0.376	28.9	0.646	< LOD	< LOD	< LOD
0.751	22.3	1.22	< LOD	< LOD	< LOD
1.13	19.1	1.70	< LOD	< LOD	< LOD
1.50	13.7	1.83	< LOD	< LOD	< LOD
1.88	11.0	1.47	< LOD	< LOD	< LOD
2.25	8.27	0.964	< LOD	< LOD	< LOD
3.00	5.80	0.205	< LOD	< LOD	< LOD
3.76	3.05	0.114	< LOD	< LOD	< LOD
5.63	< LOD	0.0285	< LOD	< LOD	< LOD
9.01	< LOD	< LOD	< LOD	< LOD	< LOD
13.5	< LOD	< LOD	< LOD	< LOD	< LOD
18.0	< LOD	< LOD	< LOD	< LOD	< LOD

High Dose Rate Experiments for CO₂ Production

Sample Preparation Techniques

The solution preparation techniques that were followed for high dose rate studies were nearly identical to those used for low dose rate work. As before, “short air” and “long air” tubes were prepared on the benchtop, while “long oxygen” and “long nitrogen” tubes were prepared in the glovebox. The only difference in the sample preparation

technique was that the aluminum foil layer between the tube and septum was omitted. Experiments revealed that the presence of the thin aluminum foil layer prevented the formation of a seal that was sufficiently gas-tight to prevent the escape of radiolysis gases, namely CO_2 , formed over the timespan of several days of irradiation; however, the seal was sufficient to prevent the escape of gases formed over the timespan of 15 to 24 hours. For this reason, all samples used for studies relating to CO_2 production were sealed with septa and open screw-top caps only. Triple-layer, Teflon backed septa (Alltech, model 7848) were purchased for this purpose. Each septum was used once, and was discarded after being pierced for headspace analysis.

Experimental Techniques

Sample irradiation procedure

After the dose rate of the freshly charged irradiator had been determined by Fricke dosimetry using geometry C, as described in Chapter 3, aqueous benzene samples were irradiated using an inner sample position of the solid-block aluminum holder. Each sample tube was irradiated for times of two hours to a maximum of 7 days, which corresponded to a dose of 2.78 Mrad to 240 Mrad. Since the dose rate using geometry C was approximately four times the dose rate of geometry B, the longest irradiation time period of 7 days using geometry C was equivalent to approximately 28 days using geometry B.

Sample development procedure

Samples were developed immediately upon removal from the irradiator in order to determine the amount of radiolytically produced CO_2 (g). The headspace was removed in accordance with the procedure outlined in detail in Chapter 5. In this procedure, the irradiated tube was inverted and the headspace was withdrawn into a valved syringe by

displacing the headspace of the vial with 1 M H_2SO_4 . The contents of the valved syringe were injected into the gas chromatograph as described in Chapter 5.

Sample quantitation procedure

The gas chromatography procedure for the quantitation of CO_2 in a sealed radiolysis vessel, as described in Chapter 5, was applied to all samples. This procedure consisted of preparing a daily air calibration plot that was used to eliminate detector drift. The peak size of the radiolytically produced CO_2 peak, the detector's attenuation setting, and the slope ratio of CO_2 (relative to air) were used to calculate the number of μmoles of CO_2 in the headspace. This calculation was repeated for all high dose rate samples.

Results

The amount of radiolytically produced CO_2 was measured for each system in accordance with the procedure that was described in detail in Chapter 5. Table 13 contains the amount of CO_2 (in μmoles) versus dose (in Mrad) for each of the four systems studied: short air, long oxygen, long air and long nitrogen.

Table 13: Listing of μmoles of CO_2 versus dose in Mrad for each of the four systems (LOD = Limit of Detection).

Dose (Mrad)	Short Air (μmoles)	Long Oxygen (μmoles)	Long Air (μmoles)	Long Nitrogen (μmoles)
0	0	0	0	0
2.78	0.1291	0.8511	0.2028	< LOD
5.56	0.1882	1.003	0.5071	< LOD
8.34	0.2366	1.357	0.5320	< LOD
11.1	0.4947	3.901	0.8429	< LOD
20.8		11.55		0.4259
22.2		12.50		
22.9		17.11		
25.0		19.45		
33.3	4.768	45.03	7.063	4.365
58.4	12.61	66.86	32.66	6.368
100	19.36	119.0	44.33	12.57
167	27.80	177.1	90.11	26.61
233	35.78	185.0	102.3	41.95

GC-MS Experiments for Qualitative Determination of Trace Products

The gamma radiolysis of aqueous benzene solutions results in a complex product mixture, with several classes of products and isomers being formed. Many of the products are very low in concentration. For this reason, radiolysis experiments were undertaken with the radiolysis mixture analyzed using the instrumental technique of GC-MS in order to qualitatively identify radiolysis products.

Description of GC-MS Instrumentation

The GC-MS instrumental setup consisted of a Hewlett-Packard Gas Chromatograph (model 5890) that was coupled to a Hewlett-Packard Mass Analyzer (model 5971), a mass analyzer of the quadrupole design. The GC column used for separations was an HP-DB5, a moderately polar, open tubular, capillary column of dimensions 25 m (length) \times 0.52 mm (inner diameter). Elutions were performed using various temperature programs and injection volumes from 1 μ L to 5 μ L of solution. The method used for all runs was the QUALORG program, which controlled instrumental settings such as injector temperature, column temperature and mass analyzer settings. The output from the instrument consisted of a real-time chromatogram with mass spectral information available for each point on the chromatogram. The on-board mass spectral library file NBS-75K was used for mass fragmentation matching, which yielded compound identification. Hard-copies of the data were obtained via an HP 5L LaserJet printer.

Description of Experiments

Numerous radiolysis experiments were performed with the product mixture analyzed via GC-MS in hopes of determining qualitative identities of trace products. Three different types of sample cells and geometries were used for these experiments.

Geometry B experiments, GCMS1 – GCMS5

In experiments GCMS1 – GCMS4, air-saturated aqueous benzene samples were prepared by adding 50.0 μL benzene (Fisher ACS grade, thiophene free) to 50.00 mL MQ water in a 50.00 mL volumetric flask through the use of a precalibrated GC syringe. After mixing was complete, samples were prepared by pipetting 5.000 mL aliquots into “long” chromatography vials identical to those used in the large headspace studies listed earlier in this chapter. Each vial was capped with an layer of aluminum foil, a rubber septum and an open, screw-top cap. Samples were irradiated for specified times and doses as listed in Table 14 using geometry B. An inner-hole of the solid-block aluminum sample holder was used for irradiation. In experiments GCMS1, GCMS3 and GCMS4, the radiolysis mixtures were poured into 10 mL centrifuge tubes (Kimex) and centrifuged using a Fisher brand centrifuge for 30 minutes each because each sample contained a precipitate. Each tube was decanted, and the resulting pellet was dissolved in approximately 2.0 mL MeOH (Fisher, ACS grade). The MeOH solutions were dried over anhydrous Na_2SO_4 (Fisher, ACS grade). In experiment GCMS2, the radiolysis mixture was extracted by adding approximately 2 mL diethyl ether, Et_2O , (Fisher, ACS grade) to the radiolysis vessel and shaking. The organic layer was allowed to separate, removed from the vessel, and dried over anhydrous Na_2SO_4 .

In experiment GCMS5, an air-saturated aqueous benzene sample was prepared by pipetting 5.000 mL MQ water into a long chromatography vial. An aliquot of 50.0 μL benzene (Fisher, thiophene free) was added to the tube using a precalibrated GC syringe. The tube was shaken and irradiated. The volume of benzene used in this experiment resulted in a saturated solution. The sample was irradiated for 5.5 hours, which resulted in a dose of 1.07 Mrad. After irradiation, the radiolysis mixture was poured into a 10 mL

centrifuge tube (Kimex) and centrifuged for 30 minutes. The supernatant was removed, and the pellet was dissolved in a 2.0 mL volume of MeOH (Fisher, ACS grade). The MeOH solution was dried over anhydrous Na_2SO_4 (Fisher).

Experimental parameters such as length of irradiation, dose, and sample workup method for experiments GCMS1 – GCMS5 are listed in Table 14. For injections, aliquots of 1 μL to 3 μL were injected into the GC-MS instrumental setup previously described. Temperature programs consisting of holding the GC at 40°C for 5 minutes, then ramping the temperature at 4°C or 5°C per minute to a final temperature of 250°C were used for these experiments. The oven of the GC was held at 250°C for a minimum of 20 minutes after each experimental run in order to remove tightly held components.

Table 14: Experimental parameters for geometry B gas chromatography experiments GCMS1 – GCMS5.

Experiment Number	t_{irradn} (hours:minutes)	Dose (Mrad)	workup method
1	5:30	1.07	pellet in MeOH
2	7:30	1.56	extraction with Et_2O
3	15:00	2.91	pellet in MeOH
4	28:00	5.43	pellet in MeOH
5	5:30	1.07	pellet in MeOH

Geometry C experiments, GCMS6 – GCMS10

For experiments GCMS6 and GCMS7, two air-saturated aqueous benzene samples were prepared on the benchtop by adding a 50.0 μL aliquot of benzene (Fisher, thiophene free) to 50.00 mL MQ water in a 50.00 mL volumetric flask. Aliquots of 5.000 mL were pipetted into long chromatography vials. Each vial was capped with a foil covered septum and open-top screw cap. The two samples were irradiated using geometry C in an inner sample position of the solid aluminum block sample holder. Upon removal from the irradiator, the radiolysis mixture in vial 1 was poured into a

10 mL centrifuge tube (Kimex) and centrifuged for 30 minutes. The resulting pellet was dissolved in a 2.0 mL volume of MeOH (Fisher, ACS grade). To vial 2, a 2.0 mL volume of diethyl ether, Et₂O, (Fisher, ACS grade) was added and the vial was shaken. The layers were allowed to separate. The Et₂O layer was removed and dried over anhydrous Na₂SO₄ (Fisher, ACS grade). The MeOH pellet solution was used for experiment GCMS6, and the Et₂O extract solution was used for experiment GCMS7.

For experiments GCMS8 – GCMS10, three nitrogen-saturated samples were prepared in the glovebox following the procedure listed earlier in this chapter. In this procedure, 50.00 mL MQ water was sparged with nitrogen and 50.0 μ L benzene (Fisher, thiophene free) was added. After mixing, three samples were prepared in the glovebox by pipetting 5.000 mL aliquots of solution into long chromatography vials. Each vial was closed with a foil covered septum and open-top screw cap. Samples were removed from the glovebox and inserted into the irradiator an inner sample position of geometry C. After irradiation, the radiolysis mixture in vial 1 was poured into a 10 mL centrifuge tube (Kimex) and centrifuged for 30 minutes. The resulting pellet, which was only present in trace amount, was dissolved in a 2.0 mL volume of MeOH (Fisher, ACS grade). To vial 2, a 2.0 mL aliquot of Et₂O (Fisher, ACS grade) was added, and to vial 3, a 2.0 mL aliquot of CH₂Cl₂ (Fisher, ACS grade) was added. Vials 2 and 3 were shaken and the layers were allowed to separate. The organic layers were removed and dried over anhydrous Na₂SO₄ (Fisher, ACS grade).

Each solution was injected into the GC-MS setup previously described. Aliquots of 1 μ L to 3 μ L were used for injection. A temperature program consisting of holding the

temperature at 40°C for 5 minutes, ramping the temperature at 5°C per minute up to a final temperature of 250°C was used for these experiments.

Table 15 contains experimental parameters for experiments GCMS6 – GCMS10. Included in the table are time of irradiation, dose as determined by Fricke dosimetry, headspace gas and sample workup method.

Table 15: Experimental parameters for geometry C gas chromatography experiments GCMS6 – GCMS10.

Experiment Number	t _{irradn} (hours:minutes)	Headspace gas	Dose (Mrad)	workup method
6	2:00	Air	2.4	pellet in MeOH
7	2:00	Air	2.4	extraction with Et ₂ O
8	2:00	N ₂	2.4	pellet in MeOH
9	2:00	N ₂	2.4	extraction with Et ₂ O
10	2:00	N ₂	2.4	extraction with CH ₂ Cl ₂

Roundbottom flask low dose rate experiments. GCMS11 – GCMS14

For experiment GCMS11, a volume of 450 mL MQ water was placed inside a 500 mL roundbottom flask on the benchtop. This flask had been modified to serve as a radiolysis vessel. A cross-section diagram of this vessel showing the center source hole and exit (fill) port is shown in Figure 37. An aliquot of 3.000 mL benzene (Fisher, thiophene free) was added to the flask. This amount of benzene resulted in a saturated solution. The exit port of the vessel was stoppered using a foil covered cork and wrapped with parafilm (American National Can). The vessel was irradiated for 66 hours using the older, decayed source that was used in geometry B. Since this vessel was never used with Fricke dosimetry, the exact dose rate is unknown. However, the average dose rate throughout the volume of the vessel is much lower than that of geometry B. After

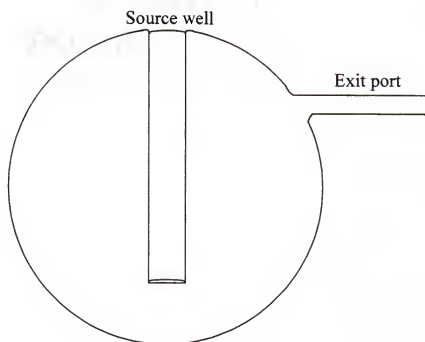


Figure 37: Cross section of the 500 mL roundbottom flask modified for use as an irradiation vessel.

irradiation, the entire radiolysis mixture was poured into a 500 mL separatory funnel. A small portion of concentrated NaCl solution was added, and the organic products were extracted using 3×25 mL volumes of CH_2Cl_2 (Fisher, ACS grade). The organic extracts were combined and dried over anhydrous Na_2SO_4 (Fisher, ACS grade).

In experiments GCMS12 – GCMS14, a volume of 450 mL MQ water was placed inside the same 500 mL modified roundbottom flask on the benchtop. To this vessel, an aliquot of 3.000 mL benzene (Fisher, thiophene free) was added, which resulted in a saturated solution. The exit port on the vessel was stoppered using a foil covered cork and wrapped with parafilm (American National Can). The vessel was irradiated using the weaker source that was used in geometry B for a total of 11 days. Upon removal from the irradiator, the radiolysis mixture had separated into two layers: an aqueous layer and a solid precipitate layer. The aqueous layer was decanted and poured into a 500 mL separatory funnel. The aqueous layer was acidified with 1 M HCl and extracted with 3×20 mL aliquots of CH_2Cl_2 (Fisher, ACS grade). The organic layers were combined and dried over anhydrous Na_2SO_4 (Fisher, ACS grade). A small portion of the solid precipitate layer was dissolved in acetone (Fisher, ACS grade). The acetone solution was dried over anhydrous Na_2SO_4 (Fisher, ACS grade). The acetone dissolved precipitate solution was used for experiment GCMS12, and the CH_2Cl_2 extract solution was used for experiments GCMS13 and GCMS14.

In experiments GCMS11 – GCMS13, aliquots of 1 μL to 3 μL were injected into the GC-MS apparatus previously described. A temperature program consisting of holding the oven at 40°C for 5 minutes, ramping the temperature at 5°C per minute up to 250°C , and holding the temperature at 250°C for 5 minutes was used for these injections.

In experiment GCMS14, a “wet-needle” injection was made of the CH_2Cl_2 extract solution used in GCMS13. A “wet-needle” injection is made by drawing 1 μL of solution into the GC syringe, and then expelling the 1 μL . Several 5 μL volumes of air are then drawn into and expelled from the syringe. Finally, a volume of 1 μL of air is injected into the GC unit. Since the needle of the syringe is still “wet” with solution even after two or three “pumps” of air, a very small amount of solution is injected into the GC. When making a “wet-needle” injection, the solvent-delay of the GC-MS unit is over-ridden. This command instructs the instrument to begin acquiring mass spectral data immediately. Normally, the solvent delay is never over-ridden, for the large volume of solvent (~1 to 10 nL assuming a 1 μL injection and a 1:100 injection split) is far too large for the MS unit to process. Over-riding the solvent delay during a normal injection will cause the MS unit to shut down and the run must be discarded. For experiment GCMS14, a “wet-needle” injection was made and the components were eluted isothermally at 40°C. The run was allowed to proceed for approximately 5 minutes, after which the column was baked at 250°C for a minimum of 30 minutes.

Results

For each experiment, a chromatogram was obtained via the LaserJet printer attached to the system. The onboard computer mass spectral library file NBS-75K was used to qualitatively identify peaks on the chromatogram. The computer spectral search program returned a “qual” number with each peak identification. The qual number is an indicator of the probability of certain match and ranges from 0 (no match) to 100 (near perfect match). Each of the following data tables is arranged in order of decreasing qual number. It is recommended that the data tables be interpreted in the following manner: compounds with qual numbers greater than 70 should be considered as likely products,

compounds with qual numbers between 40 and 70 should be viewed with skepticism but still considered as possible products, and compounds with qual numbers less than 40 should be considered as unlikely products. Compounds with qual numbers less than 40 were included in the data tables by the author for the sake of completeness.

In addition, a short summary of the experimental parameters such as headspace gas, benzene concentration, irradiation geometry, absorbed dose and sample workup method is included below the caption of each GC-MS chromatogram.

Experiments GCMS1 – GCMS5

The chromatograms obtained in experiments GCMS1 – GCMS5 are shown in Figure 38-Figure 42. Typical radiolysis products include benzaldehydes, phenol, biphenyl, reduced biphenyls, terphenyls, phenylphenols, naphthalenes and alkyl benzenes. Complete listings of identifications are tabulated in Table 16-Table 20.

Experiments GCMS6 – GCMS10

The chromatograms obtained in experiments GCMS6 – GCMS10 are shown in Figure 43-Figure 47. Typical radiolysis products include phenol, biphenyl, reduced biphenyls, naphthalenes, alkenes and aldehydes. Complete tabulations of radiolysis compounds are given in Table 21-Table 25. Also listed as an identified compound is butylated hydroxytoluene, an additive that is dissolved into diethyl ether for stabilization.

Experiments GCMS11 – 14

The chromatograms obtained in experiments GCMS11 – GCMS14 are shown in Figure 48-Figure 51. Typical radiolysis products for experiment GCMS11 include reduced benzenes, phenol, biphenyl, reduced biphenyls, naphthalenes, hydroxybiphenyls, anthracenes and terphenyls. A complete listing of products from GCMS11 is given in Table 26. Typical radiolysis products for experiment GCMS12 include hexadienes,

phenol, biphenyl, reduced biphenyls, hydroxybiphenyls, naphthalenes, and several ring-opened products. Table 27 gives a complete list of products in GCMS12. Typical radiolysis products for experiment GCMS13 include those listed in GCMS11 and 12 as well as pentanal, pentanone and hexanone derivatives. Table 28 contains a complete listing of the products found in experiment GCMS13. Products identified in the "wet-needle" experiment GCMS14 include hexadienes, acetone, salicyl alcohol, benzenecarboperoxoic acids, hexanones and methyl pentanones (ring-opened products). A complete listing is given in Table 29.

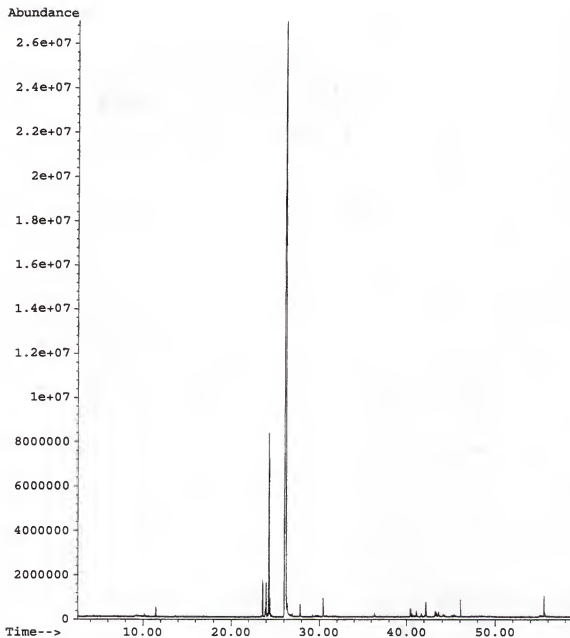


Figure 38: GC-MS chromatogram for experiment GCMS1.

In this experiment, a “long air” aqueous benzene sample of concentration 11.20 mM was irradiated to an absorbed dose of 1.07 Mrad using geometry B. The sample was centrifuged. The resulting pellet was dissolved in MeOH and injected into the GC-MS unit.

Table 16: Mass spectral data for experiment GCMS1.

Retention Time (min)	Compound Name	Molecular Formula	Molecular Weight	Qual Number
24.001	Benzene, 1-cyclohexen-1-yl-	C ₁₂ H ₁₄	158	95
24.328	Benzene, 1,4-cyclohexadien-1-yl-	C ₁₂ H ₁₂	156	93
43.221	Benzene, 1,1'-(1,3,5-hexatriene-1,6-diyl)-	C ₁₈ H ₁₆	232	91
23.589	Benzene, 2,5-cyclohexadieny-1-yl-	C ₁₂ H ₁₂	156	90
36.357	m-Hydroxybiphenyl	C ₁₂ H ₁₀ O	170	81
11.488	Benzene, butoxy-	C ₁₀ H ₁₄ O	150	80
26.134	Biphenyl	C ₁₂ H ₁₀	154	80
23.911	2-Cyclopentene, 1-propanal-	C ₈ H ₁₂ O	124	78
41.122	o-Terphenyl	C ₁₈ H ₁₄	230	76
41.671	Bicyclo[3.1.0]hex-2-ene, 5,6-diphenyl-	C ₁₈ H ₁₆	232	74
40.439	Acenaphthylene, 1,2,2a,3,4,5-hexahydro-	C ₁₂ H ₁₄	158	50
10.154	Benzaldehyde	C ₇ H ₆ O	106	47
30.440	p-Hydroxybiphenyl	C ₁₂ H ₁₀ O	170	46
24.443	Benzene, 3-cyclohexen-1-yl	C ₁₂ H ₁₄	158	45
26.954	Naphthalene, 2,6-dimethyl-	C ₁₂ H ₁₂	156	42

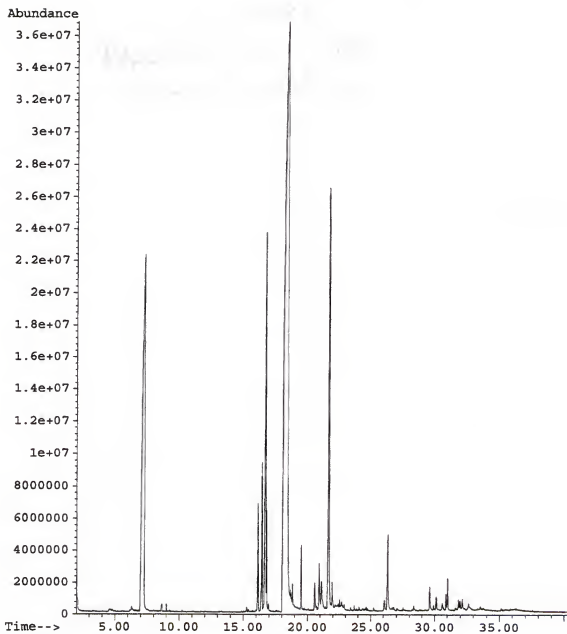


Figure 39: GC-MS chromatogram for experiment GCMS2.

In this experiment, a "long air" aqueous benzene sample of concentration 11.20 mM was irradiated to an absorbed dose of 1.56 Mrad using geometry B. The entire sample was extracted with Et₂O. The ether solution was injected into the GC-MS unit.

Table 17: Mass spectral data for experiment GCMS2.

Retention Time (min)	Compound	Molecular Formula	Molecular Weight	Qual Number
30.601	Benzene, 1,1'-(1,3,5-hexatriene-1,6-diyl)-	C ₁₈ H ₁₆	232	96
32.167	Bicyclo[3.1.0]hex-2-ene, 5,6-diphenyl-	C ₁₈ H ₁₆	232	96
16.123	Benzene, 2,5-cyclohexadien-1-yl-	C ₁₂ H ₁₂	156	95
16.421	Benzene, 1-cyclohexen-1-yl-	C ₁₂ H ₁₄	158	95
16.681	Benzene, 1,4-cyclohexadien-1-yl-	C ₁₂ H ₁₂	156	95
19.492	Benzene, 1,3-cyclohexadien-1-yl-	C ₁₂ H ₁₂	156	95
35.143	m-Terphenyl	C ₁₈ H ₁₄	230	95
18.306	Acenaphthene	C ₁₂ H ₁₀	54	94
26.311	p-Hydroxybiphenyl	C ₁₂ H ₁₀ O	170	94
21.629	o-Hydroxybiphenyl	C ₁₂ H ₁₀ O	170	93
8.645	Benzeneacetaldehyde	C ₈ H ₈ O	120	92
7.101	Phenol	C ₆ H ₆ O	94	91
18.196	Biphenyl	C ₁₂ H ₁₀	154	91
16.481	1-Phenyl-1-cyclohexene	C ₁₂ H ₁₄	158	90
16.826	Benzene, 3-cyclohexen-1-yl-	C ₁₂ H ₁₄	158	90
30.137	o-Terphenyl	C ₁₈ H ₁₄	230	90
27.522	Benzene, (1-ethyldecyl)-	C ₁₈ H ₃₀	246	86
20.904	Cyclohexanol, 2-phenyl	C ₁₂ H ₁₆ O	176	83
20.555	Naphthalene, 2-ethenyl-	C ₁₂ H ₁₀	154	81
6.319	Benzaldehyde	C ₇ H ₆ O	106	76
4.788	5-Hexenal	C ₆ H ₁₀ O	98	72
15.390	2-Norbomanone	C ₇ H ₁₀ O	110	72
24.090	Benzene, 2-heptynyl-	C ₁₃ H ₁₆	172	72
24.344	Benzophenone	C ₁₃ H ₁₀ O	182	70
28.358	Benzene, (1-methylundecyl)-	C ₁₈ H ₃₀	246	70
15.988	Dispiro[2.0.2.2]octane	C ₈ H ₁₂	108	68
16.336	5-Tetradecen-3-yne, (Z)	C ₁₄ H ₂₄	192	64
21.199	1,4-Ethanonaphthalen-2-ol, 1,2,3,4-tetrahydro-	C ₁₂ H ₁₄ O	174	64
21.941	Benzene, (methylenecyclopropyl)-	C ₁₀ H ₁₀	130	64
22.890	9-Methylbenzonorbomen-2-one	C ₁₂ H ₁₂ O	172	64
29.917	6-Hepten-2-one, 7-phenyl-	C ₁₃ H ₁₆ O	188	64
30.677	Benzene, 1,1'-(3-cyclohexen-1-ylidene)bis	C ₁₈ H ₁₈	234	62
4.531	Tridecanal	C ₁₃ H ₂₆ O	198	59
31.626	Bis(2-methoxyethyl), phthalate	C ₁₄ H ₁₈ O ₆	282	59
16.366	1,3,5-Dodecatriene	C ₁₂ H ₂₀	164	56
21.419	Acenaphthylene, 1,2,2a, 3,4,5-hexahydro-	C ₁₂ H ₁₄	158	55
23.698	Dodecane	C ₁₂ H ₂₆	150	55

25.240	Benzene, (1-ethylnonyl)-	$C_{17}H_{28}$	232	55
9.262	Acetophenone	C_8H_8O	120	53
32.632	Benzene, diethenyl-	$C_{10}H_{10}$	130	53
33.757	1,2,3,4-Tetrahydrobenz[A]anthracene	$C_{18}H_{16}$	232	51
16.960	2-Pentadecen-4-yne, (Z)	$C_{15}H_{26}$	206	50
24.653	Benzofuran, 3-methyl-2-(1-methylethenyl)	$C_{12}H_{12}O$	172	50
26.800	Benzene, (1-butyloctyl)-	$C_{18}H_{30}$	246	50
27.069	Benzene, (1-propylnonyl)-	$C_{18}H_{30}$	246	50
3.316	Cyclopentene, 1-ethyl-	C_7H_{12}	96	46
24.538	Benzene, (1-butylheptyl)-	$C_{17}H_{28}$	232	46
26.090	Benzene, (1-methyldecyl)-	$C_{17}H_{23}$	232	46
15.256	1,3-Cyclohexadiene	C_6H_8	80	43
16.561	Cis-Bicyclo[4.2.0]oct-3-en-7-one	$C_8H_{10}O$	122	42
21.825	Butylated Hydroxytoluene	$C_{15}H_{24}O$	220	42
22.680	Benzene, 1-hexynyl-	$C_{12}H_{14}$	158	42
26.690	Benzene, (1-pentylheptyl)-	$C_{18}H_{30}$	246	42
22.415	Benzene, diethenyl-	$C_{10}H_{10}$	130	41
24.762	Benzene, (1-propyloctyl)-	$C_{17}H_{28}$	232	38
22.510	1-Naphthol, 5,7-dimethyl-	$C_{12}H_{12}O$	172	35
22.176	Benzene, 2-heptynyl-	$C_{13}H_{16}$	172	30
14.856	Tetradecanoic acid, 2-hydroxy-, methyl ester-	$C_{15}H_{30}O_3$	258	22
11.696	4-Pentenoic acid, 2-acetyl-4-methyl-, methyl ester	$C_9H_{14}O_3$	170	12

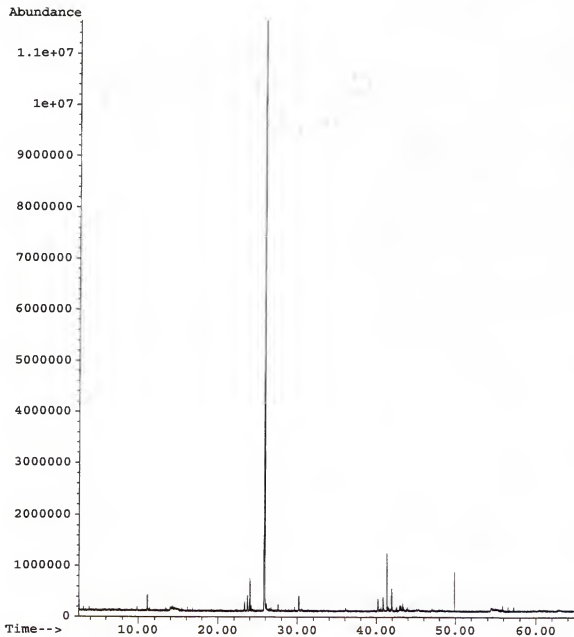


Figure 40: GC-MS chromatogram for experiment GCMS3.

In this experiment, a “long air” aqueous benzene sample of concentration 11.20 mM was irradiated to an absorbed dose of 2.91 Mrad using geometry B. The sample was centrifuged. The resulting pellet was dissolved in MeOH and injected into the GC-MS unit.

Table 18: Mass spectral data for experiment GCMS3.

Retention Time (min)	Compound	Molecular Formula	Molecular Weight	Qual Number
24.030	Benzene, 1,4-cyclohexadien-1-yl-	C ₁₂ H ₁₄	156	97
23.333	Benzene, 2,5-cyclohexadien-1-yl-	C ₁₂ H ₁₂	156	95
40.844	o-Terphenyl	C ₁₈ H ₁₄	230	92
11.097	Phenol	C ₆ H ₆	94	87
30.179	o-Hydroxybiphenyl	C ₁₂ H ₁₀ O	170	87
25.806	Biphenyl	C ₁₂ H ₁₀	154	80
23.738	Benzene, 1-cyclohexen-1-yl-	C ₁₂ H ₁₄	158	76
41.916	Bicyclo[3.1.0]hex-2-ene, 5,6-diphenyl-	C ₁₆ H ₁₆	232	64
26.099	Naphthalene, 2,6-dimethyl-	C ₁₂ H ₁₂	156	55
26.692	Benzene, 1,3-cyclohexadien-1-yl-	C ₁₂ H ₁₂	156	53
40.187	6-Hepten-2-one, 7-phenyl-	C ₁₃ H ₁₆ O	188	53
43.334	1,2,3,4-Tetrahydrobenz[A]anthracene	C ₁₈ H ₁₆	232	53
24.159	Benzene, 3-cyclohexen-1-yl	C ₁₂ H ₁₄	158	52
9.840	Benzaldehyde	C ₇ H ₆ O	106	47
27.590	Naphthalene, 2,7-dimethyl-	C ₁₂ H ₁₂	156	47
41.407	Benzene, 1,1'-(1,3,5-hexatriene-1,6-diyl)-	C ₁₈ H ₁₆	232	38
43.092	Naphthalene, 1,2-dihydro-	C ₁₀ H ₁₀	130	38
43.917	Acenaphthylene, 1,2,2a, 3,4,5-hexahydro-	C ₁₂ H ₁₄	158	38
36.108	p-Hydroxybiphenyl	C ₁₂ H ₁₀ O	170	35
47.032	p-Terphenyl	C ₁₈ H ₁₄	230	18
14.031	2-Heptanone, 6-methyl-	C ₈ H ₁₆ O	128	16
13.385	Benzeneacetaldehyde	C ₈ H ₈ O	120	10

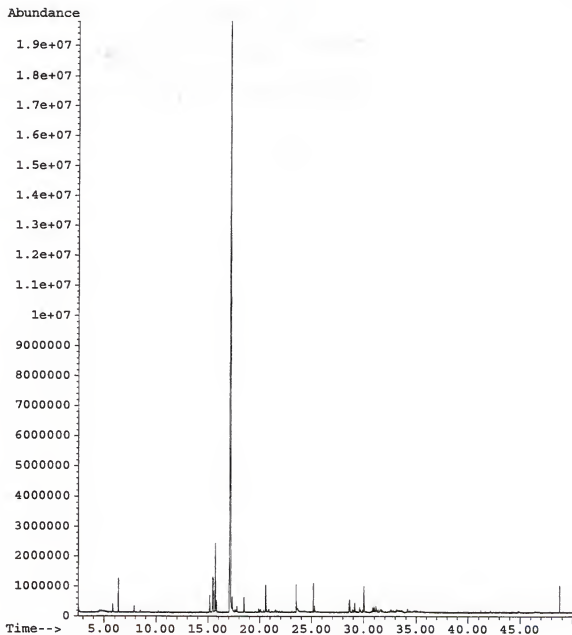


Figure 41: GC-MS chromatogram for experiment GCMS4.

In this experiment, a “long air” aqueous benzene sample of concentration 11.20 mM was irradiated to an absorbed dose of 5.43 Mrad using geometry B. The sample was centrifuged. The resulting pellet was dissolved in MeOH and injected into the GC-MS unit.

Table 19: Mass spectral data for experiment GCMS4.

Retention Time (min)	Compound	Molecular Formula	Molecular Weight	Qual Number
30.861	Benzene, 1,1'-(1,3,5-hexatriene-1,6-diyl-	C ₁₈ H ₁₆	232	94
15.456	Benzene, 1-cyclohexen-1-yl-	C ₁₂ H ₁₄	158	90
15.699	Benzene, 1,4-cyclohexadien-1-yl-	C ₁₂ H ₁₂	156	90
20.575	o-Hydroxybiphenyl	C ₁₂ H ₁₀ O	170	90
18.489	Benzene, 1,3-cyclohexadien-1-yl-	C ₁₂ H ₁₂	156	89
5.809	Benzaldehyde	C ₇ H ₆ O	106	87
6.337	Phenol	C ₆ H ₆ O	94	87
15.154	Benzene, 2,5-cyclohexadien-1-yl-	C ₁₂ H ₁₂	156	87
15.804	Benzene, 3-cyclohexen-1-yl-	C ₁₂ H ₁₄	158	87
17.128	Biphenyl	C ₁₂ H ₁₀	154	87
31.159	Bicyclo[3.1.0]hex-2-ene, 5,6-diphenyl	C ₁₈ H ₁₆	232	83
17.783	Naphthalene, 1,5-dimethyl	C ₁₂ H ₁₂	156	76
29.139	o-Terphenyl	C ₁₈ H ₁₄	230	72
34.154	p-Terphenyl	C ₁₈ H ₁₄	230	72
17.614	1-Phenyl-1-cyclohexene	C ₁₂ H ₁₄	158	70
7.887	Benzene, propyl	C ₉ H ₁₂	120	64
25.271	p-Hydroxybiphenyl	C ₁₂ H ₁₀ O	170	64
34.867	m-Terphenyl	C ₁₈ H ₁₄	230	64
15.426	Benzene, cyclohexyl	C ₁₂ H ₁₆	160	60
28.624	6-Hepten-2-one, 7-phenyl	C ₁₃ H ₁₆ O	188	50
20.046	Naphthalene, 1,2-dihydro	C ₁₀ H ₁₀	130	47
8.489	Acetophenone	C ₈ H ₈ O	120	46
23.512	3-Pentenoic acid, 4-methyl	C ₆ H ₁₀ O ₂	114	40
28.931	1,4-Ethanonaphthalen-2-ol, 1,2,3,4-tetra	C ₁₂ H ₁₄ O	174	40
20.863	Benzene, (methylenecyclopropyl)-	C ₁₀ H ₁₀	130	38
31.580	6-Hepten-2-one, 7-phenyl	C ₁₃ H ₁₆ O	188	38
19.887	Benzaldehyde, 4-pentyl-	C ₁₂ H ₁₆ O	176	30

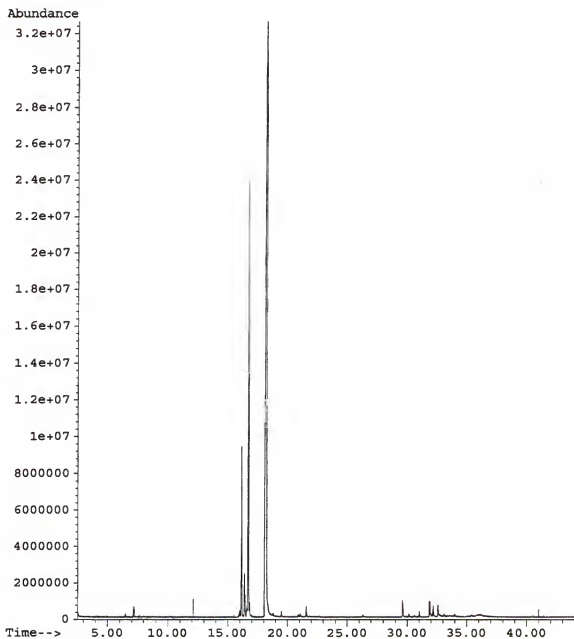


Figure 42: GC-MS chromatogram for experiment GCMS5.

In this experiment, an air-saturated, aqueous benzene sample was prepared by adding 50.0 μL benzene to 5.000 mL MQ water, which resulted in a saturated solution. The sample was irradiated to an absorbed dose of 1.07 Mrad using geometry B. The sample was centrifuged. The resulting pellet was dissolved in MeOH and injected into the GC-MS unit.

Table 20: Mass spectral data for experiment GCMS5.

Retention Time (min)	Compound	Molecular Formula	Molecular Weight	Qual Number
18.138	Biphenyl	C ₁₂ H ₁₀	154	98
16.694	Benzene, 2,5-cyclohexadien-1-yl-	C ₁₂ H ₁₄	156	97
16.450	1-Phenyl-1-cyclohexene	C ₁₂ H ₁₄	158	94
19.480	Benzene, 1,5-cyclohexadien-1-yl-	C ₁₂ H ₁₂	156	93
29.617	Benzene, 1,1'-(1,3,5-hexatriene-1,6-diyl)	C ₁₈ H ₁₆	232	93
32.173	Benzene, 1,1'-(1,3,5-hexatriene-1,6-diyl)	C ₁₈ H ₁₆	232	93
31.870	Bicyclo[3.1.0]hex-2-ene, 5,6-diphenyl	C ₁₈ H ₁₆	232	91
7.171	Phenol	C ₆ H ₆ O	94	90
16.151	Benzene, 2,5-cyclohexadien-1-yl-	C ₁₂ H ₁₂	156	90
21.572	o-Hydroxybiphenyl	C ₁₂ H ₁₀ O	170	90
30.146	o-Terphenyl	C ₁₈ H ₁₄	230	81
6.488	Benzaldehyde	C ₇ H ₆ O	106	76
16.814	Benzene, 3-cyclohexen-1-yl-	C ₁₂ H ₁₄	158	72
32.570	1-Naphthalenol, 1,2,3,4-tetrahydro	C ₁₀ H ₁₂ O	148	40

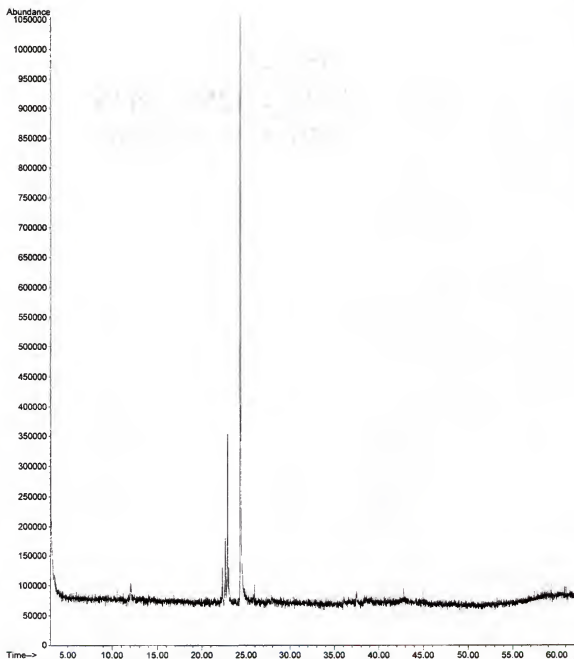


Figure 43: GC-MS chromatogram for experiment GCMS6.

In this experiment, a “long air” aqueous benzene sample of concentration 11.20 mM was irradiated to an absorbed dose of 2.4 Mrad using geometry C. The sample was centrifuged. The resulting pellet was dissolved in MeOH and injected into the GC-MS unit.

Table 21: Mass spectral data for experiment GCMS6.

Retention Time (min)	Compound	Molecular Formula	Molecular Weight	Qual Number
22.857	Benzene, (1,4-cyclohexadien-1-yl)-	C ₁₂ H ₁₂	156	97
22.604	Cyclohexene, 1-phenyl-	C ₁₂ H ₁₄	158	93
22.297	Benzene, 1,3-cyclohexadien-1-yl-	C ₁₂ H ₁₂	156	81
22.988	Benzene, 3-cyclohexen-1-yl-	C ₁₂ H ₁₄	158	76
24.424	Biphenyl	C ₁₂ H ₁₀	154	76
12.027	Phenol	C ₆ H ₆ O	94	72
22.769	1,3-Cyclohexadiene	C ₆ H ₈	80	72

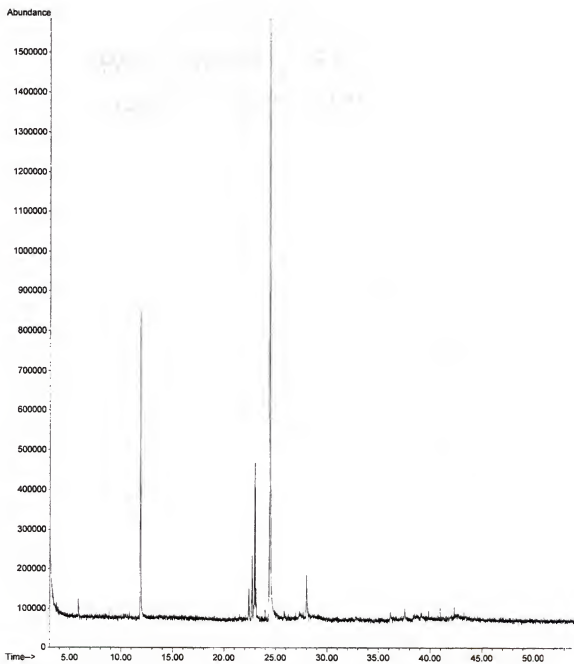


Figure 44: GC-MS chromatogram for experiment GCMS7.

In this experiment, a "long air" aqueous benzene sample of concentration 11.20 mM was irradiated to an absorbed dose of 2.4 Mrad. The entire sample was extracted with Et₂O. The ether solution was injected into the GC-MS unit.

Table 22: Mass spectral data for experiment GCMS7.

Retention Time (min)	Compound	Molecular Formula	Molecular Weight	Qual Number
22.698	Cyclohexene, 1-phenyl-	C ₁₂ H ₁₄	158	94
24.452	Biphenyl	C ₁₂ H ₁₀	154	93
11.857	Phenol	C ₆ H ₆ O	94	91
27.992	Butylated Hydroxytoluene	C ₁₅ H ₂₄ O	220	91
22.939	Benzene, 2,5-cyclohexadien-1-yl-	C ₁₂ H ₁₂	156	90
22.380	Benzene, 1,5-cyclohexadien-1-yl-	C ₁₂ H ₁₂	156	86
23.071	Benzene, 3-cyclohexen-1-yl-	C ₁₂ H ₁₄	158	59

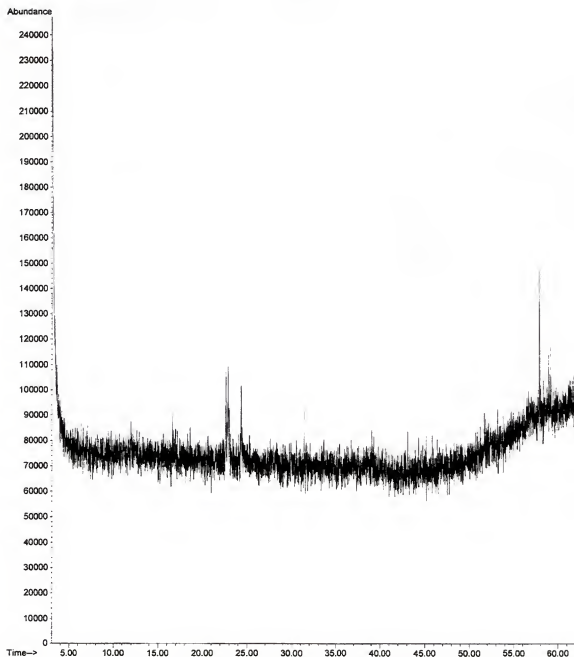


Figure 45: GC-MS chromatogram for experiment GCMS8.

In this experiment, a “long nitrogen” aqueous benzene sample of concentration 11.20 mM was irradiated to an absorbed dose of 2.4 Mrad using geometry C. The sample was centrifuged. The resulting pellet (present in trace quantity) was dissolved in MeOH and injected into the GC-MS unit.

Table 23: Mass spectral data for experiment GCMS8.

Retention Time (min)	Compound	Molecular Formula	Molecular Weight	Qual Number
22.852	Benzene, 2,5-cyclohexadien-1-yl-	C ₁₂ H ₁₂	156	92
22.622	Cyclohexene, 1-phenyl	C ₁₂ H ₁₄	158	81
24.321	Biphenyl	C ₁₂ H ₁₀	154	81
22.775	9,12,15-Octadecatrien-1-ol, (Z,Z,Z)-	C ₁₈ H ₃₂ O	264	68
22.995	Benzene, 3-cyclohexen-1-yl-	C ₁₂ H ₁₄	158	53

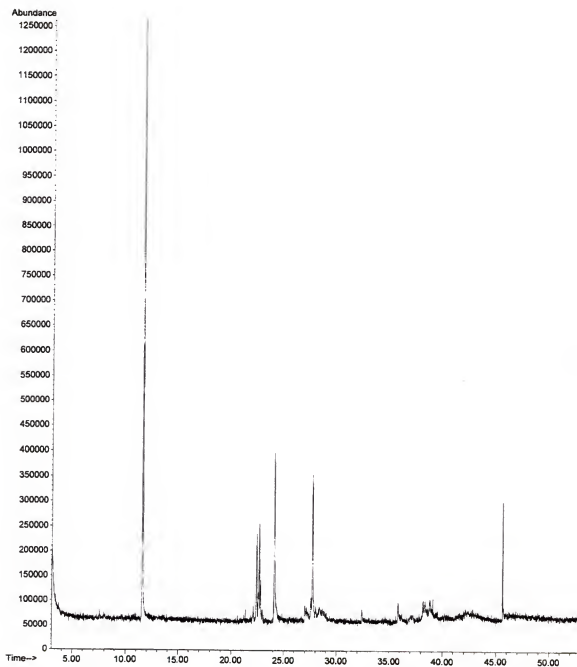


Figure 46: GC-MS chromatogram for experiment GCMS9.

In this experiment, a “long nitrogen” aqueous benzene sample of concentration 11.20 mM was irradiated to an absorbed dose of 2.4 Mrad using geometry C. The entire sample was extracted with Et₂O. The ether solution was injected in to the GC-MS unit.

Table 24: Mass spectral data for experiment GCMS9.

Retention Time (min)	Compound	Molecular Formula	Molecular Weight	Qual Number
22.651	Benzene, 2,5-cyclohexadien-1-yl-	C ₁₂ H ₁₂	156	97
27.705	Butylated Hydroxytoluene	C ₁₅ H ₂₄ O	220	95
11.600	Phenol	C ₆ H ₆ O	94	91
22.399	Cyclohexene, 1-phenyl	C ₁₂ H ₁₄	158	83
22.771	Benzene, 3-cyclohexen-1-yl-	C ₁₂ H ₁₄	158	81
24.098	Naphthalene, 2-ethenyl-	C ₁₂ H ₁₀	154	81
22.541	1,3,5-Dodecatriene	C ₁₂ H ₂₀	164	78
27.562	Biphenyl	C ₁₂ H ₁₀	154	74
22.092	Benzene, 1,3-cyclohexadien-1-yl-	C ₁₂ H ₁₂	156	64
38.197	Bicyclo[2.1.1]hexane, 1,4-diphenyl	C ₁₈ H ₁₈	234	43

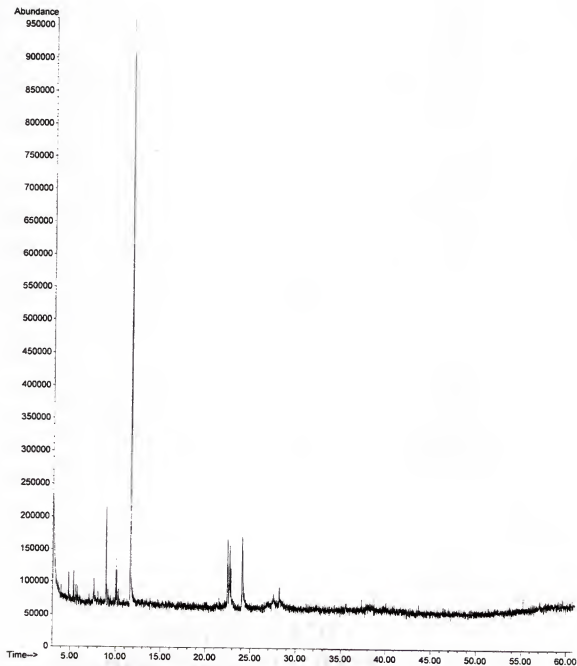


Figure 47: GC-MS chromatogram for experiment GCMS10.

In this experiment, a "long nitrogen" aqueous benzene sample of concentration 11.20 mM was irradiated to an absorbed dose of 2.4 Mrad using geometry C. The entire sample was extracted with CH_2Cl_2 . The methylene chloride solution was injected into the GC-MS unit.

Table 25: Mass spectral data for experiment GCMS10.

Retention Time (min)	Compound	Molecular Formula	Molecular Weight	Qual Number
22.700	Benzene, (1,4-cyclohexadien-1-yl)-	C ₁₂ H ₁₂	156	95
11.627	Phenol	C ₆ H ₆ O	94	91
22.459	Cyclohexene, 1-phenyl	C ₁₂ H ₁₄	158	90
24.081	Biphenyl	C ₁₂ H ₁₀	154	81
22.810	Benzene, 3-cyclohexen-1-yl-	C ₁₂ H ₁₄	158	76
8.919	2-Butenal, 3-methyl-	C ₅ H ₈ O	84	72
10.026	Cyclohexane, (1,2,2-trimethylbutyl)-	C ₁₃ H ₂₆	182	72
10.103	Cyclohexane, 1-methyl-2-propyl	C ₁₀ H ₂₀	140	64
4.808	2,3-Dimethyl-1-hexene	C ₈ H ₁₆	112	59
5.794	1,1'-Bicyclohexyl, 2-(2-methylpropyl)-	C ₁₆ H ₃₀	222	55
10.278	Phytol	C ₂₀ H ₄₀ O	296	53
22.579	1,4-Cyclohexadene-1-carboxylic acid, methyl ester-	C ₈ H ₁₀ O ₂	138	53
5.345	2-Hexene, 3,5,5-trimethyl-	C ₉ H ₁₈	126	49

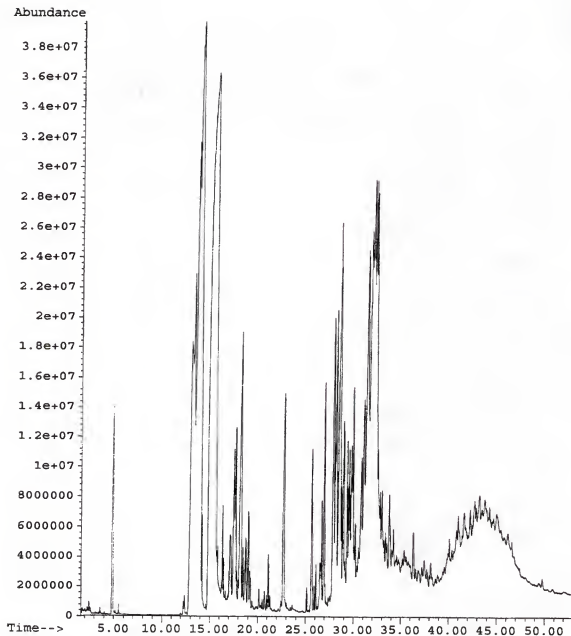


Figure 48: GC-MS chromatogram for experiment GCMS11.

In this experiment, volumes of 3.000 mL benzene and 450 mL MQ water were placed into a 500 mL roundbottom irradiation flask on the benchtop, which resulted in a saturated solution. The flask was irradiated for 66 hours using the old, weak source used in geometry B. The entire sample was extracted with CH_2Cl_2 . The methylene chloride solution was injected into the GC-MS unit.

Table 26: Mass spectral data for experiment GCMS11.

Retention Time (min)	Compound	Molecular Formula	Molecular Weight	Qual Number
26.104	o-Terphenyl	C ₁₈ H ₁₄	230	99
33.739	[1,1':3',1''-Terphenyl]-4'-ol	C ₁₈ H ₁₄ O	246	98
11.992	Benzene, 2,5-cyclohexadien-1-yl-	C ₁₂ H ₁₂	156	97
22.652	p-Hydroxybiphenyl	C ₁₂ H ₁₀ O	170	97
13.073	Benzene, 1,5-cyclohexadien-1-yl-	C ₁₂ H ₁₂	156	96
16.319	Benzene, (1,4-cyclohexadien-1-yl-)	C ₁₂ H ₁₂	156	96
14.055	Benzene, 3-cyclohexen-1-yl	C ₁₂ H ₁₄	158	94
15.245	Acenaphthene	C ₁₂ H ₁₀	154	93
17.509	Cyclohexanol, 2-phenyl	C ₁₂ H ₁₆ O	176	93
31.047	m-Terphenyl	C ₁₈ H ₁₄	230	92
1.588	Octane	C ₈ H ₁₈	114	91
2.483	1,3,5,7-Cyclooctatetraene	C ₈ H ₈	104	91
4.825	Phenol	C ₆ H ₆ O	94	91
14.763	Biphenyl	C ₁₂ H ₁₀	154	91
18.245	o-Hydroxybiphenyl	C ₁₂ H ₁₀ O	170	91
3.584	Benzaldehyde	C ₇ H ₆ O	106	90
25.123	Benzene, 1,1'-(1,3,5-hexatriene-1,6-diyl	C ₁₈ H ₁₆	232	90
32.340	Naphth[1,2-b]oxirene, 1a,2,3,7b-tetrahydro	C ₁₀ H ₁₀ O	146	87
2.577	Benzene, 1,2-dimethyl	C ₈ H ₁₀	106	83
12.805	2-Cyclopentene-1-propanal	C ₈ H ₁₂ O	124	83
1.652	Benzene	C ₆ H ₆	78	81
33.520	1,1'-Biphenyl, phenoxy-	C ₁₈ H ₁₄ O	246	81
1.996	1,3-Hexadien-5-yne	C ₆ H ₆	78	80
2.070	1,3,5-Cyclooctatriene	C ₈ H ₁₀	106	80
3.819	Cis-Bicyclo[4.2.0]octa-3,7-diene	C ₈ H ₁₀	106	78
12.362	3-Penten-1-yne, 3-methyl-, (Z)-	C ₆ H ₈	80	78
5.513	Benzeneacetaldehyde	C ₈ H ₈ O	120	76
22.437	[1,1'-Biphenyl]-3-ol	C ₁₂ H ₁₀ O	170	76
3.299	Cyclohexane, 1,3-bis(methylene)-	C ₈ H ₁₂	108	72
4.383	2,4-Hexadiyne	C ₆ H ₆	78	72
25.719	Benzene, 1,3-diethenyl	C ₁₀ H ₁₀	130	72
15.723	Naphthalene, 2-ethenyl-	C ₁₂ H ₁₀	154	70
7.058	Cyclohexane, 1,3-bis(methylene)-	C ₈ H ₁₂	108	64

17.695	Benzene, (1-methyl-2-cyclopropen-1-yl)-	$C_{10}H_{10}$	130	64
20.131	Naphthalene, 1,2-dihydro-	$C_{10}H_{10}$	130	64
21.097	1-Naphthol, 6,7-dimethyl-	$C_{12}H_{12}O$	172	64
25.923	Acenaphthylene, 1,2,2a,3,4,5-hexahydro-	$C_{12}H_{14}$	158	64
28.739	Naphthalene, 1,2-dihydro	$C_{10}H_{10}$	130	64
6.318	1,3-Hexadien-5-yne	C_6H_6	78	59
13.616	1,3-Cyclohexadiene	C_6H_8	80	59
2.405	Cyclohexanol	$C_6H_{12}O$	100	58
28.572	1-Naphthalenol, 1,2,3,4-tetrahydro-	$C_{10}H_{12}O$	148	56
30.159	4b,5,6,10b,11,12-Hexahydrochrysene (cis)	$C_{18}H_{18}$	234	55
14.560	1,3-Cyclopentadiene, methyl-	C_6H_8	80	53
19.185	Benzofuran, 3-methyl-2-(1-methylethenyl)	$C_{12}H_{12}O$	172	50
26.424	Naphthalene, 1,4,6-trimethyl	$C_{13}H_{14}$	170	50
23.436	1,1-Diphenylbutane	$C_{16}H_{18}$	210	47
32.819	Naphthalene, 1,2-dihydro-1-phenyl	$C_{16}H_{14}$	206	47
23.640	1-Naphthol, 6,7-dimethyl	$C_{12}H_{12}O$	172	46
32.029	9,10-Dimethylanthracene	$C_{16}H_{14}$	206	46
14.150	2-Pentadecen-4-yne, (Z)	$C_{15}H_{26}$	206	45
18.720	Naphthalene, 2,-dimethyl-	$C_{12}H_{12}$	156	45
26.686	2-(2-Naphthyl)propanoic acid	$C_{13}H_{12}O_2$	200	43
29.753	Benzeneacetaldehyde, .alpha.-phenyl-	$C_{14}H_{12}O$	96	43
34.228	2-Cyclohexen-1-one, 4,4-diphenyl-	$C_{18}H_{16}O$	248	43
21.257	1,1-Diphenylpropane	$C_{15}H_{16}$	196	42
20.459	Benzene, 1,3,5-trimethyl-	C_9H_{12}	120	41
34.558	Benzaldehyde, 3-methoxy-	$C_8H_8O_2$	136	41
9.824	Benzene, 1-cyclopenten-1-yl	$C_{11}H_{12}$	144	38
26.570	Naphthalene, 2-methyl-1-propyl	$C_{14}H_{16}$	184	38
29.936	Naphthalene, 1,6-dimethyl-	$C_{12}H_{12}$	156	38
36.899	2-Propyn-1-ol, 3-(4-methylphenyl)-	$C_{10}H_{10}O$	146	38
38.160	1,2-Diphenylethylene	$C_{14}H_{12}$	180	38
18.635	Benzene, (3-methylcyclopentyl)-	$C_{12}H_{16}$	160	30

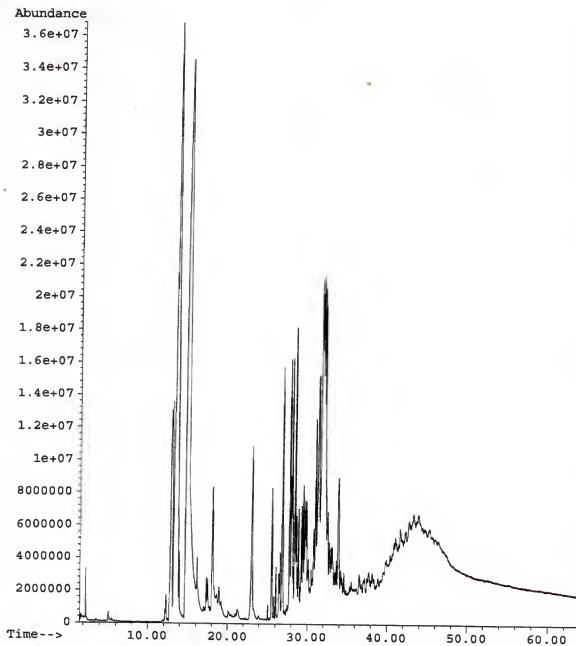


Figure 49: GC-MS chromatogram for experiment GCMS12.

In this experiment, volumes of 3.000 mL benzene and 450 mL MQ water were placed into a 500 mL roundbottom irradiation flask on the benchtop, which resulted in a saturated solution. The flask was irradiated for 11 days using the old, weak source used in geometry B. A small amount of the solids in the flask was dissolved in acetone. The acetone solution was injected into the GC-MS unit.

Table 27: Mass spectral data for experiment GCMS12.

Retention Time (min)	Compound	Molecular Formula	Molecular Weight	Qual Number
31.020	m-Terphenyl	C ₁₈ H ₁₄	230	98
32.522	[1,1':3',1''-Terphenyl]-2'-ol	C ₁₈ H ₁₄ O	246	98
33.829	[1,1':3',1''-Terphenyl]-4'-ol	C ₁₈ H ₁₄ O	246	97
13.019	Benzene, 1,4-cyclohexadien-1-yl-	C ₁₂ H ₁₂	156	95
12.869	Benzene, 2,5-cyclohexadien-1-yl-	C ₁₂ H ₁₂	156	94
23.016	[1,1'-Biphenyl]-3-ol	C ₁₂ H ₁₀ O	170	94
25.061	Benzene, 1,1'-(1,3,5-hexatriene-1,6-diyl)-	C ₁₈ H ₁₆	232	93
26.046	o-Terphenyl	C ₁₈ H ₁₄	230	93
33.605	1,1'-Biphenyl, phenoxy-	C ₁₈ H ₁₄ O	246	93
31.620	p-Terphenyl	C ₁₈ H ₁₄	230	92
13.742	Benzene, 3-cyclohexen-1-yl-	C ₁₂ H ₁₄	158	90
22.347	1,2-Diphenylethylene	C ₁₄ H ₁₂	180	90
15.098	Biphenyl	C ₁₂ H ₁₀	154	89
14.620	Naphthalene, 2-ethenyl	C ₁₂ H ₁₀	154	87
18.089	o-Hydroxybiphenyl	C ₁₂ H ₁₀ O	170	87
17.304	Trans-2-Phenyl-1-cyclohexanol	C ₁₂ H ₁₆ O	176	86
34.144	2,5-Cyclohexadien-1-one, 4,4-diphenyl-	C ₁₈ H ₁₄ O	246	80
12.285	1,3-Isobenzofurandione, 3a, 4,7,7a-tetrahydro-	C ₈ H ₈ O ₃	152	78
32.969	Bicyclo[3.1.0]hexan-2-one, 6,6-diphenyl-	C ₁₈ H ₁₆ O	248	76
5.272	Phenol	C ₆ H ₆ O	94	74
1.608	1,3-Hexadien-5-yne	C ₆ H ₆	124	72
5.085	Acetic acid, phenyl ester	C ₈ H ₈ O ₂	136	72
25.871	6-Hepten-2-one, 7-phenyl-	C ₁₃ H ₁₆ O	188	72
3.562	2,5-Heptadiyn-4-one	C ₇ H ₆ O	106	64
17.459	Benzene, 1,3-diethenyl	C ₁₀ H ₁₀	130	64
20.102	9-Methylbenzonorbornen-2-one	C ₁₂ H ₁₂ O	172	64
26.910	Bicyclo[3.1.0]hex-2-ene, 5,6-diphenyl-	C ₁₈ H ₁₆	232	64
29.726	Benzene, 1,1'-(3-methylbutylidene)bis-	C ₁₇ H ₂₀	224	64
37.048	Bicyclo[3.1.0]hex-3-en-2-one, 6,6-diphenyl-	C ₁₈ H ₁₄ O	246	64
23.351	p-Hydroxybiphenyl	C ₁₂ H ₁₀ O	170	60
32.181	1(2H)-Naphthalenone, 3,4-dihydro-	C ₁₀ H ₁₀ O	146	58

28.448	1-Naphthalenol, 1,2,3,4-tetrahydro-	C ₁₀ H ₁₂ O	148	56
28.737	Acenaphthylene, 1,2,2a,3,4,5-hexahydro-	C ₁₂ H ₁₄	158	55
31.849	Phenanthrene, 2,7-dimethyl-	C ₁₆ H ₁₄	206	55
2.421	Salicyl Alcohol	C ₇ H ₈ O ₂	124	53
13.243	2-Cyclopentene-1-propanal	C ₈ H ₁₂ O	124	53
29.132	2-Cyclohexen-1-one, 4,4-diphenyl	C ₁₈ H ₁₆ O	248	51
10.652	Naphthalene, 1,4,5,8-tetrahydro-	C ₁₀ H ₁₂	132	50
28.160	Benzene, diethenyl-	C ₁₀ H ₁₀	130	50
17.773	Acenaphthylene, 1,2,2a,3,4,5-hexahydro-	C ₁₂ H ₁₄	158	49
37.210	Benzeneacetaldehyde, .alpha.-phenyl-	C ₁₄ H ₁₂ O	196	49
28.601	2-Pentenoic acid, 5-phenyl-, methyl ester	C ₁₂ H ₁₄ O ₂	190	47
29.021	2-(2-Naphthyl)propanoic acid	C ₁₃ H ₁₂ O ₂	200	47
38.075	Benzenepropanol, .gamma.-phenyl-	C ₁₅ H ₁₆ O	212	47
14.412	Benzene, 1,3-cyclohexadien-1-yl-	C ₁₂ H ₁₂	156	46
23.910	1-Naphthol, 6,7-dimethyl-	C ₁₂ H ₁₂ O	172	46
20.998	Phenol, 4-cyclohexyl-	C ₁₂ H ₁₆ O	176	45
18.915	1H-Indene, 1-methyl-	C ₁₀ H ₁₀	130	44
1.805	2-Pentanone, 4-hydroxy-4-methyl-	C ₆ H ₁₂ O ₂	116	43
6.197	2,4-Hexadiyne	C ₆ H ₆	78	43
9.709	1,3,5-Cyclooctatriene	C ₈ H ₁₀	106	43
12.127	1,3,5-Hexatriene, (Z)-	C ₆ H ₈	80	43
20.470	Benzene, 2-heptynyl	C ₁₃ H ₁₆	172	43
32.069	Phenanthrene, 3,6-dimethyl-	C ₁₆ H ₁₄	206	43
13.887	2-Pentadecen-4-yne, (Z)-	C ₁₅ H ₂₆	206	42
30.122	Benzene, 1-methyl-4-(1-propynyl)-	C ₁₀ H ₁₀	130	42
32.939	Naphthalene, 1,2-dihydro-4-phenyl-	C ₁₆ H ₁₄	206	42
34.841	1-Phenyl-1-pentyne	C ₁₁ H ₁₂	144	40
5.504	Benzeneacetaldehyde	C ₈ H ₈ O	120	38
13.392	1,4-Cyclohexadiene	C ₆ H ₈	80	38
21.243	1-Naphthol, 6,7-dimethyl-	C ₁₂ H ₁₂ O	172	38
29.898	Naphthalene, 1,6-dimethyl-	C ₁₂ H ₁₂	156	38
38.416	Benzenepropanoic acid, .beta.-phenyl-	C ₁₅ H ₁₄ O ₂	226	38

31.315	Naphth[1,2-b]oxirene, 1a,2,3,7b-tetrahydro-	$C_{10}H_{10}O$	146	35
2.145	3-Hydroxy-2-pentanone	$C_5H_{10}O_2$	102	30
35.507	Naphthalene, 1,2-dihydro-2,5,8- trimethyl-	$C_{13}H_{16}$	172	25
38.889	Naphthalene, 1,4,6-trimethyl-	$C_{13}H_{14}$	170	25
33.097	Phenol, 2-undecyl-	$C_{17}H_{28}O$	248	22

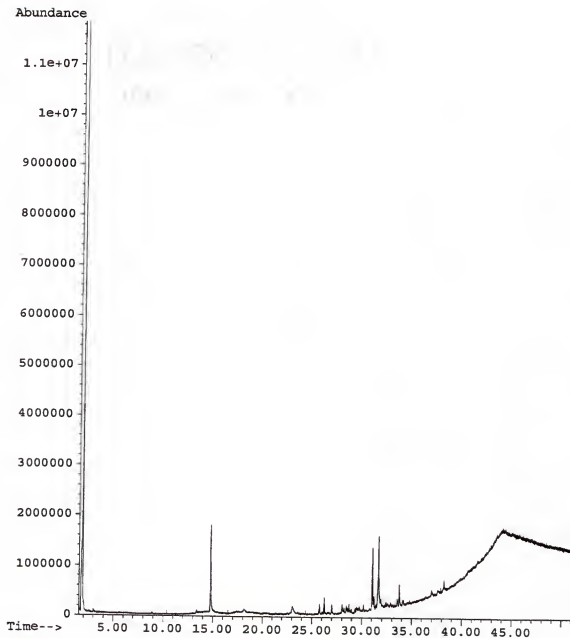


Figure 50: GC-MS chromatogram for experiment GCMS13.

In this experiment, volumes of 3.000 mL benzene and 450 mL MQ water were placed into a 500 mL roundbottom irradiation flask on the benchtop, which resulted in a saturated solution. The flask was irradiated for 11 days using the old, weak source used in geometry B. The aqueous layer was acidified and extracted with CH_2Cl_2 . The CH_2Cl_2 solution was injected into the GC-MS unit. This same solution was used for injection GCMS14.

Table 28: Mass spectral data for experiment GCMS13.

Retention Time (min)	Compound	Molecular Formula	Molecular Weight	Qual Number
31.067	m-Terphenyl	C ₁₈ H ₁₄	230	98
26.230	o-Terphenyl	C ₁₈ H ₁₄	230	95
33.765	[1,1':3',1''-Terphenyl]-4'-ol	C ₁₈ H ₁₄ O	246	95
14.734	Biphenyl	C ₁₂ H ₁₀	154	87
23.099	[1,1'-Biphenyl]-3-ol	C ₁₂ H ₁₀ O	170	87
31.604	p-Terphenyl	C ₁₈ H ₁₄	230	86
33.516	2,5-Cyclohexadien-1-one, 4,4-diphenyl	C ₁₈ H ₁₄ O	246	83
18.165	o-Hydroxybiphenyl	C ₁₂ H ₁₀ O	170	70
1.853	2-Pentanone, 4-hydroxy-4-methyl-	C ₆ H ₁₂ O ₂	116	64
29.356	Bicyclo[3.1.0]hex-2-ene, 5,6-diphenyl-	C ₁₈ H ₁₆	232	64
25.743	Benzene, 1,3-diethenyl-	C ₁₀ H ₁₀	130	59
28.725	1,4-Ethanonaphthalen-2-ol, 1,2,3,4-tetra	C ₁₂ H ₁₄ O	174	59
28.443	1-Naphthalenol, 1,2,3,4-tetrahydro-	C ₁₀ H ₁₂ O	148	50
28.034	Benzene, diethenyl-	C ₁₀ H ₁₀	130	49
30.162	1-Phenyl-1-pentyne	C ₁₁ H ₁₂	144	49
13.398	Benzene, cyclohexyl-	C ₁₂ H ₁₆	160	46
26.058	Acenaphthylene, 1,2,2a,3,4,5-hexahydro-	C ₁₂ H ₁₄	158	43
1.593	Pentanal	C ₅ H ₁₀ O	86	42
38.200	Phenol, nonyl-	C ₁₅ H ₂₄ O	220	41
3.024	Ethanol, 2-butoxy	C ₆ H ₁₄ O ₂	118	38
26.973	Methanone, 2-naphthalenylphenyl-	C ₁₇ H ₁₂ O	232	38
8.880	3-Octanol, 2,2-dimethyl-	C ₁₀ H ₂₂ O	158	36
13.662	Benzene, 3-cyclohexen-1-yl-	C ₁₂ H ₁₄	158	35
29.752	Benzeneacetaldehyde, .alpha.-phenyl	C ₁₄ H ₁₂ O	196	35
2.574	2-Hexanone, 5-methyl-	C ₇ H ₁₄ O	114	32

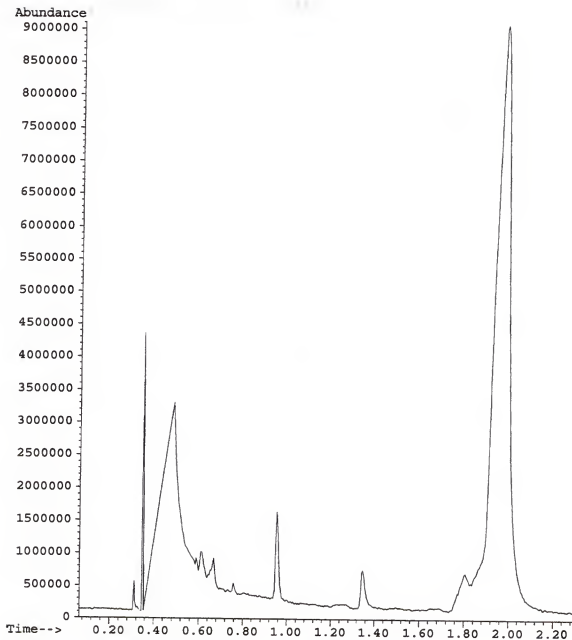


Figure 51: GC-MS chromatogram for experiment GCMS14.

In this experiment, volumes of 3.000 mL benzene and 450 mL MQ water were placed into a 500 mL roundbottom irradiation flask on the benchtop, which resulted in a saturated solution. The flask was irradiated for 11 days using the old, weak source used in geometry B. The aqueous layer was acidified and extracted with CH_2Cl_2 . The CH_2Cl_2 solution was injected into the GC-MS unit using the “wet-needle” technique and solvent-delay override command. This same solution was used for injection GCMS13.

Table 29: Mass spectral data for experiment GCMS14.

Retention Time (min)	Compound	Molecular Formula	Molecular Weight	Qual Number
0.291	4H-1,3-Benzodioxin	C ₈ H ₈ O ₂	136	78
0.958	Methyl Isobutyl Ketone	C ₆ H ₁₂ O	100	74
0.668	Salicyl Alcohol	C ₇ H ₈ O ₂	124	72
1.346	3-Penten-2-one, 4-methyl-	C ₆ H ₁₀ O	98	72
0.485	Acetone	C ₃ H ₆ O	58	58
0.613	1,3-Hexadien-5-yne	C ₆ H ₆	78	43
0.663	Benzenecarboperoxic acid, 1,1-dimethylene-	C ₁₁ H ₁₄ O ₃	194	43
1.978	2-Pentanone, 4-hydroxy-4-methyl-	C ₆ H ₁₂ O ₂	116	38
1.785	2-Heptanone, 4-methyl-	C ₈ H ₁₆ O	128	35
0.904	Oxirane, 2,3-dimethyl-, cis-	C ₄ H ₈ O	72	10

CHAPTER 7

MECHANISM AND DISCUSSION

In this work, the gamma radiolysis of aqueous benzene solutions was studied using two different headspace volumes, three different headspace gases, and two different dose rates; experiments and results were listed in Chapter 6. In this chapter, the effects of headspace volume and headspace gas on benzene destruction, initial product formation and production of CO_2 will be presented via comparison figures. A discussion of the reactions of benzene with the primary radical transients e_{aq}^- , $\text{H}\cdot$ and $\cdot\text{OH}$ will be presented for both anoxic and aerated aqueous solutions. Lastly, an explanation of system behavior based on a postulated reaction mechanism will be offered.

Effect of Headspace Volume

Initial Product Formation

The effect of headspace volume on the rate of benzene destruction and initial product formation is best illustrated by examining plots containing data from the “short air” system (short tubes with air headspaces) and data from the “long air” system (long tubes with air headspaces). Comparison plots for the short air versus long air system are shown in Figure 52-Figure 57. The same products were identified in both systems: phenol, biphenyl, and 3- and 4-phenylphenols.

Consumption of benzene

Figure 52 presents the amount of benzene in solution (in μmoles) versus dose (in Mrad) for both the short air and long air systems. Since aqueous benzene solutions for

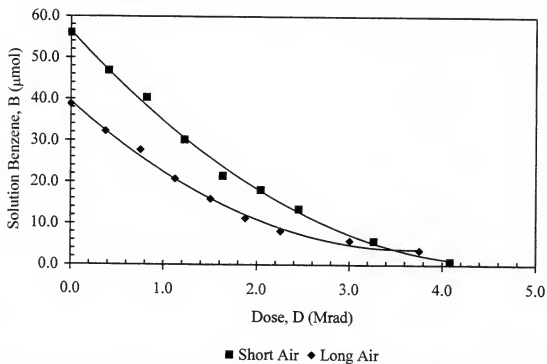


Figure 52: Plot of μmoles of benzene in solution versus dose in Mrad for both the short air and long air systems.

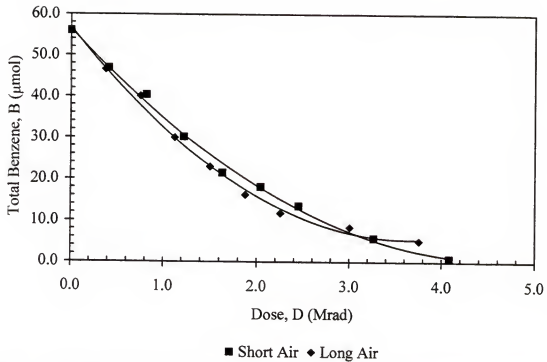


Figure 53: Plot of the total number of μmoles of benzene contained in the radiolysis vessel versus dose in Mrad for both the short air and long air systems.

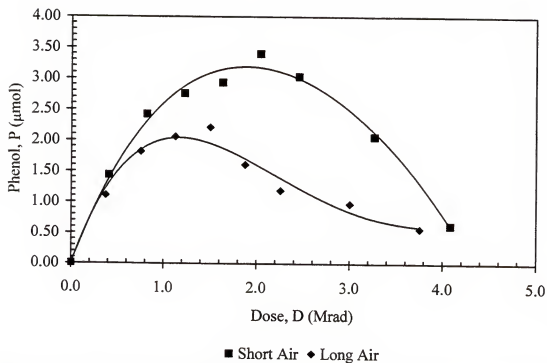


Figure 54: Plot of μ moles of phenol versus dose in Mrad for both the short air and long air systems.

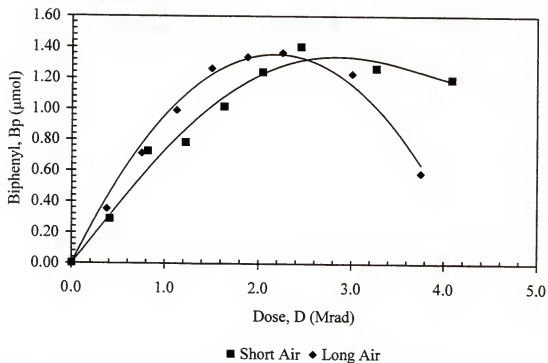


Figure 55: Plot of μ moles of biphenyl versus dose in Mrad for both the short air and long air systems.

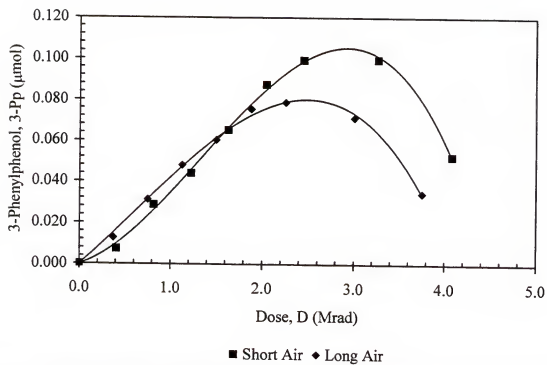


Figure 56: Plot of μ moles of 3-phenylphenol versus dose in Mrad for both the short air and long air systems.

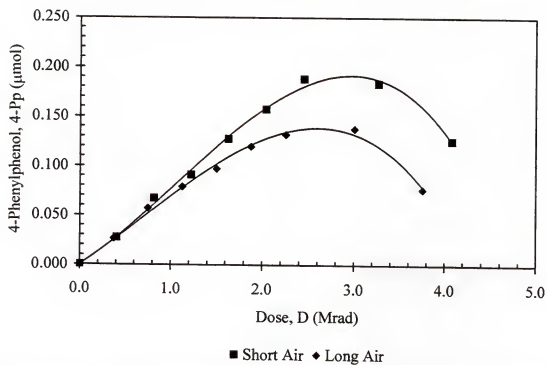


Figure 57: Plot of μmoles of 4-phenylphenol versus dose in Mrad for both the short air and long air systems.

each system were prepared equivalently (5.000 mL aliquots of a stock solution formed by diluting 50.0 μ L benzene to a final volume of 50.00 mL), the two curves of μ moles of solution benzene versus dose should begin at the same number of μ moles; however, the number of μ moles of benzene in solution in the long air system is approximately 30% less than the number of μ moles of benzene in the short air system. This difference serves to illustrate the fact that as the headspace of the closed container increases, a significant amount of the benzene escapes from solution into the headspace.

An experiment was undertaken in which several samples tubes were prepared with headspaces varying from 0 mL to 11.0 mL. The experiment was performed by preparing a stock solution by diluting 50.0 μ L benzene to a final volume of 50.00 mL, and then filling long tubes to various heights with stock solution. The height of solution in each tube was calculated so that the remaining headspace would be the desired volume. Each tube was capped and the benzene was allowed to reach equilibrium between the liquid and vapor phases. The amount of benzene remaining in solution in each tube was measured via HPLC and interpreted as a function of headspace volume. The observation was made that for the short tube system, approximately 3% of the initial benzene was in the headspace, and for the long tube system, approximately 30% of the initial benzene was in the headspace. Correction factors (3% for the short tube system and 30% for the long tube system) were applied to the data composing Figure 52 in order to determine the total amount of benzene (in μ moles) versus dose (in Mrad) for the two systems, the plot of which is shown in Figure 53.

Analysis of Figure 53 indicates that the benzene consumption curve for the short air system is linear to an absorbed dose of approximately 1.2 Mrad. At this dose,

1.2 Mrad, the amount of total benzene present in the sample tube has fallen from 57 μ moles to 31 μ moles, which corresponds to $G(-\text{benzene})$ of 4.2. Past this dose, the consumption curve for the short air system begins to flatten, as the products resulting from benzene degradation begin to compete for radical transients. The linear initial region of the curve serves to illustrate the indirect effect as described in Chapter 2, which implies that a plot of concentration versus time of irradiation (dose) should be linear. Although the total benzene curve in the long air system is not as linear as in the short air system, the first two or three points of the curve can be used to estimate a value of $G(-\text{benzene})$ in the long air system: 4.7 molecules per 100 eV.

Production of phenol

Figure 54 presents the yield of phenol (in μ moles) versus dose (in Mrad) for both the short air and long air systems. Phenol is initially produced at the same rate in both systems, a rate which corresponds to $G(\text{phenol})$ of 0.58 given 1.2 μ moles of phenol present at an absorbed dose of 0.40 Mrad. However, after a dose of 0.40 Mrad has been absorbed, the two production curves begin to diverge. In the long air system, the amount of phenol reached a maximum value of 2.1 μ moles at a dose of 1.1 Mrad. In the short air system, the amount of phenol reached a maximum value of 3.2 μ moles at a dose of 1.9 Mrad. Further irradiation in each system resulted in the continued consumption of phenol.

Production of biphenyl

Figure 55 illustrates the production and consumption of biphenyl versus dose for both the short air and long air systems. For the short air system, the production curve of biphenyl versus dose is linear to an absorbed dose of 1.7 Mrad. The amount of biphenyl

present at this dose is 1.1 μmoles , which corresponds to $G(\text{biphenyl})$ of 0.12. For the long air system, the production curve is linear to an absorbed dose of 1.1 Mrad. The amount of biphenyl present at this dose is 1.0 μmoles , which corresponds to $G(\text{biphenyl})$ of 0.18. Further irradiation in both the short air and long air systems resulted in the continued consumption of biphenyl.

Production of 3-phenylphenol

Figure 56 presents the yield of 3-phenylphenol (in μmoles) versus dose (in Mrad) for the short air and long air systems. The production curves for both systems are linear to an absorbed dose of 1.6 Mrad, at which the μmoles of compound present was equal to 0.064. At this point, $G(3\text{-phenylphenol})$ is equal to 0.0077. Further irradiation resulted in the continued consumption of 3-phenylphenol for each system.

Production of 4-phenylphenol

Figure 57 shows the yield of 4-phenylphenol (in μmoles) versus dose (in Mrad) for both the short air and long air systems. The production curves for both systems are linear up to an absorbed dose of 1.0 Mrad. At this dose, the amount of 4-phenylphenol present in each system is 0.075 μmoles , which corresponds to a value for $G(4\text{-phenylphenol})$ of 0.014. Continued irradiation resulted in further consumption of 4-phenylphenol for each system.

Table 30 lists the initial G-values for benzene and the quantified radiolysis products for both the short air and long air systems. For each compound, the dose D (in Mrad) at which the production curve strayed from linearity is listed along with the amount (in μmoles) of compound present at that dose. The amount of compound present is given as $\Delta_{\mu\text{moles}}$, which is the difference between the amount present at the specified

dose and the amount present at the onset of radiation. The dose and the change in amount were used to calculate each G-value.

Table 30: Listing of initial G-values for benzene and quantified radiolysis products for the short air and long air systems.

Compound	Short Air System			Long Air System		
	Dose	$\Delta_{\mu\text{moles}}$	G	Dose	$\Delta_{\mu\text{moles}}$	G
-Benzene	1.2	26	4.2	1.1	27	4.7
Phenol	0.40	1.2	0.58	0.40	1.2	0.58
Biphenyl	1.7	1.1	0.12	1.1	1.0	0.18
3-Phenylphenol	1.6	0.064	0.0077	1.6	0.064	0.0077
4-Phenylphenol	1.0	0.075	0.014	1.0	0.075	0.014

Mineralization to Produce CO₂

Figure 58 shows the yield of CO₂ (in μmoles) versus dose (in Mrad) for both the short air and long air systems. In each system, essentially no CO₂ is produced until a dose of 33 Mrads has been absorbed. After this dose, the amount of radiolytically produced CO₂ begins to increase. The maximum amount of CO₂ produced in the short air system is 35.8 μmoles , and in the long air system is 102 μmoles . Assuming complete degradation of all benzene (56.0 μmoles C₆H₆ which equals 336 μmoles carbon), these amounts represent percent degradations of 10.7% and 30.5%, respectively.

Effect of Headspace Gas

Initial Product Formation

The effect of headspace gas on the rate of benzene destruction and initial product formation is best illustrated by comparing plots arising from the long oxygen system, long air system and long nitrogen system. Comparison plots for these three systems are shown in Figure 59-Figure 64. Although long tube irradiations were allowed to proceed until a dose of 18 Mrad was absorbed, the comparison plots for the three long systems are shown for absorbed doses of up to 6.0 Mrad, which is sufficient dose to illustrate

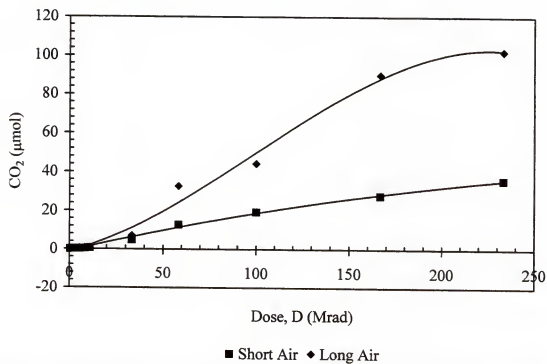


Figure 58: Plot of μmoles of CO_2 versus dose in Mrad for both the short air and long air systems.

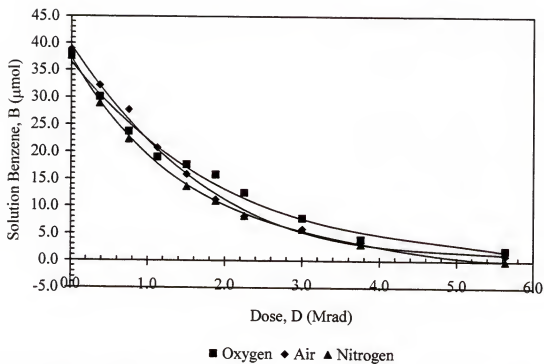


Figure 59: Plot of μ moles of benzene in solution versus dose in Mrad for the long oxygen, long air and long nitrogen systems.

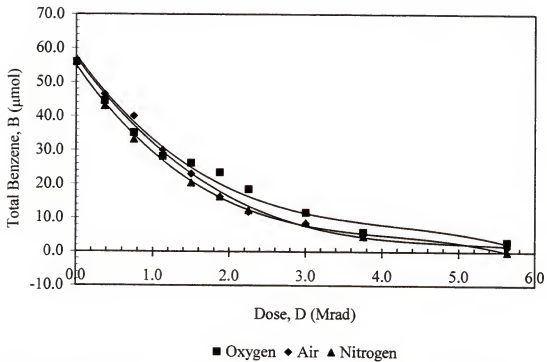


Figure 60: Plot of total number of μmoles of benzene versus dose in Mrad for the long oxygen, long air and long nitrogen systems.

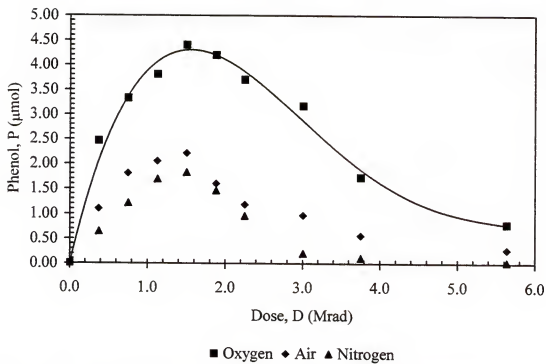


Figure 61: Plot of μ moles of phenol versus dose in Mrad for the long oxygen, long air and long nitrogen systems.

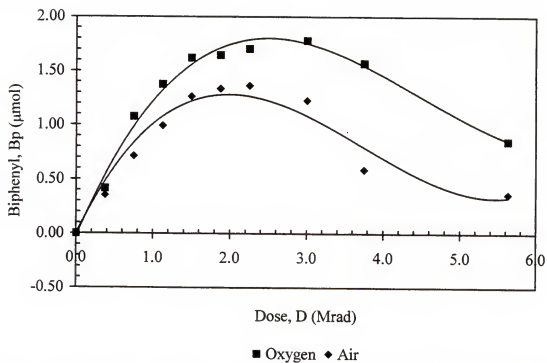


Figure 62: Plot of μ moles of biphenyl versus dose in Mrad for the long oxygen and long air systems. Biphenyl was not observed in the long nitrogen system.

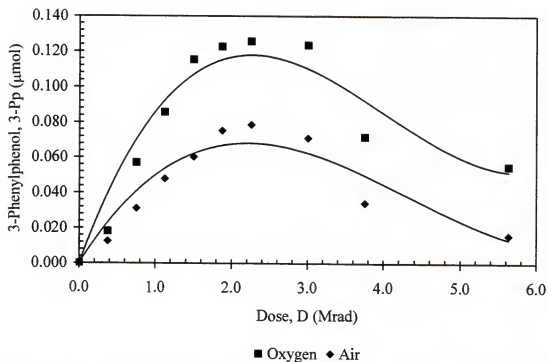


Figure 63: Plot of μ moles of 3-phenylphenol versus dose in Mrad for the long oxygen and long air systems. The compound 3-phenylphenol was not observed in the long nitrogen system.

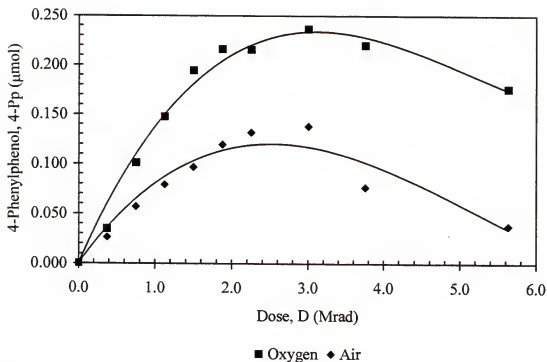


Figure 64: Plot of μ moles of 4-phenylphenol versus dose in Mrad for the long oxygen and long air systems. The compound 4-phenylphenol was not observed in the long nitrogen system.

headspace gas effects. The same products were quantified in the long oxygen and long air systems: phenol, biphenyl, and 3- and 4-phenylphenol. Phenol was the only product quantified in the long nitrogen system.

Consumption of benzene

Figure 59 presents the amount of benzene in solution (in μmoles) versus dose (in Mrad) for the long oxygen, long air and long nitrogen systems. The number of μmoles of benzene in solution at the onset of the experiment was calculated to equal approximately 38 μmoles for each of the three systems. As discussed previously, a significant percentage (*ca.* 30%) of the total benzene escaped into the headspace in each of the long tubes. As before, a correction factor was applied to the data composing Figure 59 to yield the total amount of benzene (in μmoles) versus dose (in Mrad) for the three long systems, the plot of which is shown in Figure 60.

In contrast to the short air system, the curves of benzene consumption versus dose for the three long systems are nonlinear, even over the first 0.5 Mrad of absorbed dose. This is a consequence of the lower concentration of benzene in solution as compared to the short air system, in which only 3% of the benzene was found to exist in the headspace volume. As the irradiation proceeded and the benzene in solution was consumed, benzene in the headspace began to re-dissolve into solution. The effect of this re-dissolving of benzene is a leveling off of each consumption curve of benzene for the long tube systems, thus deviating the curve from linearity. However, the initial value of $G(-\text{benzene})$ may be estimated by examining the first few points of the curve. The initial value of $G(-\text{benzene})$ was approximated as 4.7 for each of the three long systems.

Production of phenol

Figure 61 shows the yield of phenol (in μmoles) versus dose (in Mrad) for the three long systems. Each system is characterized by a high initial rate of phenol production (from 0 to 0.40 Mrad). If one calculates $G(\text{phenol})$ for each systems based on initial rates, values of $G(\text{phenol})$ of 1.2, 0.58 and 0.29 are obtained for the long oxygen, long air and long nitrogen systems given amounts of 2.5, 1.2, and 0.60 μmoles of phenol present at an absorbed dose of 0.40 Mrad. In addition, the phenol production maximizes at an absorbed dose of 1.5 Mrad. The μmoles of phenol at this maximum are 4.4 μmoles for the long oxygen, 2.3 μmoles for the long air, and 2.1 μmoles for the long nitrogen. Past a dose of 1.5 Mrad, the μmoles of phenol for each system decreases as the phenol is consumed.

Production of biphenyl

Figure 62 shows the μmoles of biphenyl versus dose for the long oxygen and long air systems. Strikingly, biphenyl was not detected at any value of absorbed dose in the long nitrogen system. The production curve of biphenyl for the long oxygen system is linear to an absorbed dose of 0.70 Mrad, at which the amount of compound present was 1.1 μmoles . The value of $G(\text{biphenyl})$ at this point is 0.27. The production curve of biphenyl for the long air system is linear to an absorbed dose of 1.1 Mrad, at which the amount of compound present is equal to 1.0 μmoles . The value of $G(\text{biphenyl})$ at this point is calculated to equal 0.18. Each production curve reaches a maximum value of biphenyl of 1.8 μmoles for the long oxygen system and 1.4 μmoles for the long air system at 2.4 Mrad, and past this dose consumption of biphenyl continues.

Production of 3-phenylphenol

The production curves of 3-phenylphenol for both the long oxygen and long air systems are shown in Figure 63. As with biphenyl, 3-phenylphenol was not observed in the long nitrogen system. The production curve of 3-phenylphenol for the long oxygen system was linear to 1.3 Mrad. The amount of compound present at this dose was equal to 0.10 μ moles, which corresponds to a value for $G(3\text{-phenylphenol})$ of 0.015. The production curve in the long air system is linear to an absorbed dose of 1.6 Mrad, at which the amount of compound present was equal to 0.064 μ moles. This yields a G -value of 0.077 for the long air system. In each system, the amount of 3-phenylphenol reaches a maximum value at a dose of 2.2 Mrad: 1.7 μ moles for the long oxygen system, and 1.2 μ moles for the long air system. Past this dose of maximum μ moles, each production curve decreases as 3-phenylphenol is consumed.

Production of 4-phenylphenol

Figure 64 presents the experimental data for the production of 4-phenylphenol versus dose for both the long oxygen and long air systems. As with 3-phenylphenol, 4-phenylphenol was not observed in the long nitrogen system. The production curve in the long oxygen system is linear up to 1.1 Mrad, at which the amount of 4-phenylphenol present was equal to 0.14 μ moles. The value of $G(4\text{-phenylphenol})$ at this point is equal to 0.025. The production curve for the long air system is linear to an absorbed dose of 1.0 Mrad, at which the amount of 4-phenylphenol present was equal to 0.075 μ moles. These values correspond to $G(4\text{-phenylphenol})$ of 0.014 for the long air system. The amount of 4-phenylphenol was found to reach a maximum value at a dose of 3.0 Mrad. The amount of compound present in the long oxygen system was 0.24 μ moles, and the

amount present in the long air system was 0.12 μmoles . Upon further irradiation, the amount of 4-phenylphenol lessens due to consumption.

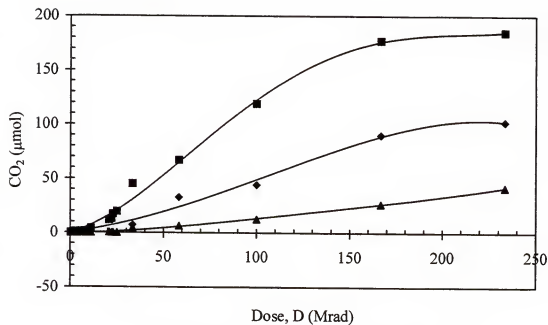
Table 31 lists the initial G-values for benzene and quantified radiolysis products for the long oxygen, long air and long nitrogen systems. The initial G-value is calculated by looking at the portion of the production curve from the start of the experiment to the dose at which the curve deviated from linearity. The table contains the dose D, in Mrad, at which each production curve strayed from linearity, and the difference (Δ) in μmoles of compound present at this dose from the amount present at the beginning of the radiolysis experiment.

Table 31: Listing of initial G-values for benzene and quantified radiolysis products for the long oxygen, long air and long nitrogen systems (LOD = Limit of Detection).

Compound	Long Oxygen System			Long Air System			Long Nitrogen System		
	D	$\Delta_{\mu\text{moles}}$	G	D	$\Delta_{\mu\text{moles}}$	G	D	$\Delta_{\mu\text{moles}}$	G
Benzene	1.1	27	4.7	1.1	27	4.7	1.1	27	4.7
Phenol	0.40	2.5	1.2	0.40	1.2	0.58	0.40	0.60	0.29
Biphenyl	0.70	1.1	0.27	1.1	1.0	0.18	< LOD		
3-Phenylphenol	1.3	0.10	0.15	1.6	0.064	0.0077	< LOD		
4-Phenylphenol	1.1	0.14	0.25	1.0	0.075	0.014	< LOD		

Mineralization to Produce CO_2

Figure 65 shows experimental results for the yield of CO_2 (in μmoles) versus dose (in Mrad) for the long oxygen, long air and long nitrogen systems. The characteristics of the production curves are similar to the short air/long air curves: minimal production during the first 20 Mrad, a rapid rise in CO_2 production, and a leveling off in production past approximately 160 Mrad. The maximum amount of CO_2 was found to be 185 μmoles , 102 μmoles and 41.9 μmoles for the long oxygen, long air and long nitrogen systems, respectively. These amounts correspond to degradation percents of 55.1%, 30.5% and 12.5% for the long oxygen, long air and long nitrogen systems, respectively.



■ Long Oxygen ♦ Long Air ▲ Long Nitrogen

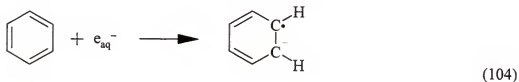
Figure 65: Plot of μmoles of CO_2 versus dose in Mrad for the long oxygen, long air and long nitrogen systems.

Reactions of Benzene with Radical Transients

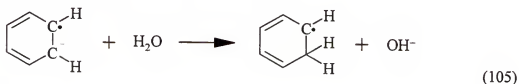
Anoxic Solutions

Hydrated electron

In the early days of radiation chemistry, the two reactive species in gamma irradiated aqueous solution were assumed to be $\text{H}\cdot$ and $\cdot\text{OH}$, which were responsible for reduction and oxidation of substrates, respectively. By the late 1950's, however, studies in which yields were measured as a function of pH [79] or a kinetic salt effect was measured [80] indicated the presence of two different reducing species in gamma irradiated water: $\text{H}\cdot$ and e_{aq}^- . The UV-VIS spectrum of the hydrated electron was finally measured by Hart and Boag in 1962 [81]. The hydrated electron reacts with benzene by addition, forming the cyclohexadienyl radical anion.

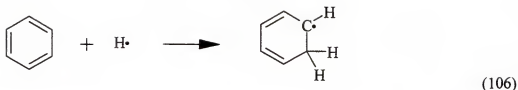


Koehler and Solar measured the rate constant of addition and found it to equal $9.0 \times 10^6 \text{ M}^{-1} \text{ s}^{-1}$ [82]. Marketos and Mantaka determined a rate constant of $1.3 \times 10^7 \text{ M}^{-1} \text{ s}^{-1}$ for Reaction (104) [83]. The cyclohexadienyl radical anion immediately protonates to form the cyclohexadienyl radical, $\text{C}_6\text{H}_7\cdot$.



Hydrogen atom

The hydrogen atom reacts with benzene by addition to form the cyclohexadienyl radical.

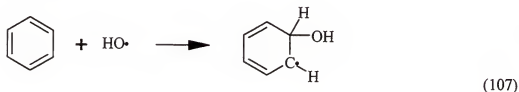


The rate constant for $\text{H}\cdot$ addition to benzene has been measured by Roduner and Bartels as $1.1 \times 10^9 \text{ M}^{-1}\text{s}^{-1}$ [84], and by Anderson to equal the same value, $1.1 \times 10^9 \text{ M}^{-1}\text{s}^{-1}$ [85].

The cyclohexadienyl radical has been well characterized. Gordon and Schmidt found that the radical has a UV absorbance at a wavelength of 312 nm with molar absorptivity of $5310 \text{ M}^{-1}\text{cm}^{-1}$ [59]. Marketos measured an absorbance at 311 nm with molar absorptivity of $5350 \text{ M}^{-1}\text{cm}^{-1}$ for the cyclohexadienyl radical [83]. Cercek measured the absorbance at a wavelength of 260 nm and calculated a molar absorptivity of $630 \text{ M}^{-1}\text{cm}^{-1}$ [86]. Further reactions of the cyclohexadienyl radical are discussed later in this chapter.

Hydroxyl radical

The hydroxyl radical reacts with benzene by addition, forming the hydroxycyclohexadienyl radical.



The rate constant for $\cdot\text{OH}$ addition has been reported as $7.8 \times 10^9 \text{ M}^{-1}\text{s}^{-1}$ by Gordon [59] and as $8.2 \times 10^9 \text{ M}^{-1}\text{s}^{-1}$ by Patterson [87]. A similar value of $7.8 \times 10^9 \text{ M}^{-1}\text{s}^{-1}$ has been determined by Anderson [85]. The radical adduct has been the subject of numerous studies. Cercek monitored the absorbance of the $\cdot\text{OH}$ /benzene adduct at a wavelength of 275 nm and determined a molar absorptivity of $1950 \text{ M}^{-1}\text{cm}^{-1}$ [86]. Marketos

determined an absorbance at 313 nm with molar absorptivity of $4700 \text{ M}^{-1}\text{cm}^{-1}$ for the adduct [83].

Aerated Solutions

Hydrated electron

In the presence of oxygen, e_{aq}^- is scavenged by oxygen to form the peroxy radical anion.



The rate constant for Reaction (29) has been reported as $9.5 \times 10^9 \text{ M}^{-1}\text{s}^{-1}$ by Milosavljevic [88], and as $1.2 \times 10^{10} \text{ M}^{-1}\text{s}^{-1}$ by Gordon [89]. The product of this reaction, the peroxy radical anion, is relatively inert in the presence of organic substrates. Further scavenging of e_{aq}^- by the peroxy radical anion leads to the formation of the superoxide ion.



Gruenbein reported the rate constant for formation of the superoxide ion as $1.3 \times 10^{10} \text{ M}^{-1}\text{s}^{-1}$ [32]. Single and double protonation of the superoxide ion leads to formation of the hydrogen peroxide anion and hydrogen peroxide, H_2O_2 , respectively.



The acid/base properties of hydrogen peroxide have been well characterized [20].

Hydrogen atom

As with the hydrated electron, a similar scavenging reaction occurs between the hydrogen atom and oxygen.



The rate constant for addition of $H\cdot$ to O_2 has been reported as $2.1 \times 10^{10} M^{-1}s^{-1}$ by Gordon [90]. The product, the hydroperoxyl radical, reacts rather slowly with organic molecules.

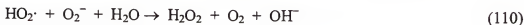
The hydroperoxyl radical and the peroxy anion radical are related through an acid/base equilibrium reaction with a pK_a of 4.88 [91].



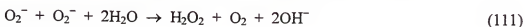
In aqueous solution, the fate of the hydroperoxyl radical is disproportionation, leading to the formation of hydrogen peroxide and oxygen.



The measured rate constant for this reaction has been reported as $7.6 \times 10^5 M^{-1}s^{-1}$ [91]. A similar reaction to produce H_2O_2 is known to occur between $HO_2\cdot$ and O_2^- .



The rate constant for Reaction (110) is $8.5 \times 10^7 M^{-1}s^{-1}$ [91]. Lastly, if the pH is sufficiently basic such that all $HO_2\cdot$ exists as O_2^- , a disproportionation reaction to produce H_2O_2 is possible, but the reaction rate is slow, $1 \times 10^2 M^{-1}s^{-1}$ [91].



Thus, in oxygen containing aqueous solution at a pH less than 7, both of the reducing radicals e_{aq}^- and $H\cdot$ are scavenged by oxygen to form O_2^- and $HO_2\cdot$, respectively. The hydroperoxyl radical or peroxy radical anion reacts to form hydrogen peroxide, H_2O_2 , and oxygen. The presence of H_2O_2 in irradiated solution leads to formation of additional $\cdot OH$ by reaction with e_{aq}^- with a rate constant of $1.2 \times 10^{10} M^{-1}s^{-1}$ [89].



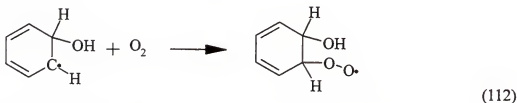
A similar reaction also occurs between H_2O_2 and $\text{H}\cdot$.



The rate constant for Reaction (41) has been measured by Sweet as $9 \times 10^7 \text{ M}^{-1}\text{s}^{-1}$ [92].

Hydroxyl radical

In aerated solution, the hydroxyl radical is not scavenged by oxygen. Addition of $\cdot\text{OH}$ to the benzene ring occurs as in anoxic solutions (Reaction (107)) to form the hydroxycyclohexadienyl radical. Oxygen adds to this radical to form the peroxyhydroxycyclohexadienyl radical with a rate constant of $5.0 \times 10^8 \text{ M}^{-1}\text{s}^{-1}$, as reported by Dorfman [93]. Based on pulse radiolysis experimentation, Ramanan measured a rate constant of $3.9 \times 10^8 \text{ M}^{-1}\text{s}^{-1}$ for the addition reaction [94].



Further reactions of the peroxy adduct are discussed later in this chapter.

Discussion of Reaction Mechanism

The study of the gamma radiolysis of aqueous benzene solutions began in the late 1940's with the observations of Stein and Weiss [95]. Over the past fifty years, numerous researchers have contributed to the understanding of the system. However, as previous work was intended to determine initial products or rate constants, doses were selected so that only a small percentage (*ca.* 3 to 10%) of initial reactant benzene was consumed. To date, there have been no studies of the gamma radiolysis of aqueous benzene solutions over a radiolysis timespan sufficient to destroy all benzene as well as first generation radiolysis products. In addition, yields of radiolysis products such as

G(phenol) and G(biphenyl) reported in the older literature (especially in the 1950's and early 1960's) seem to be contradictory for similar systems (oxygen- or N_2O -saturated aqueous benzene solutions). The rationalization for these discrepancies is that the analytical methods available at the time were inadequate. Many of the earlier works relied on simple extractions, simple chemical tests and/or UV-VIS spectrophotometry for identification of radiolysis products and calculation of yields. It is certain that in many cases researchers reported yields resulting from analytical tests in which mixtures of similarly reacting products were analyzed that were assumed to be one radiolysis product. For this reason, older literature in which analytical methods such as chromatography, sophisticated chemical tests and/or sophisticated extractions were not employed must be viewed with suspicion.

An analysis of the recent literature reveals that there are two generally accepted mechanistic pathways that may be followed in the gamma radiolysis of aqueous benzene solutions. The choice of pathway is dependent upon the presence or absence of oxygen in the radiolysis solution and/or headspace.

Mechanistic Pathway for Oxygenated Systems

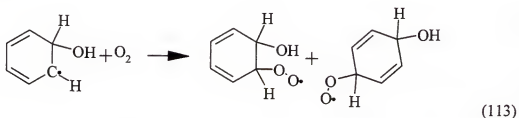
Reaction of e_{aq}^- and $H\cdot$

As mentioned previously, in oxygenated aqueous solution e_{aq}^- and $H\cdot$ are effectively scavenged by O_2 to form O_2^- and $HO_2\cdot$, respectively. The disproportionation of $HO_2\cdot$ (Reaction (39)), reaction between $HO_2\cdot$ and O_2^- (Reaction (110)), or disproportionation of O_2^- (Reaction (111)) leads to formation of H_2O_2 . The reaction of H_2O_2 with e_{aq}^- forms additional $\cdot OH$ via Reaction (28). As long as oxygen is available, the two reducing radicals e_{aq}^- and $H\cdot$ are removed from solution via Reactions (29) and

(43). The amount of $\cdot\text{OH}$ is increased, and the solution may be considered entirely oxidizing in character.

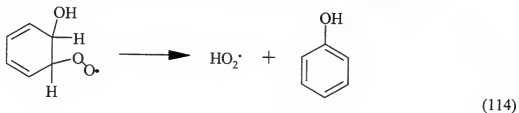
Reaction of $\cdot\text{OH}$

As discussed above, the hydroxyl radical adds to the benzene ring via Reaction (107) to form the hydroxycyclohexadienyl radical. Oxygen then adds to the $\cdot\text{OH}/\text{benzene}$ adduct to form the peroxyhydroxycyclohexadienyl radical in a mixture of ortho and para isomers.



The ratio of ortho to para addition has been investigated. Pan and von Sonntag concluded that oxygen addition to the hydroxycyclohexadienyl radical is a reversible process, and that the two peroxyhydroxycyclohexadienyl radicals resulting from oxygen addition are in equilibrium with the hydroxycyclohexadienyl radical. More importantly, they found that the peroxy radical that results from ortho addition only accounts for a small percentage of the radical mixture [96]. In their study, they measured a value for the rate constant for Reaction (113) of $1.5 \times 10^8 \text{ M}^{-1} \text{ s}^{-1}$.

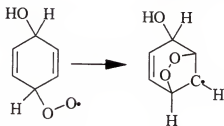
The decay of the peroxyhydroxycyclohexadienyl radical follows one of two pathways. The peroxy radical is known to eliminate $\text{HO}_2\cdot$ to form phenol.



Dorfman was among the first to determine that production of $\text{HO}_2\cdot$ paralleled the production of phenol, resulting in the inclusion of Reaction (114) in his kinetic scheme [93]. The elimination of $\text{HO}_2\cdot$ to form phenol has been suggested by numerous other workers in the field [97-100].

Pan and von Sonntag proposed that elimination of $\text{HO}_2\cdot$ to form phenol arises from the ortho isomer of the peroxyhydroxycyclohexadienyl radical and not the para isomer [96]. They based their decision on the $\text{H}\cdots\text{O}_2$ distance between $\text{H}\cdot$ at the α -position to the $-\text{OH}$ group of 1.8 Å and 3.85 Å in the ortho and para isomers, respectively. They were able to determine a rate constant for elimination of $\text{HO}_2\cdot$, $2.0 \times 10^4 \text{ s}^{-1}$.

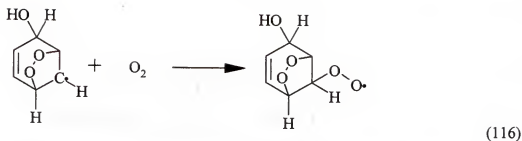
In comparison, the peroxyhydroxycyclohexadienyl radical may also undergo an intramolecular peroxide forming reaction that eventually leads to ring opening.



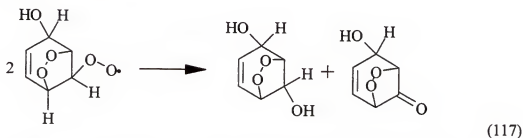
(115)

An intramolecular peroxide forming reaction has been included in the mechanistic scheme for oxygenated solutions for many years [97]. However, the most complete mechanistic and kinetic study on the ring opening reaction was done by Pan, Schuchmann and von Sonntag [96]. Through their experiments, they provided a rate constant for Reaction (115) of $5.0 \times 10^2 \text{ s}^{-1}$.

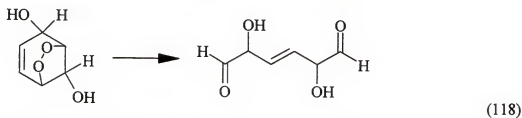
Once formed, the peroxide reacts with another molecule of oxygen.



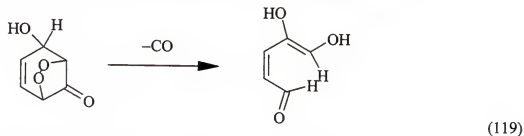
According to Pan, two product molecules from Reaction (116) disproportionate to yield an alcohol and a ketone.



The alcohol product of Reaction (117) then undergoes a ring scission reaction to produce dihydroxymucondialdehyde, one of their observed products.



According to Pan, the ketone product of Reaction (117) eliminates CO .

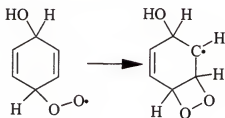


Lastly, the product from Reaction (119) undergoes keto-enol tautomerization to yield another of their observed products.



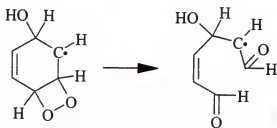
(120)

The inclusion of intramolecular peroxide forming reactions as shown in Reaction (115) to explain ring scission is not new. In 1969, Srinvisan and Balakrishnan included the reaction in their mechanistic analysis of the oxygen-saturated aqueous benzene system [97]. These researchers also assumed that elimination of $\text{HO}_2\cdot$ to form phenol occurs from the ortho peroxy radical, and that ring opening occurs from the para peroxy radical. One interesting note concerning their mechanism is that intramolecular peroxide formation was assumed to form a four-membered ring instead of a five-membered ring as in the mechanism of Pan.



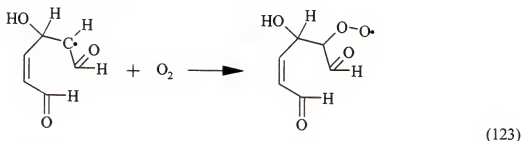
(121)

According to Srinvisan, ring scission would now occur.

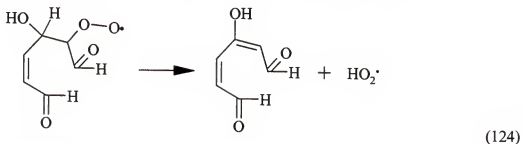


(122)

The product of Reaction (122) then reacts with oxygen.



Elimination of HO_2^\cdot led to the formation of β -hydroxymucondialdehyde.



Compounds such as β -hydroxymucondialdehyde and mucondialdehyde have been widely reported as oxidation products “other than phenol” in the gamma radiolysis of aqueous benzene solutions [101-103].

Ring-opened compounds similar to mucondialdehyde were identified via GC-MS experiments in this work. The compound 3-hydroxy-2-pentanone was identified in experiment GCMS12. The mass spectral data for experiment GCMS12 are contained in Table 27. Likewise, the compound 4-hydroxy-4-methyl-2-pentanone was identified in experiment GCMS14; the mass spectral data for this experimental run are contained in Table 29.

Further reaction of ring-opened products with $\cdot\text{OH}$ in the presence of oxygen leads to compounds such as alcohols, aldehydes, ketones and carboxylic acids containing fewer and fewer carbon atoms. It is assumed that extended radiation to doses 10 to 50 times that used in the present work for initial product determination would result in the breakdown of benzene to form CO_2 , a process termed mineralization by workers in the

field. A discussion of differences in CO₂ production for each system is provided later in this dissertation.

Mechanistic Pathway for Anoxic Systems

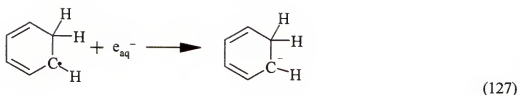
Reaction of e_{aq}^- and $H\cdot$

In deaerated solutions, the reactions of e_{aq}^- and $H\cdot$ with benzene must be considered. As illustrated previously, e_{aq}^- reacts with benzene to form the cyclohexadienyl radical anion, which immediately protonates to form the cyclohexadienyl radical, $C_6H_7\cdot$, via Reactions (104) and (105). Since $H\cdot$ reacts with benzene to form the same product in a one-step process (Reaction (106)), the types of compounds that are formed by the cyclohexadienyl radical may be considered as a class.

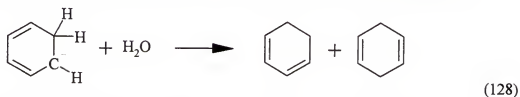
The number of papers describing the gamma irradiation of aqueous benzene solutions under reducing conditions comprises approximately 5% of the total number published. In one such paper, Studier and Hart examined the reduction of benzene in alkaline solution [104]. The system was studied under a high pressure of H₂ so that the following transformations would take place.



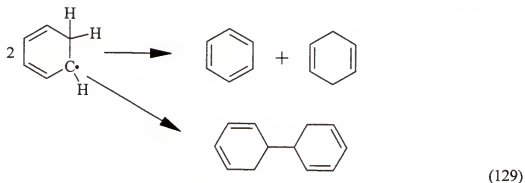
After a short period of irradiation, reduction products such as cyclohexadienes and phenylcyclohexadienes were detected. To explain the origin of these reduced products, they assumed that the cyclohexadienyl radical would react with an electron by addition, forming the cyclohexadienyl radical anion.



Protonation of the radical anion would lead to both 1,3- and 1,4-cyclohexadiene.



Sequential e_{aq}^- attack on either of the cyclohexadienes would lead to cyclohexene and cyclohexane by the same mechanism. If the cyclohexadienyl radical did not undergo attack by e_{aq}^- via Reaction (127), the radical could disproportionate to form benzene and cyclohexadiene, or could couple to form any of several isomers of reduced biphenyl.

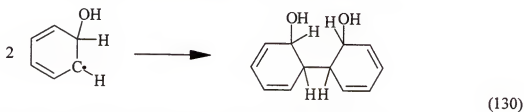


Likewise, in 1970 Michael and Hart explored the aqueous benzene system and found that the yields of reduced products increased when the aqueous system was modified via Reactions (125) and (126) such that $\text{H}\cdot$ and $\cdot\text{OH}$ were converted into e_{aq}^- [105]. They measured products such as 1,3-cyclohexadiene, 1,4-cyclohexadiene, various isomers of C_6H_{10} (cyclohexene), $\text{C}_{12}\text{H}_{14}$ (bicyclohexadienes) as well as C_6H_{12} (cyclohexane) and $\text{C}_{12}\text{H}_{22}$ (bicyclohexyl). Michael and Hart justified the formation of these compounds using a mechanism similar to that shown in Reaction (127) -

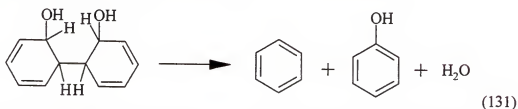
Reaction (129). They also reported the e_{aq}^- addition rate constant for 1,3-cyclohexadiene as $1.0 \times 10^9 \text{ M}^{-1} \text{ s}^{-1}$. However, they were only able to place upper limits on the addition rate constants of 1,4-cyclohexadiene and cyclohexene of $7.5 \times 10^5 \text{ M}^{-1} \text{ s}^{-1}$ and $10^6 \text{ M}^{-1} \text{ s}^{-1}$, respectively.

Reaction of $\cdot\text{OH}$

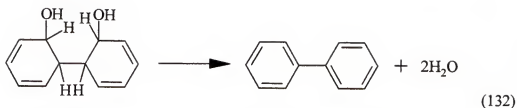
In deaerated aqueous solutions of benzene, the $\cdot\text{OH}$ adds to the benzene ring to form the hydroxycyclohexadienyl radical as in the oxygenated system. However, since oxygen is absent, peroxy formation is not possible. The fate of the hydroxycyclohexadienyl radical has been the subject of numerous studies. In 1971, Mantaka and Marketos studied the N_2O -saturated aqueous benzene system [106]. At this point, the reader is reminded that the presence of N_2O converts e_{aq}^- into $\cdot\text{OH}$ via Reaction (61), thus converting the system to oxidizing-only in character. This modification was discussed at length in Chapter 2. Mantaka and Marketos proposed that in the absence of oxygen, hydroxycyclohexadienyl radicals dimerize.



The dimer may disproportionate to form benzene, phenol and water.

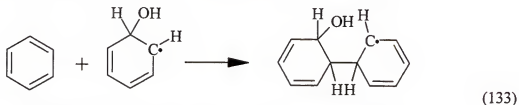


Alternatively, the dimer may eliminate two molecules of water to form biphenyl.

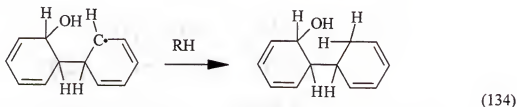


Consideration of their mechanism for the formation of phenol and biphenyl led to the calculation of the disproportion to dimerization ratio, which was obtained by dividing $G(\text{phenol})$ by $G(\text{biphenyl})$. For their results, Mantaka and Marketos calculated a ratio of 0.48. Mantaka and Marketos summarized their results by stating that in anoxic solutions, the formation of dimers is of central importance.

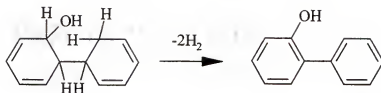
In 1974, Bhatia studied the N₂O-saturated aqueous benzene system [107]. In addition to phenol and biphenyl, Bhatia observed the production of various isomers of phenylphenols. Bhatia rationalized their production by assuming that the hydroxycyclohexadienyl radical can combine with reactant benzene in addition to reacting via the dimerization mechanism of Mantaka, Reaction (130). In Bhatia's explanation, the hydroxycyclohexadienyl radical reacts with benzene.



The product of Reaction (133) then abstracts H• from another species.



Lastly, the elimination of 2 molecules of H₂ leads to formation of the observed phenylphenols.



(135)

In 1978, Klein and Schuler studied the N_2O -saturated system and calculated that $G(\text{phenol})$ was equal to 0.8 and $G(\text{dimeric products})$ was equal to 4.1 [108]. Based on their results, a disproportionation to dimerization ratio of 0.20 was calculated.

Application of Mechanisms to Our Systems

In the previous section, the accepted mechanisms for the radiolysis of aqueous benzene solutions were discussed. A mechanism for radiolysis in the presence of oxygen was presented that resulted in the formation of phenol and ring-opened products. Different mechanisms for reaction of $\cdot OH$ or e_{aq}^- were presented in anoxic solutions. To date, no studies have been performed in which oxygen-saturated solutions or anoxic solutions were irradiated until doses were absorbed sufficient to transform all reactant benzene to first, second or even third generation products, that is, doses of *ca.* 10 to 20 Mrad. An analysis of the literature reveals that in all previous studies in which oxygen-saturated solutions were irradiated, the time of irradiation was adjusted so that the sample only absorbed a few krad at most. In addition, in radiolysis experiments of anoxic solutions, the solutions were always saturated with N_2O in order to study $\cdot OH$ oxidation reactions, or the solutions were treated with high pressures of H_2 in order to study e_{aq}^- reduction reactions. In no previous work have both $\cdot OH$ and e_{aq}^- been allowed to react with benzene in the study of anoxic aqueous benzene solutions. Therefore, an explanation of the observed behavior in the four systems studied in this research project

(short air, long air, long oxygen and long nitrogen) requires careful consideration and proper application of the three limiting-case mechanisms described earlier.

To rationalize benzene destruction and product yields, one must consider the amount of oxygen present in each of the four systems, since the presence or absence of oxygen determines the choice of mechanistic pathways leading to production of CO_2 .

Calculation of Available Oxygen

Short air system

It has been reported that the concentration of oxygen in air-saturated water in contact with air at a pressure of 1 atm is 0.25 mM [14]. For 5.000 mL of air-saturated aqueous solution, the amount of oxygen can be calculated:

$$(5.000 \text{ mL}) \left(0.25 \frac{\text{mmol}}{\text{L}} \right) \left(\frac{1 \text{ L}}{1000 \text{ mL}} \right) \left(\frac{1000 \mu\text{mol}}{1 \text{ mmol}} \right) = 1.25 \mu\text{moles} \quad (136)$$

To calculate the amount of oxygen per mL of air, the oxygen percent composition of air (20.9% [109]) and the molar gas volume at 25°C and 760 mm Hg are used.

$$(1 \text{ mL air}) \left(\frac{0.209 \text{ mL O}_2}{1 \text{ mL air}} \right) \left(\frac{1 \text{ mmol}}{24.41 \text{ mL}} \right) \left(\frac{1000 \mu\text{mol}}{1 \text{ mmol}} \right) = 8.19 \frac{\mu\text{moles O}_2}{\text{mL air}} \quad (137)$$

Each short air tube contained a 5.000 mL volume of aqueous benzene solution and a 3.0 mL headspace volume filled with air. The total amount of oxygen can be calculated by summing the contributions from Equations (136) and (137).

$$1.25 \mu\text{mol O}_2 + (3.0 \text{ mL air}) \left(8.19 \frac{\mu\text{mol O}_2}{\text{mL air}} \right) = 25.8 \mu\text{moles O}_2 \quad (138)$$

Thus, the amount of oxygen available in each short air tube was taken to equal 25.8 $\mu\text{moles O}_2$.

Long air system

Each long air tube was prepared by adding 5.000 mL of air-saturated solution to a long tube. The volume of headspace in each long tube was equal to 11.0 mL. The total amount of oxygen available in each long air tube is calculated by using the factors from Equations (136) and (137).

$$1.25\mu\text{mol O}_2 + (11.0\text{mL air})\left(8.19\frac{\mu\text{mol O}_2}{\text{mL air}}\right) = 91.3\mu\text{moles O}_2 \quad (139)$$

The amount of oxygen in each long air tube was taken to equal 91.3 $\mu\text{moles O}_2$.

Long oxygen system

The aqueous solubility of oxygen at 1 atm pressure and 25°C is equal to 1.31 mM [68]. Using this solubility value, the amount of oxygen in 5.000 mL of oxygen-saturated solution can be calculated.

$$(5.000\text{mL})\left(1.31\frac{\text{mmol}}{\text{L}}\right)\left(\frac{1\text{L}}{1000\text{mL}}\right)\left(\frac{1000\mu\text{mol}}{1\text{mmol}}\right) = 6.55\mu\text{moles} \quad (140)$$

The amount of oxygen contained in 11.0 mL of gas (headspace volume of long tubes) at room temperature and room pressure was determined using the molar gas volume at lab conditions, 24.41 mL/mmol.

$$(11.0\text{mL})\left(\frac{1\text{mmol}}{24.41\text{mL}}\right)\left(\frac{1000\mu\text{mol}}{1\text{mmol}}\right) = 451\mu\text{moles} \quad (141)$$

Thus, the total amount of oxygen present in a long oxygen tube was taken as the sum of the amounts listed in Equations (140) and (141), 458 μmoles of oxygen.

Long nitrogen system

In the long nitrogen system, the MQ water was sparged with nitrogen before sample preparation took place in the nitrogen-filled glovebox. Therefore, the amount of oxygen in each long nitrogen tube was assumed to be zero.

Determination of Radical Production Rates

As described above, the selection of mechanistic pathway is based upon the availability of oxygen for peroxyhydroxycyclohexadienyl radical formation. In solutions containing oxygen, e_{aq}^- and $H\cdot$ are scavenged by oxygen via Reactions (29) and (43). In addition, in oxygen containing solutions the formation of the hydroxycyclohexadienyl radical is followed by oxygen attack to form the peroxyhydroxycyclohexadienyl radical via Reaction (112). Since the total amount of oxygen in the sample tube was known for each system, the rate of radical production was calculated for e_{aq}^- , $H\cdot$ and $\cdot OH$.

Rate of production of hydrated electron

The rate of production of e_{aq}^- was calculated by employing the dose rate as determined by Fricke dosimetry, the value of $G(e_{aq}^-)$, and the sample volume. For example, the short air studies were performed during the summer of 1995. The dose rate during this time was equal to 3.178×10^{17} eV/(mL*min). Using the value of $G(e_{aq}^-)$ given by Draganic [22], 2.63 molecules per 100 eV, and the sample volume, 5.000 mL, the production rate was calculated as shown.

$$\left(3.178 \times 10^{17} \frac{\text{eV}}{\text{mL min}}\right) (5.000 \text{ mL}) \left(\frac{2.63 \text{ molec}}{100 \text{ eV}}\right) \left(\frac{1 \text{ mol}}{6.02 \times 10^{23} \text{ molec}}\right) = 6.94 \times 10^{-8} \frac{\text{mol}}{\text{min}} \quad (142)$$

The production rate was then converted to $\mu\text{moles per hour}$.

$$\left(6.94 \times 10^{-8} \frac{\text{mol}}{\text{min}}\right) \left(\frac{60 \text{ min}}{\text{hr}}\right) \left(\frac{1 \times 10^6 \mu\text{mol}}{\text{mol}}\right) = 4.16 \frac{\mu\text{moles}}{\text{hr}} \quad (143)$$

This value was taken as the production rate of e_{aq}^- , 4.16 $\mu\text{moles } e_{aq}^-$ per hour.

Rate of production of hydrogen atom

The rate of production of $H\cdot$ over the time period during which the short air studies were done was calculated in the same manner as in Equations (142) and (143) except that the value of $G(H\cdot)$ was used instead of $G(e_{aq}^-)$. Using the value of $G(H\cdot)$ given by Draganic [22], 0.55 molecules per 100 eV, the rate of production of $H\cdot$ was calculated to equal 0.871 $\mu\text{moles } H\cdot$ per hour.

Rate of production of hydroxyl radical

The rate of production of $\cdot OH$ during the short air studies was calculated using Equations (142) and (143) with the value of $G(\cdot OH)$ given by Draganic [22], 2.72 molecules per 100 eV. Using this value, the rate of production of $\cdot OH$ during these studies was calculated to equal 4.31 $\mu\text{moles } \cdot OH$ per hour.

The rates of production of the radical transients e_{aq}^- , $H\cdot$ and $\cdot OH$, as well as the rates of production of the molecular species H_3O^+ and H_2O_2 were calculated for each system, and are given in Table 32. Each production rate is based on the average dose rate that was obtained during that particular phase of the project. Values for each $G(\text{species})$ were taken from Draganic [22] and are listed in Chapter 2. The reader should note that similar to the yields of e_{aq}^- , $H\cdot$ and $\cdot OH$, $G(H_3O^+)$ refers to a transient species and not to a stable species. Presumably, H_3O^+ reacts with anions in solution to form neutral products and does not build up resulting in acidification of the irradiated solution.

Table 32: Rates of production, R, of radical and molecular products during the four experiments using geometry B.

System	Dose Rate (eV/mL*min)	R(e_{aq}^-) (μ mol/hr)	R(H \cdot) (μ mol/hr)	R(\cdot OH) (μ mol/hr)	R(H ₃ O ⁺) (μ mol/hr)	R(H ₂ O ₂) (μ mol/hr)
Short air	3.178×10^{17}	4.16	0.871	4.31	4.16	1.08
Long oxygen	3.050×10^{17}	4.00	0.836	4.14	4.00	1.03
Long air	2.890×10^{17}	3.79	0.792	3.92	3.79	0.979
Long nitrogen	2.814×10^{17}	3.69	0.771	3.81	3.69	0.954

Discussion of Product Formation in Each System

Long nitrogen system

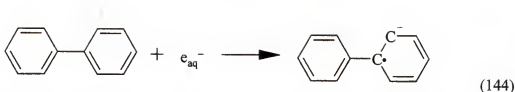
The long nitrogen system has been chosen for discussion first, because the experimental results are the most explainable from the four systems. Since the system contained no oxygen, all \cdot OH adds to the benzene ring via the addition mechanism of Mantaka, Reaction (130) – Reaction (132). Mantaka's mechanism results in the formation of a dimer of the hydroxycyclohexadienyl radical, which can disproportionate to form phenol and benzene, or can eliminate 2 molecules of water to form biphenyl. As mentioned earlier, previous researchers who studied the \cdot OH addition reaction in anoxic solutions routinely calculated the ratio of disproportionation to dimerization by dividing G(phenol) by G(biphenyl). The values of G(phenol) and G(biphenyl) were usually found to equal approximately 0.4 and 1.0, respectively. Although reported yields varied somewhat, the ratio tended to fall between 0.2 to 0.5, implying that biphenyl was the major product in a 2:1 or 3:1 ratio.

Figure 62 shows the amount of biphenyl (in μ moles) versus dose (in Mrad) for the long oxygen and long air systems: however, biphenyl was not quantified at any measured dose in the long nitrogen system. Since biphenyl was the major product in earlier anoxic radiolysis studies, the absence of biphenyl is at first a perplexing issue.

The resolution of this quandary lies in the fact that in all the anoxic studies previously mentioned, the solutions were saturated with N_2O . As discussed in Chapter 2, N_2O converts e_{aq}^- into $\cdot OH$ via Reaction (61). Due to the presence of N_2O , the anoxic solutions mentioned earlier were oxidizing-only in character.

In the nitrogen-saturated solutions studied in this work, N_2O was not used. Therefore, both oxidation and reduction of substrate were possible in our case. The reaction between benzene and e_{aq}^- , Reaction (104), has a rate constant of approximately $1 \times 10^7 \text{ M}^{-1} \text{ s}^{-1}$. The reaction between benzene and $\cdot OH$, Reaction (107), has a rate constant of $8 \times 10^9 \text{ M}^{-1} \text{ s}^{-1}$. Based on $G(\cdot OH)$ of 2.72 and $G(e_{aq}^-)$ of 2.63, calculation reveals that 99.8% of the radical reactions with benzene occur with $\cdot OH$. It is certain, however, that reactions between benzene and e_{aq}^- do occur to form cyclohexadienes as in the mechanism suggested by Studier, Hart and Michael [104, 105]. The initial yield of phenol in the long nitrogen system is calculated to equal 0.29 molecules per 100 eV. This yield is comparable to those reported in the literature for N_2O -saturated aqueous benzene solutions. The value of $G(-\text{benzene})$ at the beginning of irradiation for the long nitrogen system is equal to approximately 4.7. With $G(\text{phenol})$ equal to 0.29, it is obvious that most of the benzene is reacting to form products other than phenol.

The question remains as to the absence of biphenyl in the long nitrogen system. Based on analyses of rate constants and GC-MS work (to be discussed shortly), we propose that biphenyl is formed as predicted by the Mantaka mechanism. However, since e_{aq}^- is not being scavenged in our nitrogen-saturated solutions, we suggest that most biphenyl is attacked by e_{aq}^- immediately upon formation.



The rate constant for addition of e_{aq}^- to biphenyl has been measured by Sehested and Hart as $1.2 \times 10^{10} \text{ M}^{-1} \text{ s}^{-1}$ [110], a value near the diffusion-controlled limit. In contrast, the rate constant for addition of e_{aq}^- to benzene is $1 \times 10^7 \text{ M}^{-1} \text{ s}^{-1}$. It is concluded that

Reaction (144) is the predominate fate of e_{aq}^- in the system. Biphenyl can also be attacked by $\cdot\text{OH}$ with a rate constant of $9.0 \times 10^9 \text{ M}^{-1} \text{ s}^{-1}$ [110]. However, since the rate constant of benzene + $\cdot\text{OH}$ is of the same magnitude as biphenyl + $\cdot\text{OH}$, the majority of $\cdot\text{OH}$ will attack benzene and not biphenyl except in the final stages of an extended radiolysis experiment.

The attack of e_{aq}^- on biphenyl leads to reduced products such as those seen in the work of Michael and Hart [105]: in particular, 1,3-cyclohexadiene, 1,4-cyclohexadiene, and various isomers of C_6H_{10} (cyclohexene), C_6H_{12} (cyclohexane), $\text{C}_{12}\text{H}_{14}$ (bicyclohexadienes) and $\text{C}_{12}\text{H}_{22}$ (bicyclohexyl). These reduced products were discussed earlier in this Chapter. HPLC chromatograms of long nitrogen samples showed no products other than phenol using any of the seven mobile phases mentioned in Chapter 6. Reduced benzenes and reduced biphenyls are nearly insoluble in water. Since development of the irradiated tubes was accomplished by sampling directly from the aqueous phase in a recently mixed radiolysis vessel, it is quite likely that these reduced products have such low water solubility that the amounts injected into the HPLC were below the detection limit at 254 nm.

Evidence of formation of reduced biphenyls was seen via GC-MS experiments. As was presented in Chapter 6 in experiments GCMS8 – GCMS10, three long nitrogen

samples were irradiated until doses of approximately 2.4 Mrad were absorbed. In GCMS8, the precipitate pellet (present in trace quantities in comparison to air-saturated samples) was dissolved in MeOH. In GCMS9, the radiolysis sample was extracted with Et₂O. In GCMS10, the radiolysis sample was extracted with CH₂Cl₂. From the mass spectral data, compounds such as phenylcyclohexadienes, phenylcyclohexene, 1,3,5-dodecatriene, 1,4-diphenylbicyclo[2.1.1]hexane, 2,3-dimethyl-1-hexene, 3,5,5-trimethyl-2-hexene and numerous other reduction products were found by way of mass-spectral matching.

Continued irradiation of nitrogen-saturated samples leads to production of CO₂ as shown in Figure 65. However, the percent degradation for the long nitrogen system after an absorbed dose of 250 Mrad is only 12.5%. Obviously, degradation can occur without added oxygen, but the pathway to degradation is inefficient in comparison to oxygen containing systems. Degradation in the long nitrogen system must occur from phenol and/or these reduced benzene moieties, and not from intramolecular peroxide formation as in samples containing oxygen. Although relatively small amounts of CO₂ were observed in the nitrogen-saturated system, CO₂ is not an initial product but is formed only after extended irradiation.

As mentioned earlier, biphenyl formation was not observed in the long nitrogen system. This observation was repeatable provided that the glovebox was well purged with nitrogen and that the sample-cell enclosure was tight. Failure to purge the glovebox well with nitrogen resulted in the appearance of a peak for biphenyl in the HPLC chromatograms. In fact, the absence or presence of biphenyl served as a visual indicator of the state of the glovebox purge. This observation serves to strengthen our proposed

mechanism for anoxic aqueous benzene solutions. If oxygen is present in the sample vial, the reducing radicals e_{aq}^- and $H\cdot$ are scavenged by oxygen, and the concentration of biphenyl continues to rise until the small amount of oxygen is depleted. As soon as the oxygen is depleted, previously formed biphenyl is destroyed and no additional biphenyl accumulates due to fast reaction with e_{aq}^- .

Long oxygen system

The long oxygen system will be discussed next because it forms the most interesting comparison to the long nitrogen system. In the long oxygen system, the total amount of oxygen present is 451 μ moles. The value of $G(-benzene)$ at the start of the radiolysis experiment is approximately 4.7, and the value of $G(phenol)$ is 1.2. If one assumes that all e_{aq}^- and $H\cdot$ are scavenged effectively by oxygen, then the difference between $G(-benzene)$ and $G(phenol)$ will approximate $G(peroxyhydroxycyclohexadienyl\ radical)$. Following this logic leads to $G(peroxy)$ of 3.5, which corresponds to a production rate of 5.3 μ moles peroxy per hour. Summing the production rates of e_{aq}^- , $H\cdot$, and the peroxyhydroxycyclohexadienyl radical leads to oxygen consumption of 10.1 μ moles per hour. Assuming that no other reactions consume oxygen, the oxygen in the saturated solution combined with the oxygen in the 11.0 mL headspace will last for approximately 45 hours of irradiation using the old irradiator (before reloading in 1999), or approximately 2 days. The validity of this assumption will be discussed shortly.

With oxygen present in excess, all e_{aq}^- and $H\cdot$ are effectively scavenged. After disproportionation of the resulting $HO_2\cdot$ radical, H_2O_2 is produced. As explained previously, the presence of H_2O_2 leads to the formation of extra $\cdot OH$. At the beginning of the radiolysis experiment, consumption of benzene occurs by addition of $\cdot OH$ via

Reaction (107). Formation of phenol via elimination of HO_2^\cdot from the peroxyhydroxycyclohexadienyl radical has a G-value of 1.2. Since $G(-\text{benzene})$ is the same for the long oxygen system as in the long nitrogen system, the extra $\cdot\text{OH}$ produced from H_2O_2 in the long oxygen system has the same ability to consume benzene as the combination of e_{aq}^- , H^\cdot and $\cdot\text{OH}$ in the long nitrogen system.

It is suggested that in the long oxygen system a majority of the benzene undergoes ring opening via formation of peroxyhydroxycyclohexadienyl radicals; the value of $G(\text{peroxyhydroxycyclohexadienyl})$ is 3.5. Sequential reactions of ring-opened compounds lead to formation of CO_2 . In the long oxygen system, 55.1% of initial benzene was converted to CO_2 after the absorption of 250 Mrad.

Long air system

The long air system represents an intermediate case between the long oxygen and the long nitrogen systems. As calculated previously, the total amount of oxygen in each long air tube is equal to 91.3 μmoles . In the long air system, $G(-\text{benzene})$ is equal to 4.7, which is the same value as in the other long systems. In the long air system, the value of $G(\text{phenol})$ based on the initial slope is equal to 0.58. Assuming complete scavenging of the reducing radicals at the onset of the experiment, a value of $G(\text{peroxyhydroxycyclohexadienyl})$ would be assumed to equal 4.1. If one assumes that the peroxy radical leads to formation of CO_2 , then the long air system should result in a larger amount of CO_2 being produced. However, this was not seen in the experimental results. The percent degradation of benzene in the long air system was found to equal 30.5%. This is in marked contrast to the long oxygen system, in which 55.1% of the benzene was converted to CO_2 .

The behavior of the long oxygen versus long air systems in terms of product yields and percent benzene mineralization can be rationalized. It is proposed that in static (non-stirred) solutions, the dissolution of oxygen from the headspace into solution is not an instantaneous process but rather is quite likely a slow process. For this reason, the amount of oxygen present in the long oxygen system is closer to 6.55 μmoles , which is the amount in 5.000 mL of oxygen-saturated aqueous solution, as opposed to the total contained in the solution and in the gas phase. Likewise, the amount of oxygen present in solution in each long air tube (air-saturated solution) is 1.25 μmoles . As the irradiation of each system begins, the reducing radicals are scavenged by oxygen. Both the long oxygen and long air systems follow the mechanism presented above for the radiolysis of oxygenated aqueous benzene solutions. As oxygen becomes depleted in the long air system, the mechanistic pathway followed in the system shifts to the anoxic pathway, with its $G(\text{phenol})$ of 0.2 to 0.3, and $G(\text{biphenyl})$ of 1.0. The shift in pathway causes the production rate of phenol to fall considerably. The reducing radicals now begin to consume biphenyl to form reduced products. Due to the presence of other products that compete for reaction with e_{aq}^- , biphenyl is not consumed as effectively as in the long nitrogen case. Depletion of oxygen in solution occurs later in the long oxygen system as compared to long air system. When depletion of solution oxygen occurs in the long oxygen system, the mechanistic pathway shifts to the anoxic case as in the long nitrogen system. However, oxygen continues to dissolve into solution, although slowly. The dissolution of oxygen into solution enables degradation to CO_2 . Since the 11.0 mL headspace in the long oxygen system is filled entirely with oxygen, more oxygen is available for production of CO_2 , and this is borne out in the experimental results.

The shift in mechanistic pathway in the long air system is evidenced by GC-MS data. In experiments GCMS1 – GCMS4, long air samples were prepared on the benchtop and irradiated for times of 5.5 hours, 7.5 hours, 15 hours and 28 hours. For experiments GCMS1, GCMS3 and GCMS4, methanol solutions of the resulting pellets (present in copious amounts) were injected into the GC-MS unit. For experiment GCMS2, the radiolysis solution was extracted with diethyl ether. In all four experiments, typical oxidation products such as benzaldehyde, hydroxybiphenyls and phenol were observed. In addition, reduction products such as phenylcyclohexadienes and phenylcyclohexenes were seen. The presence of these reduced products serves to justify our proposal of shift to the anoxic pathway as oxygen depletion occurs.

If one examines the yields of 3-phenylphenol and 4-phenylphenol versus dose for the long oxygen and long air systems, the shift in mechanistic pathway is also demonstrated. The amounts of phenylphenols present in the long oxygen system were found to be greater than the amount present in the long air system. Following the mechanism of Bhatia [107], phenylphenols are produced via reaction between benzene and the hydroxycyclohexadienyl radical. Elimination of H_2 yields any of several isomers of phenylphenol. The dissolution of oxygen from the headspace into solution serves to protect the phenylphenols against consumption from reducing radicals. Hence, the yield of phenylphenols present at any time is greater in the long oxygen system than in the long air system.

The differences in percent conversion of benzene to CO_2 are also explainable via our proposed shift in mechanism. Since the long oxygen solutions were initially saturated with oxygen, a significant percentage of the benzene underwent the

intramolecular peroxide forming reaction described earlier. Oxygen, resulting from dissolution of headspace oxygen into the solution, was then available for degradation of the ring-opened products as the radiolysis proceeded long-term.

Long air versus short air system

Analysis of yields of phenol, biphenyl and phenylphenols in the long air and short air systems seems to conflict with the above described shift of mechanism and slow dissolution of headspace oxygen into solution. However, as described in the beginning of this chapter, a considerable portion (*ca.* 30%) of solution benzene volatilized into the headspace in the long air system. For this reason, the yield of phenol in the long air system is smaller than in the short air system. Over the first 0.40 Mrad, the amount of benzene in solution was sufficient to produce the same amount of phenol in both of the air systems. However, after 0.40 Mrad, the amount of benzene in solution in the long air system became inadequate to produce phenol at the same rate. Likewise, the rate of production of phenylphenols for the two air systems was reasonably similar for the first 1.3 Mrad. Once the amount of benzene in solution became inadequate for phenol production, the rate of phenylphenol production also decreased. For this reason, the yields of phenylphenols in the short air system were found to be greater than the yields of phenylphenols in the long air system past a dose of 1.5 Mrad. A similar argument can be made for the difference in yields of biphenyl for the two systems.

Determination of Solution Toxicity

If Cobalt-60 gamma radiation is going to be used for radiation detoxification of polluted water, then the toxicity of the solution should decrease over time. Using published OSHA air-borne toxicity limits [111], the total solution toxicity was calculated for each system at each dose by summing the contributions from benzene and identified

radiolysis products. Individual toxicity limits for benzene and identified products are listed in Table 33. The toxicity limits listed below are threshold limits for airborne contaminants to which workers can be exposed day after day without adverse effect. The limits are given as parts per million (ppm) by volume in air at 25°C and 1 atm pressure. Strictly speaking, these values are for airborne contaminants and not solution contaminants; however, the values were used in this work to illustrate the trend of total solution toxicity versus dose.

Table 33: Airborne toxicity limits (TL) for benzene and identified products.

Compound	Toxicity Limit (ppm)	Toxicity Limit ($\mu\text{moles/mL}$)
Benzene	0.1	1.28×10^{-1}
Phenol	5.0	5.31×10^{-2}
Biphenyl	0.2	1.30×10^{-3}
Phenylphenols	0.1	5.88×10^{-4}

Short air versus long air system

Figure 66 illustrates the total toxicity of the irradiated solution versus dose for both the short air and long air systems. Over the first 2.0 Mrad, the total toxicity of each solution is approximately equal. Each toxicity curve begins at 85 Total Toxicity Units (TTU). The value of 85 TTU means that the solution is 85 times the toxicity limit. Of course, at the beginning of the experiment all toxicity is due to benzene. As radiolysis proceeds, the toxicity of the solution increases. Even though benzene is being consumed, the products that are being formed are toxic also. The net effect is an increase in the toxicity of the irradiated solution. Past 2.2 Mrad, the identified products begin to be consumed, and the total solution toxicity begins to fall.

Solution toxicity in the long systems

Figure 67 shows the total solution toxicity versus dose for the long oxygen, long air and long nitrogen systems. Each of the three curves begins at the same toxicity amount, 85 TTU. The toxicity curves for the long oxygen and long air systems rise over the first 2.2 Mrad, and then both fall. By the end of the radiation timespan (18 Mrad), both toxicity curves have fallen to beneath the toxicity of the starting solution. The toxicity curve for nitrogen falls immediately. Since phenol was the only quantified product in the long nitrogen system, the net toxicity resulting from decreasing amounts of benzene and increasing amounts of phenol still falls.

For the short air, long air and long oxygen systems, continuous irradiation eventually causes the toxicity curves to fall beneath the toxicity value of the unirradiated solution. For the long nitrogen system, the curve of toxicity versus dose falls immediately. However, are any of the solutions really detoxified? The only method for answering this question is the monitoring of CO_2 versus dose. As can be seen from the plots of CO_2 yield versus dose (Figure 58 and Figure 65), significant CO_2 is not produced until after a dose of 30 Mrad has been absorbed by the system. Obviously, between 10 Mrad (point at which toxicity curves fall beneath the starting values), and 30 Mrad (onset of CO_2 production) a multitude of compounds is being formed, each with its own toxicity limit. Although each of these compounds is formed in small yield, the total concentration is large enough to be significant. Therefore, one can never validly discuss solution toxicity without adequate carbon mass balance or CO_2 production information. Although chromatograms from analytical instrumentation such as HPLC or GC-MS may not indicate the presence of any product compound, it is quite likely that many compounds are present in the so-called "detoxified" sample, but they are present in

concentrations that are below the Limit of Detection (LOD) for the particular method.

The production of CO₂ for hydrocarbon systems is the only foolproof indicator to tell whether or not the solution is actually detoxified.

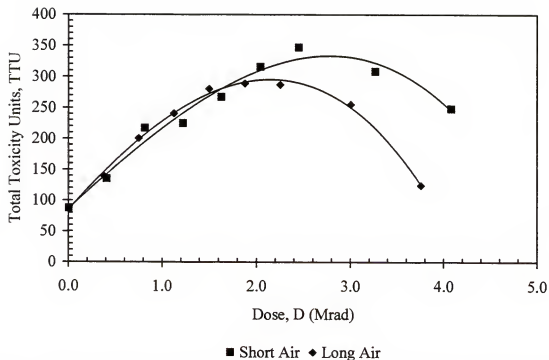
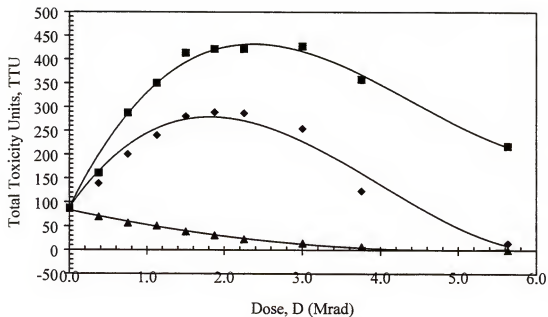


Figure 66: Plot of Total Toxicity Units (TTU) versus dose in Mrad for the short air and long air systems.



■ Long Oxygen ♦ Long Air ▲ Long Nitrogen

Figure 67: Plot of Total Toxicity Units (TTU) versus dose in Mrad for the long oxygen, long air and long nitrogen systems. Data are shown for the first 15 hours of irradiation.

CHAPTER 8 CONCLUSION AND FUTURE WORK

Summary of Results

For three of the four systems studied in this project (short air, long oxygen and long air), phenol and biphenyl were determined to be the major identified products. For the long nitrogen system, phenol was the sole identified product. Benzene was found to be consumed at nearly the same rate in each of the four systems; $G(-\text{benzene})$ was found to be in the range of 4.2 to 4.7 molecules per 100 eV. Initial yields of phenol, $G(\text{phenol})$, were determined for each system and were found to equal 0.58, 1.2, 0.58 and 0.29 for the short air, long oxygen, long air and long nitrogen systems, respectively. The yield of biphenyl, $G(\text{biphenyl})$, was also determined for each of the three systems in which biphenyl was identified as a product. Values for $G(\text{biphenyl})$ of 0.12, 0.27 and 0.18 were calculated for the short air, long oxygen and long air systems, respectively. The compounds 3- and 4-phenylphenol were also identified as minor products in the short air, long oxygen and long air systems. Their yields are given in Chapter 7 in Table 30 and Table 31. Lastly, the percent conversion of benzene to CO_2 was determined for each of the four systems after a dose of 250 Mrad had been absorbed: the values found were 10.7%, 55.1%, 30.5% and 12.5% for the short air, long oxygen, long air and long nitrogen systems, respectively. A proposed mechanism for radiolysis of each system was presented. Product yields were discussed in view of the proposed mechanism.

Implications for Detoxification Applicability

The results obtained in this project definitely support the use of ionizing radiation for solution detoxification. However, as demonstrated in Chapter 7, the availability of oxygen is the predominate factor for production of CO_2 , which is the final degradation product. Even though the initial benzene is destroyed, many of the radiolysis products that are formed during the benzene destruction timescale are more toxic than the initial benzene, so that the total toxicity of the irradiated benzene system tends to increase rather than decrease during the initial irradiation period. The possibility of similar behavior must be considered in the case of other water pollutants. Each case (or class of related compounds) needs to be evaluated before this detoxification method is given blanket approval for a particular contaminant. Ultimately, general approval might be possible for sufficiently low pollutant concentrations along with sufficiently large doses.

Several general statements concerning the applicability of ionizing radiation for solution detoxification can be made.

1. The practicality of this method will differ for various contaminants.
2. The concentration level of both the contaminant and of "benign" impurities is important; the latter may compete for $\cdot\text{OH}$ or e_{aq}^- .
3. One-step conversion of solute to CO_2 is unlikely in most systems, especially aromatic systems.
4. In the case of benzene (and similar compounds), the formation of 5 or 6 major products and as many as 20 to 30 minor products can be expected.
5. If the original concentration of contaminant is near the analytical threshold, conversion of that single species to 5, 10 or more products may drop all concentrations below detection limits—yet the water is not really "detoxified". Therefore, carbon mass balance or CO_2 production information is necessary before detoxification can be validly discussed.

6. In some cases, sequential conversion of reactant into successively higher molecular weight products can occur, following an $A \rightarrow B \rightarrow C$ kinetic scheme. However, at each stage, degradation of reactant moieties into lower molecular weight or oxidized fragments can compete.
7. Since products may be more toxic per mole than reactant, it is possible that total toxicity will increase initially, before decreasing at higher dose.
8. Greater total dose will always give more substrate destruction; higher dose rate may not do so.

Future Work

As asserted in Chapter 7, the dissolution of oxygen from the headspace volume into solution is a slow process. One extension of this work that should be performed is the repetition of radiolyses under dynamic conditions instead of static conditions. This could be accomplished by continually stirring the sample during irradiation or shaking the sample every few hours. Although the results in this proposed experimental scheme are predictable (faster consumption of solid products, greater production of CO_2), it would be interesting to quantify the speed of oxygen dissolution into solution by comparing the results obtained in this "static" project with the results obtained in the suggested "dynamic" project.

Since oxygen availability is the determining factor for production of CO_2 , the effect of higher pressures of oxygen in the headspace should also be investigated for both the static and dynamic systems. By careful experimental design, it should be possible to determine a correlation between such factors as initial solute concentration, pressure of oxygen in the headspace and the rate of CO_2 production for both the static and dynamic systems.

LIST OF REFERENCES

1. Getoff, N., *Radiation and Photoinduced Degradation of Pollutants in Water. A Comparative Study*. Radiation Physics and Chemistry, 1991. 37: p. 673-680.
2. Al-Ekabi, H. and N. Serpone, *Kinetic Studies in Heterogeneous Photocatalysis. 1. Photocatalytic Degradation of Chlorinated Phenols in Aerated Aqueous Solutions of TiO_2 Supported on a Glass Matrix*. Journal of Physical Chemistry, 1988. 92: p. 5726-5731.
3. Fujihira, M. and Y. Satoh, *Heterogeneous Photocatalytic Oxidation of Aromatic Compounds on TiO_2* . Nature, 1981. 293: p. 206-208.
4. Theurich, J., M. Lindner, and D.W. Bahnemann, *Photocatalytic Degradation of 4-Chlorophenol in Aerated Aqueous Titanium Dioxide Suspensions: A Kinetic and Mechanistic Study*. Langmuir, 1996. 12: p. 6368-6376.
5. Sclafani, A., L. Palmisano, and E. Davi, *Photocatalytic Degradation of Phenol in Aqueous Polycrystalline TiO_2 Dispersions: The Influence of Fe^{3+} , Fe^{2+} , and Ag^+ on the Reaction Rate*. Journal of Photochemistry and Photobiology. A: Chemistry, 1991. 56: p. 113-123.
6. Stafford, U., K.A. Gray, and P.V. Kamat, *Radiolytic and TiO_2 Assisted Photocatalytic Degradation of 4-Chlorophenol. A Comparative Study*. Journal of Physical Chemistry, 1994. 98: p. 6343-6351.
7. Kim, D.H. and M.A. Anderson, *Solution Factors Affecting the Photocatalytic and Photoelectrocatalytic Degradation of Formic Acid Using Supported TiO_2 Thin Films*. Journal of Photochemistry and Photobiology. A: Chemistry, 1996. 94: p. 221-229.
8. Hashimoto, K., T. Kawai, and T. Sakata, *Photocatalytic Reactions of Hydrocarbons and Fossil Fuels with Water. Hydrogen Production and Oxidation*. Journal of Physical Chemistry, 1984. 88: p. 4083-4088.
9. Anpo, M., N. Aikawa, S. Kodama, and Y. Kubokawa, *Photocatalytic Hydrogenation of Alkynes and Alkenes with Water over TiO_2 . Hydrogenation Accompanied by Bond Fission*. Journal of Physical Chemistry, 1984. 88: p. 2569-2572.

10. Matsumura, M., M. Hiramoto, T. Iehara, and H. Tsubomura, *Photocatalytic and Photoelectrochemical Reactions of Aqueous Solutions of Formic Acid, Formaldehyde, and Methanol on Platinized CdS Powder and at a CdS Electrode*. Journal of Physical Chemistry, 1984. 88: p. 248-250.
11. Nickelsen, M.G., W.J. Cooper, C.N. Kurucz, and T.D. Waite, *Removal of Benzene and Selected Alkyl-Substituted Benzenes from Aqueous Solution Utilizing Continuous High-Energy Electron Irradiation*. Environmental Science & Technology, 1992. 26: p. 144-152.
12. Nickelsen, M.G., W.J. Cooper, K. Lin, C.N. Kurucz, and T.D. Waite, *High Energy Electron Beam Generation of Oxidants for the Treatment of Benzene and Toluene in the Presence of Radical Scavengers*. Water Research, 1994. 28: p. 1227-1237.
13. Crawford, C.L., M.R. Gholami, R.N. Bhawe, and R.J. Hanrahan, *Pulse Radiolysis of Aqueous Solutions of Sodium Tetraphenylborate*. Radiation Physics and Chemistry, 1994. 44: p. 309-315.
14. Gupta, A.K., R.J. Hanrahan, and D.D. Walker, *Use of Co-60 Gamma Irradiation to Simulate Decomposition of Tetraphenylborate Precipitates from High Level Radioactive Waste*. Radiochimica Acta, 1993. 60: p. 43-51.
15. Lederer, C.M., J.M. Hollander, and I. Perlman, *Table of Isotopes*. Sixth ed. 1967, John Wiley and Sons: New York. 594.
16. Spinks, J.W.T. and R.J. Woods, *An Introduction to Radiation Chemistry*. Second ed. 1976, John Wiley and Sons: New York. 504.
17. Swallow, A.J., *Radiation Chemistry: An Introduction*. First ed. 1973, John Wiley and Sons: New York. 275.
18. Bethe, H.A. and J. Ashkin, *Experimental Nuclear Physics*, ed. E. Segre. Vol. 1. 1953, John Wiley and Sons: New York. 166.
19. Christophorou, L.G., R.N. Compton, G.S. Hurst, and P.W. Reinhardt, *Dissociative Electron Capture by Benzene Derivatives*. Journal of Chemical Physics, 1966. 45: p. 536-547.
20. Spinks, J.W.T. and R.J. Woods, *An Introduction to Radiation Chemistry*. Third ed. 1990, Wiley-Interscience: New York. 574.
21. Friedlander, G., J.W. Kennedy, E.S. Macias, and M. Miller, *Nuclear and Radiochemistry*. Third ed. 1981, Wiley-Interscience: New York. 684.
22. Draganic, I.G. and Z.D. Draganic, *The Radiation Chemistry of Water*. Physical Chemistry, ed. E.M. Loebl. Vol. 26. 1971, Academic Press: New York. 242.

23. Buxton, G.V., *Basic Radiation Chemistry of Liquid Water*, in *The Study of Fast Processes and Transient Species by Electron Pulse Radiolysis*, J.H. Baxendale and F.D. Busi, Editors. 1981, Reidel Publishing Company: New York. p. 267-287.
24. Mozumder, A. and J.L. Magee, *Theory of Radiation Chemistry. VII. Structure and Reactions in Low LET Tracks*. Journal of Chemical Physics, 1966. 45: p. 3332-3341.
25. Schmidt, K.H. and D.M. Bartels, *Lack of Ionic Strength Effect in the Recombination of Hydrated Electrons*. Chemical Physics, 1995. 190: p. 145-152.
26. Christensen, H., K. Sehested, and T. Logager, *Temperature Dependence of the Rate Constant for Reactions of Hydrated Electrons with H, OH and H₂O₂*. Radiation Physics and Chemistry, 1994. 43: p. 527-531.
27. Chen, R., Y. Avotins, and G.R. Freeman, *Solvent Effects on the Reactivity of Solvated Electrons with Ions in Isobutanol/Water Mixed Solvents*. Canadian Journal of Chemistry, 1994. 72: p. 1083-1093.
28. Felix, W.D., B.L. Gall, and L.M. Dorfman, *Pulse Radiolysis Studies. IX. Reactions of the Ozonide Ion in Aqueous Solution*. Journal of Physical Chemistry, 1967. 71: p. 384-392.
29. Matheson, M.S. and J. Rabani, *Pulse Radiolysis of Aqueous Solutions. I. Rate Constants for Reaction of e_{aq}^- with Itself and Other Transients. II. The Interconvertibility of e_{aq}^- and H*. Journal of Physical Chemistry, 1965. 69: p. 1324-1335.
30. Elliot, A.J., D.R. McCracken, G.V. Buxton, and N.D. Wood, *Estimation of Rate Constants for Near-Diffusion-Controlled Reactions in Water at High Temperatures*. Journal of the Chemical Society, Faraday Transactions, 1990. 86: p. 1539-1547.
31. Elliot, A.J., *A Pulse Radiolysis Study of the Temperature Dependence of Reactions Involving H, OH and e_{aq}^- in Aqueous Solutions*. Radiation Physics and Chemistry, 1989. 34: p. 753-758.
32. Gruenbein, W., A. Henglein, G. Stevens, and G. Beck, *Vielfachpuls-Radiolyse: Sukzessive Anlagerung Zweier Hydratisierter Elektronen und Sauerstoff, Nitrobenzol und Nitromethan*. Ber. Bunsenges. Phys. Chem., 1971. 75: p. 126-134.
33. Buxton, G.V., C.L. Greenstock, W.P. Helman, and A.B. Ross, *Critical Review of Rate Constants for Reactions of Hydrated Electrons, Hydrogen Atoms and Hydroxyl Radicals (OH/O⁻) in Aqueous Solutions*. Journal of Physical Chemistry Reference Data, 1988. 17: p. 513-886.

34. Han, P. and D.M. Bartels, *H/D Isotope Effects in Water Radiolysis. 4. The Mechanism of $H_{aq} \rightleftharpoons e_{aq}^-$ Interconversion*. Journal of Physical Chemistry, 1992. 96: p. 4899-4906.
35. Sehested, K. and H. Christensen, *The Rate Constant of the Bimolecular Reaction of Hydrogen Atoms at Elevated Temperatures*. Radiation Physics and Chemistry, 1990. 35: p. 499-500.
36. Thomas, J.K., *Rates of Reaction of the Hydroxyl Radical*. Transactions of the Faraday Society, 1965. 61: p. 702-707.
37. Hart, E.J. and M. Anbar, *The Hydrated Electron*. 1970, Wiley-Interscience: New York. 267.
38. Christensen, H. and K. Sehested, *Reaction of Hydroxyl Radicals with Hydrogen at Elevated Temperatures. Determination of the Activation Energy*. Journal of Physical Chemistry, 1983. 87: p. 118-120.
39. Christensen, H., K. Sehested, and H. Corfitzen, *Reactions of Hydroxyl Radicals with Hydrogen Peroxide at Ambient and Elevated Temperatures*. Journal of Physical Chemistry, 1982. 86: p. 1588-1590.
40. Buxton, G.V., *Radiation Chemistry of the Liquid State: (1) Water and Homogeneous Aqueous Solutions*, in *Radiation Chemistry: Principles and Applications*, Farhataziz and M.A.J. Rodgers, Editors. 1987, VCH Publishers: New York. p. 321-349.
41. Mezyk, S.P. and D.M. Bartels, *Direct EPR Measurement of Arrhenius Parameters for the Reactions of H Atoms with H_2O_2 and D Atoms with D_2O_2 in Aqueous Solution*. Journal of the Chemical Society, Faraday Transactions, 1995. 91: p. 3127-3132.
42. Feng, P.Y., A. Brynjolfsson, J.W. Halliday, and R.D. Jarrett, *High-Intensity Radiolysis of Aqueous Ferrous Sulfate-Cupric Sulfate-Sulfuric Acid Solutions*. Journal of Physical Chemistry, 1970. 74: p. 1221-1227.
43. Ilan, Y. and J. Rabani, *On Some Fundamentals in Radiation Chemistry. Nanosecond Pulse Radiolysis*. International Journal of Radiation Physics and Chemistry, 1976. 8: p. 609-611.
44. Anbar, M., Farhataziz, and A.B. Ross, *Selected Specific Rates of Reactions of Transients from Water in Aqueous Solution. II. Hydrogen Atom*. National Standard Reference Data Series, U.S. National Bureau of Standards, 1975. 51: p. 56.
45. Buxton, G.V., *Pulse Radiolysis of Aqueous Solutions. Rate of Reaction of OH with OH^-* . Transactions of the Faraday Society, 1970. 66: p. 1656-1660.

46. Merenyi, G. and J.S. Lind, *Role of a Peroxide Intermediate in the Chemiluminescence of Luminol. A Mechanistic Study*. Journal of the American Chemical Society, 1980. 102: p. 5830-5835.
47. Rabani, J. and M.S. Matheson, *The Pulse Radiolysis of Aqueous Solutions of Potassium Ferrocyanide*. Journal of Physical Chemistry, 1966. 70: p. 761-769.
48. Elliot, A.J. and G.V. Buxton, *Temperature Dependence of the Reactions $\text{OH} + \text{O}_2^-$ and $\text{OH} + \text{HO}_2$ in water up to 200 C*. Journal of the Chemical Society, Faraday Transactions, 1992. 88: p. 2465-70.
49. Hickel, B. and K. Sehested, *Activation Energies for the Reactions $\text{O}^- + \text{H}_2$ and $\text{O}^- + \text{D}_2$ in Aqueous Solution*. Journal of Physical Chemistry, 1991. 95: p. 744-747.
50. Elliot, A.J. and D.K. McCracken, *Effect of Temperature on O^- Reactions and Equilibria: A Pulse Radiolysis Study*. Radiation Physics and Chemistry, 1989. 33: p. 69-74.
51. Sehested, K., J. Holcman, E. Bjergbakke, and E.J. Hart, *Ultraviolet Spectrum and Decay of the Ozonide Ion Radical, O_3^- , in Strong Alkaline Solution*. Journal of Physical Chemistry, 1982. 86: p. 2066-2069.
52. Schwarz, H.A., *Free Radicals Generated by Radiolysis of Aqueous Solutions*. Journal of Chemical Education, 1981. 58: p. 101-105.
53. Thomas, J.K., *Advances in Radiation Chemistry*, in *Advances in Radiation Chemistry*, M. Burton and J.L. Magee, Editors. 1969, Wiley-Interscience: New York. p. 410.
54. Klaning, U.K. and K. Sehested, *Standard Gibbs Energy of Formation of the Hydroxyl Radical in Aqueous Solution. Rate Constants for the Reaction $\text{ClO}_2^- + \text{O}_3 \rightleftharpoons \text{O}_3^- + \text{ClO}_2$* . Journal of Physical Chemistry, 1985. 89: p. 760-763.
55. Schwarz, H.A. and R.W. Dodson, *Equilibrium Between Hydroxyl Radicals and Thallium(II) and the Oxidation Potential of $\text{OH}(\text{aq})$* . Journal of Physical Chemistry, 1984. 88: p. 3643-3647.
56. Dorfman, L.M. and G.E. Adams, *Reactivity of the Hydroxyl Radical in Aqueous Solutions*. NSRDS-NBS 46. 1973, U.S. Dept. Commerce - National Bureau of Standards: Washington, D. C. 59.
57. Janata, E. and R.H. Schuler, *Rate Constant for Scavenging e_{aq}^- in N_2O -Saturated Solutions*. Journal of Physical Chemistry, 1982. 86: p. 2078-2084.

58. Schuler, R.H., L.H. Amy, and B. Behar, *Track Effects in Radiation Chemistry. Concentration Dependence*. Journal of Physical Chemistry, 1981. 85: p. 192-199.
59. Gordon, S., K.H. Schmidt, and E.J. Hart, *A Pulse Radiolysis Study of Aqueous Benzene Solutions*. Journal of Physical Chemistry, 1977. 81: p. 104-109.
60. Buxton, G.V., *Pulse Radiolysis Studies of Aqueous Solutions*, in *Pulse Radiolysis*, Y. Tabata, Editor. 1991, CRC Press: Boca Raton. p. 397-429.
61. Denaro, A.R. and G.G. Jayson, *Fundamentals of Radiation Chemistry*. First ed. 1973, Butterworth & Company Ltd.: Ann Arbor. 204.
62. Allen, A.O., *The Radiation Chemistry of Water and Aqueous Solutions*. First ed. 1961, D. Van Nostrand Company: Princeton. 204.
63. Radak, B. and V. Markovic, *Calorimetry*, in *Manual on Radiation Dosimetry*, N.W. Holm and R.J. Berry, Editors. 1970, Marcel Dekker Publishing: New York. p. 45-81.
64. Fricke, H. and S. Morse, *The Chemical Action of Roentgen Rays on Dilute Ferrosulfate Solutions as a Measure of Dose*. Am. J. Roentgenol. Radium Ther., 1927. 18: p. 426-430.
65. Christensen, H. and K. Sehested, *Pulse Radiolysis At High Temperatures And High Pressures*. Radiation Physics and Chemistry, 1981. 18: p. 723-731.
66. Jonah, C.D., J.R. Miller, and M.S. Matheson, *The Reaction of e_{aq}^- and H_3O^+ . Concentration effects of acid or salts*. Journal of Physical Chemistry, 1977. 81: p. 931-934.
67. Thomas, J.K., *The Rate Constants for H Atom Reactions in Aqueous Solutions*. Journal of Physical Chemistry, 1963. 67: p. 2593-2595.
68. Gevantman, L.H., *Solubility of Selected Gases in Water*, in *Handbook of Chemistry and Physics*, D.R. Lide, Editor. 1995, CRC Press: Boca Raton. p. 6-3 - 6-6.
69. Mozumder, A., *Fundamentals of Radiation Chemistry*. First ed. 1999, Academic Press: New York. 392.
70. Vereshchinskii, I.V. and A.K. Pikaev, *Introduction to Radiation Chemistry*. First ed. 1964, Israel Program for Scientific Translations, Ltd: Jerusalem. 335.
71. Jayson, G.G., B.J. Parsons, and A.J. Swallow, *Some Simple, Highly Reactive, Inorganic Chlorine Derivatives in Aqueous Solution. Their Formation Using Pulses of Radiation and Their Role in the Mechanism of the Fricke Dosimeter*. Journal of the Chemical Society, Faraday Transactions 1, 1973. 69: p. 1597-1607.

72. Bjergbakke, E., S. Navaretne, B.J. Parsons, and A.J. Swallow, *A Quantitative Description of the Action of High-Dose Pulses of Radiation on Aerated Acid Solutions Containing Ferrous and Chloride Ions*. Radiation Physics and Chemistry, 1987. 30: p. 59-62.
73. Hanrahan, R.J., *A Co⁶⁰ Gamma Irradiator for Chemical Research*. International Journal of Applied Radiation and Isotopes, 1962. 13: p. 254-255.
74. Weiss, J., A.O. Allen, and H.A. Schwarz, *Use of the Fricke Ferrous Sulfate Dosimeter for Gamma-Ray Doses in the Range 4 to 40 kr*. Proc. 2nd Intern. Conf. Peaceful Uses of Atomic Energy. Vol. 14. 1956, United Nations: NY. 179-181.
75. Matheson, M.S. and L.M. Dorfman, *Pulse Radiolysis*. First ed. 1969, M.I.T. Press: Cambridge, MA. 202.
76. Harris, D.C., *Quantitative Chemical Analysis*. Fourth ed. 1995, W. H. Freeman and Co.: New York. 748.
77. Kern, D.M., *The Hydration of Carbon Dioxide*. Journal of Chemical Education, 1960. 31: p. 14-23.
78. Weast, R.C., ed. *Handbook of Chemistry and Physics*. 1987, CRC Press, Inc.: Boca Raton.
79. Czapski, G. and H.A. Schwarz, *The Nature of the Reducing Radical in Water Radiolysis*. Journal of Physical Chemistry, 1962. 66: p. 471-474.
80. Collinson, E., F.S. Dainton, D.R. Smith, and S. Tazuke, *Evidence for the Unit Negative Charge on the "Hydrogen Atom" Formed by the Action of Ionising Radiation on Aqueous Systems*. Proceedings of the Chemical Society, 1962. 140.
81. Hart, E.J. and J.W. Boag, *Absorption Spectrum of the Hydrated Electron in Water and in Aqueous Solutions*. Journal of the American Chemical Society, 1962. 84: p. 4090-4095.
82. Koehler, G., S. Solar, N. Getoff, A.R. Holzwarth, and K. Schaffner, *Relationship Between the Quantum Yields of Electron Photoejection and Fluorescence of Aromatic Carboxylate Anions in Aqueous Solution*. Journal of Photochemistry, 1985. 28: p. 383-391.
83. Marketos, D.G., A. Marketou-Mantaka, and G. Stein, *Reaction of the Hydrated Electron with Benzene Studied by Pulse Radiolysis*. Journal of Physical Chemistry, 1974. 78: p. 1987-1992.
84. Roduner, E. and D.M. Bartels, *Solvent and Isotope Effects on Addition of Atomic Hydrogen to Benzene in Aqueous Solution*. Ber. Bunsenges. Phys. Chem., 1992. 96: p. 1037-1042.

85. Anderson, R.F., *Oxidation of the Cyclohexadienyl Radical by Metal Ions: A Pulse Radiolysis Study*. Radiation Physics and Chemistry, 1979. 13: p. 155-157.
86. Cercek, B. and M. Kongshaug, *Phenyl and Hydroxyphenyl Radicals. Pulse Radiolysis Study of Their Spectra and Reactivity*. Journal of Physical Chemistry, 1970. 74: p. 4319-4322.
87. Patterson, L.K., K.M. Bansal, and J.H. Fendler, *Pulse Radiolytic Investigations of Hydroxyl-Radical Reactivities in Micellar Solutions*. Chemical Communications, 1971: p. 152-153.
88. Milosavljevic, B.H. and O.I. Micic, *Solvated Electron Reactions in Water-Alcohol Solutions*. Journal of Physical Chemistry, 1978. 82: p. 1359-1362.
89. Gordon, S., E.J. Hart, M.S. Matheson, J. Rabani, and J.K. Thomas, *Reactions of the Hydrated Electron*. Discussions of the Faraday Society, 1963. 36: p. 193-205.
90. Gordon, S., E.J. Hart, and J.K. Thomas, *The Ultraviolet Spectra of Transients Produced in the Radiolysis of Aqueous Solutions*. Journal of Physical Chemistry, 1964. 68: p. 1262-1264.
91. Behar, D., G. Czapski, J. Rabani, L.M. Dorfman, and H.A. Schwarz, *The Acid Dissociation Constant and Decay Kinetics of the Perhydroxyl Radical*. Journal of Physical Chemistry, 1970. 74: p. 3209-3213.
92. Sweet, J.P. and J.K. Thomas, *Absolute Rate Constants for H Atom Reactions in Aqueous Solutions*. Journal of Physical Chemistry, 1964. 68: p. 1363-1364.
93. Dorfman, L.M., I.A. Taub, and R.E. Buehler, *Pulse Radiolysis Studies. I. Transient Spectra and Reaction-Rate Constants in Irradiated Aqueous Solutions of Benzene*. Journal of Chemical Physics, 1962. 36: p. 3051-3061.
94. Ramanam, G., *A Pulse Radiolysis Study of Aqueous Oxygenated Benzene in the Presence of Nitrous Oxide*. Journal of the Indian Chemical Society, 1977. 53: p. 957-964.
95. Stein, G. and J. Weiss, *Chemical Actions of Ionising Radiations on Aqueous Solutions. Part II. The Formation of Free Radicals. The Action of X-Rays on Benzene and Benzoic Acid*. Journal of the Chemistry Society, 1949: p. 3245-3257.
96. Pan, X.-M., M.N. Schuchmann, and C. von Sonntag, *Oxidation of Benzene by the OH Radical. A Product and Pulse Radiolysis Study in Oxygenated Aqueous Solution*. Journal of the Chemical Society, Perkin Transactions 2, 1993: p. 289-297.
97. Srinivasan, T.K.K., I. Balakrishnan, and M.P. Reddy, *On the Nature of the Products of Gamma Radiolysis of Aerated Aqueous Solutions of Benzene*. Journal of Physical Chemistry, 1969. 73: p. 2071-2073.

98. Kartosheva, L.I. and A.V. Pikaev, *Initial Yields of Hydrogen Peroxide in the Gamma Radiolysis of Aqueous Solutions of Benzene in the Presence of Oxygen*. High Energy Chemistry, 1972. 6: p. 76-77.
99. Balakrishnan, I. and M.P. Reddy, *The Effect of Temperature on the Gamma Radiolysis of Aqueous Solutions*. Journal of Physical Chemistry, 1972. 76: p. 1273-1279.
100. Eberhardt, M.K., G.A. Martinez, J.I. Rivera, and A. Fuentes-Aponte, *Thermal Decomposition of Peroxydisulfate in Aqueous Solutions of Benzene-Nitrobenzene-Benzonitrile Mixtures. Formation of OH Radicals from Benzene Radical Cations and Water at Room Temperature*. Journal of the American Chemical Society, 1982. 104: p. 7069-7073.
101. Sworski, T.J., *Some Effects of Cobalt Gamma Radiation on Aqueous Benzene Solutions*. Journal of Chemical Physics, 1952. 20: p. 1817-1818.
102. Baxendale, J.H. and D. Smithies, *Radiation Chemistry of Aqueous Benzene Solutions*. Journal of Chemical Physics, 1955. 23: p. 604.
103. Phung, P.V. and M. Burton, *Radiolysis of Aqueous Solutions of Hydrocarbons Benzene, Benzene-d₆, Cyclohexane*. Radiation Research, 1957. 7: p. 199-216.
104. Studier, M.H. and E.J. Hart, *The Reduction of Benzene by Hydrated Electrons in Gamma Ray Irradiated Alkaline Solutions*. Journal of the American Chemical Society, 1969. 91: p. 4068-4072.
105. Michael, B.D. and E.J. Hart, *The Rate Constants of Hydrated Electron, Hydrogen Atom, and Hydroxyl Radical Reactions with Benzene, 1,3-Cyclohexadiene, 1,4-Cyclohexadiene, and Cyclohexene*. Journal of Physical Chemistry, 1970. 74: p. 2878-2884.
106. Mantaka, A., D.G. Marketos, and G. Stein, *Continuous Gamma and Pulse Radiolysis of Aqueous Benzene Solutions: Some Reactions of the Hydroxycyclohexadienyl Radical*. Journal of Physical Chemistry, 1971. 75: p. 3886-3889.
107. Bhatia, K., *Reactions of the Radiolytically Generated Hydroxycyclohexadienyl Radical in Aqueous Benzene Systems*. Radiation Research, 1974. 59: p. 537-555.
108. Klein, G.W. and R.H. Schuler, *Oxidation of Benzene by Radiolytically Produced OH Radicals*. Radiation Physics and Chemistry, 1978. 11: p. 167-171.
109. Petrucci, R.H. and W.S. Harwood, *General Chemistry. Principles and Modern Applications*. Seventh ed. 1997, Prentice-Hall: Upper Saddle River.
110. Sehested, K. and E.J. Hart, *Formation and Decay of the Biphenyl Cation Radical in Aqueous Acidic Solution*. Journal of Physical Chemistry, 1975. 79: p. 1639-1642.

111. Lide, D., ed. *Handbook of Chemistry and Physics*. 1995, CRC Press, Inc.: Boca Raton.

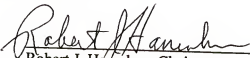
BIOGRAPHICAL SKETCH

Larry Lee Land was born in the small town of Marianna, Florida, and was reared in the even smaller town of Bonifay, Florida. He attended Bonifay Elementary School and Holmes County High School, where he earned the title of Valedictorian and most likely to succeed for the class of 1987. Larry began college at the University of Florida on full scholarship in 1987 and majored in chemistry. He graduated with a Bachelor of Science degree in 1991.


Larry began graduate studies in chemistry at the University of Florida in the fall of 1991. He served as teaching assistant for almost all of the chemistry classes offered at UF. In addition, Larry was awarded a departmental teaching award, and a University of Florida teaching award. Larry also serves as an adjunct mathematics instructor at Central Florida Community College in Ocala, Florida.

Larry married Cynthia Isabel Mendoza in March of 1995. In his spare time, Larry enjoys vocal performance and opera. Ultimately, Larry aspires to obtain a professional position as the world's first operatic chemist.

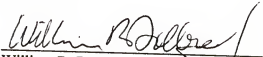
I certify that I have read this study and that in my opinion it conforms to acceptable standards of scholarly presentation and is fully adequate, in scope and quality, as a dissertation for the degree of Doctor of Philosophy.


Robert J. Hanrahan, Chairman
Professor of Chemistry

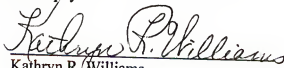
I certify that I have read this study and that in my opinion it conforms to acceptable standards of scholarly presentation and is fully adequate, in scope and quality, as a dissertation for the degree of Doctor of Philosophy.


Merle A. Battiste
Professor of Chemistry

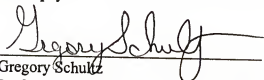
I certify that I have read this study and that in my opinion it conforms to acceptable standards of scholarly presentation and is fully adequate, in scope and quality, as a dissertation for the degree of Doctor of Philosophy.


William R. Dolbier
Professor of Chemistry

I certify that I have read this study and that in my opinion it conforms to acceptable standards of scholarly presentation and is fully adequate, in scope and quality, as a dissertation for the degree of Doctor of Philosophy.


Kathryn R. Williams
Associate Professor of Chemistry

I certify that I have read this study and that in my opinion it conforms to acceptable standards of scholarly presentation and is fully adequate, in scope and quality, as a dissertation for the degree of Doctor of Philosophy.

A handwritten signature in cursive script, reading "Gregory Schultz", written over a horizontal line.

Gregory Schultz
Professor of Biochemistry and Molecular
Biology

This dissertation was submitted to the Graduate Faculty of the Department of Chemistry in the College of Liberal Arts and Sciences and to the Graduate School and was accepted as partial fulfillment of the requirements for the degree of Doctor of Philosophy.

May, 2001

Dean, Graduate School